DUDLEY
NAVAL
MONTEREY, CALIFORNIA 93943

NAVAL POSTGRADUATE SCHOOL
Monterey, California

THESIS

GENERATION OF AN OPTIMUM HIGH SPEED
HIGH ACCURACY OPERATIONAL AMPLIFIER

by

Patrick Gariano, Jr.

September 1985

Thesis Advisor: S. Michael

Approved for public release; distribution is unlimited

T222844

SECURITY CLASSIFICATION OF THIS PAGE *(When Data Entered)*

REPORT DOCUMENTATION PAGE

READ INSTRUCTIONS BEFORE COMPLETING FORM

1. REPORT NUMBER

2. GOVT ACCESSION NO.

3. RECIPIENT'S CATALOG NUMBER

4. TITLE *(and Subtitle)*
Generation of an Optimum High Speed High Accuracy Operational Amplifier

5. TYPE OF REPORT & PERIOD COVERED
Master's Thesis; September 1985

6. PERFORMING ORG. REPORT NUMBER

7. AUTHOR(s)
Patrick Gariano, Jr.

8. CONTRACT OR GRANT NUMBER(s)

9. PERFORMING ORGANIZATION NAME AND ADDRESS
Naval Postgraduate School
Monterey, California 93943-5100

10. PROGRAM ELEMENT, PROJECT, TASK AREA & WORK UNIT NUMBERS

11. CONTROLLING OFFICE NAME AND ADDRESS
Naval Postgraduate School
Monterey, California 93943-5100

12. REPORT DATE
September 1985

13. NUMBER OF PAGES
138

14. MONITORING AGENCY NAME & ADDRESS*(if different from Controlling Office)*

15. SECURITY CLASS. *(of this report)*
UNCLASSIFIED

15a. DECLASSIFICATION/DOWNGRADING SCHEDULE

16. DISTRIBUTION STATEMENT *(of this Report)*
Approved for public release; distribution is unlimited.

17. DISTRIBUTION STATEMENT *(of the abstract entered in Block 20, if different from Report)*

18. SUPPLEMENTARY NOTES

19. KEY WORDS *(Continue on reverse side if necessary and identify by block number)*
OP-AMPS; Operational Amplifiers; Composite OP-AMPS

20. ABSTRACT *(Continue on reverse side if necessary and identify by block number)*
This research examines and discusses the feasibility of utilizing Composite Operational Amplifiers to overcome the inherent inability of IC op-amps to simultaneously perform in a very fast, very accurate mode. Composite operational amplifiers, known to provide enhanced stability, decreased sensitivity to circuit element variations, and an extended operating frequency range, can now be used to generate an operational amplifier that

DD FORM 1 JAN 73 1473 EDITION OF 1 NOV 65 IS OBSOLETE
S N 0102-LF-014-6601

SECURITY CLASSIFICATION OF THIS PAGE *(When Data Entered)*

comcurrently exhibits both high speed and high accuracy. The composite op-amp is the only generalized method known to produce an op-amp that is both very fast and very accurate. This has never before been achievable in a simple individual entity.

Approved for public release; distribution is unlimited.

Generation of an Optimum High Speed High Accuracy Operational Amplifier

by

Patrick Gariano Jr.
Lieutenant Commander, United States Navy
B.S., University of South Florida, 1972

Submitted in partial fulfillment of the
requirements for the degree of

MASTER OF SCIENCE IN ELECTRICAL ENGINEERING

from the

NAVAL POSTGRADUATE SCHOOL
September 1985

Thesis
S192
c.1

ABSTRACT

This research examines and discusses the feasibility of utilizing Composite Operational Amplifiers to overcome the inherent inability of IC op-amps to simultaneously perform in a very fast, very accurate mode. Composite operational amplifiers, known to provide enhanced stability, decreased sensitivity to circuit element variations, and an extended operating frequency range, can now be used to generate an operational amplifier that concurrently exhibits both high speed and high accuracy. The composite op-amp is the only generalized method known to produce an op-amp that is both very fast and very accurate. This has never before been achievable in a simple individual entity.

TABLE OF CONTENTS

LIST OF FIGURES

I. INTRODUCTION

A. BACKGROUND

The Operational Amplifier (op-amp) is perhaps the most widely used analog integrated circuit. It is an element common to almost every circuit design. Society's increased demands on the engineering fields over the last several decades have prompted fantastic technology changes to produce systems of ever greater performance. Paramount among the performance increases demanded are speed and accuracy as exemplified by high speed analog-to-digital (A/D) and digital-to-analog (D/A) converters with 16 bit accuracy, high speed digital signal processing applications including switched capacitor networks and sample and hold circuits, and many nonlinear applications where speed and accuracy are crucial. Hence, as an integral design element, faster and more accurate op-amps, or circuits that perform an equivalent function, are required to meet these demands.

As will be discussed later, the speed (slew rate) and accuracy (input offset voltage) of an op-amp do not go hand-in-hand. Rather, theoretical constraints encountered in the design of op-amps have precluded the fabrication of a single op-amp capable of simultaneously providing both high speed and high accuracy. Manufacturer's designation of high accuracy (on the order 3 to 5 mV) op-amps are often not sufficiently accurate for some of the requirements imposed by today's advanced systems designs. Although op-amps are commercially available with accuracies in the 100 μV range, these same op-amps have speeds (slew rates) that are typically limited to 10 V/ μS or less. In fact, one cannot purchase an op-amp that is, by today's standards, both very fast (hundreds of Volts per microsecond) and very accurate (hundreds of microvolts), but rather must utilize one that

is a compromise of these two attributes for a particular application.

This research demonstrates that in fact, an extremely fast and extremely accurate operational amplifier is now achievable via a relatively new design approach known as Composite Operational Amplifiers. This general technique for designing controlled sources by combining N basic op-amps into a composite structure has been proposed with applications to Voltage Controlled Voltage Source (VCVS) [Refs. 1,2]. The resulting composite op-amp families (N = 2, 3, or 4) were designed according to stringent performance criteria to satisfy various practical aspects of an op-amp's behavior. Included among these aspects was stability and dynamic range, extended bandwidth (BW), power supply variations, Gain Bandwidth Product (GBWP), and insensitivity to other circuit components. Relative to state-of-the-art designs using a similar number of op-amps, the improved performance of resulting active realizations was demonstrated over a wide range of signal processing applications, when Composite operational amplifiers were used to replace the regular op-amps [Refs. 1,3].

This technique has now been further extended, [Ref. 4], to generate C2OA composite operational amplifiers (CNOA , N=2) which utilize a very high accuracy op-amp and a very high speed op-amp to generate a composite amplifier possessing both of these qualities, an entity heretofore unknown.

Before discussing this technique in detail (Chapter II), the basic op-amp must first be dissected in order to determine the driving forces behind its operation. The sections immediately following will attempt to do just that as it pertains to some of the basic performance measures of an op-amp such as slew rate, bandwidth, input offset voltage, stability, insensitivity, etc.. It is essential to have a

firm grasp on each of these concepts and their interrelation. As an example, consider an "average" op-amp, such as the work-horse LM741, which is mediocre in each of these respects. Although each performance measure is important in its own right, the op-amp's overall performance and suitability for a particular application depends on the combination of the performances in each area. As an example, an op-amp may exhibit a very good slew rate, offset, bandwidth, and be insensitive to other circuit components, but have a very narrow range of stable operation (due perhaps to a very small internal compensation capacitance). It would be quite likely then for the op-amp to be beyond its range of stable operation and hence oscillate, leading to a very fast, very accurate, large bandwidth amplifier that is of limited or no practical value.

Later in this chapter, some of the more successful approaches that have been developed to increase the performance (primarily speed) of an op-amp will be discussed. But, as will be pointed out, in each case in which a substantial enhancement of slew rate was achieved, a penalty of a concomitant degradation in the input offset voltage and drift as well as some degradation in noise performance resulted.

Chapter II will discuss various theoretical aspects of the C2OAs including the development of equations to predict the best achievable input offset voltage depending upon the type of configuration used. Also a two-pole model for the composites will be developed as well as a computer program to simulate their frequency transfer characteristics. In addition, an historical perspective will be presented on the development of CNOAs and the general performance attributes that may be expected to result when this very dynamic circuit is used.

Chapter III includes the experimental results realized during the course of this investigation. Circuit topologies

will be presented as well as numerous pictoral, graphical, and tabular representations of results and trends observed.

Chapter IV presents various sample applications of C20As in both linear and nonlinear environments. These include preliminary results of the improved implementation of a square wave generator, an improved version of a precision half-wave rectifier (AM signal detector), and a novel sample and hold circuit design (for A/D, D/A, and digital signal processing applications) [Ref. 5].

B. INPUT OFFSET VOLTAGE

Ideally, an op-amp that has its inputs connected to a common ground will have an output voltage (V_o) equal to zero (Figure 1.1). Practically, however, an op-amp will exhibit some DC output voltage, called the output offset voltage (V_{oo}), even though both the inverting and the non inverting input terminals are grounded. This output is undesirable in that it represents an error voltage. The differential input voltage that must be applied between the input terminals in order to force the output to zero is termed the input offset voltage (V_{io}) and for typical general-purpose op-amps, this value is on the order of several millivolts (Figure 1.2).

The output offset voltage is caused by a mismatching between the two op-amp input terminals. This mismatching is due to the fact that the transistor pairs in the op-amp's input differential stage almost certainly will have gains and emitter resistances that are not identical. In monolithic op-amps, it is highly desirable that all of the transistors on a particular integrated circuit be identical. However, the transistors will only be "identical" within a statistical deviation about some mean. Even though all of the components are integrated onto one chip, it is not possible to avoid minor variations between the two transistors in the op-amp's input differential amplifier stage. This phenomenon then produces slight differences in the

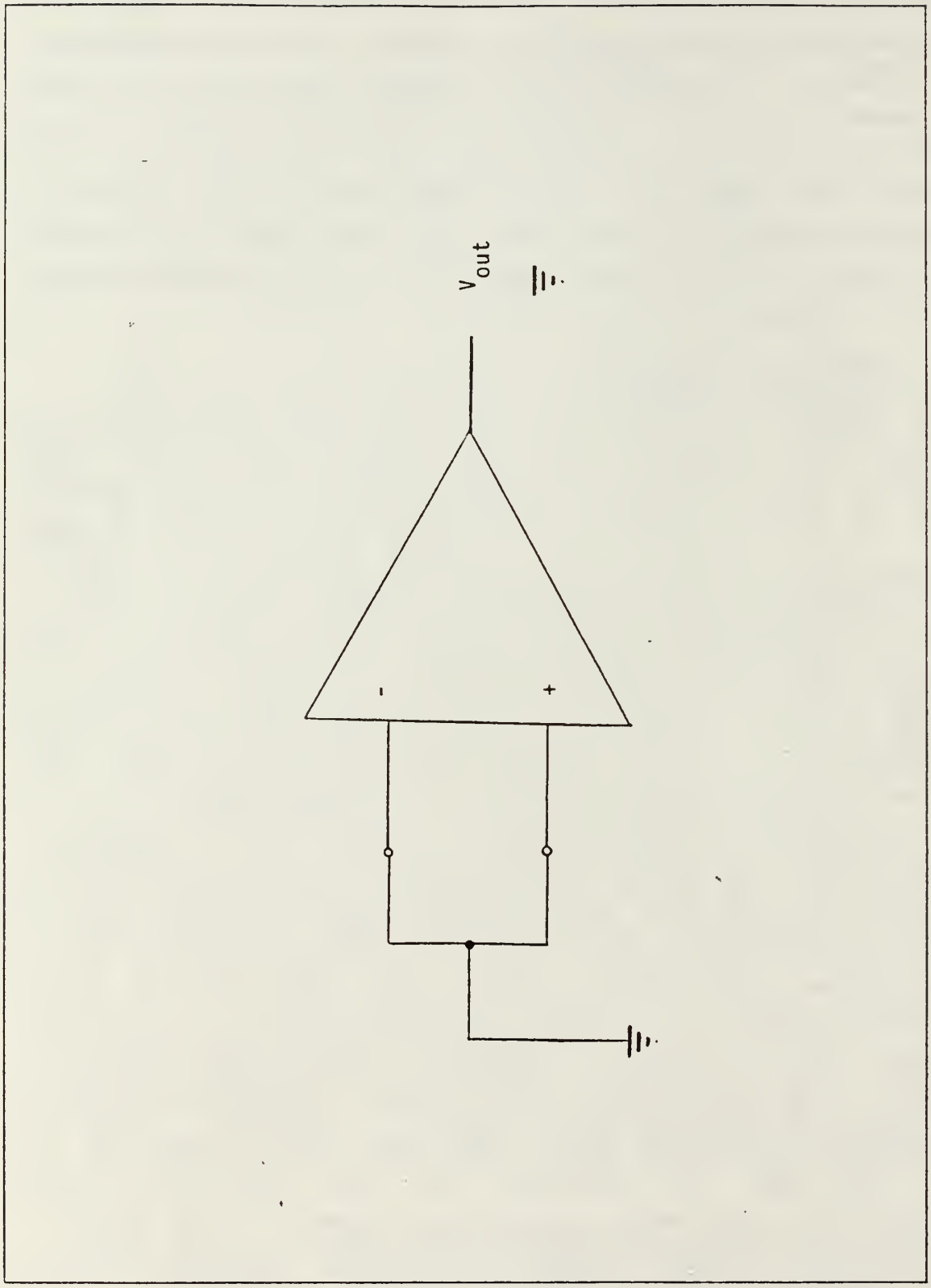

Figure 1.1 Offset Voltage Illustration

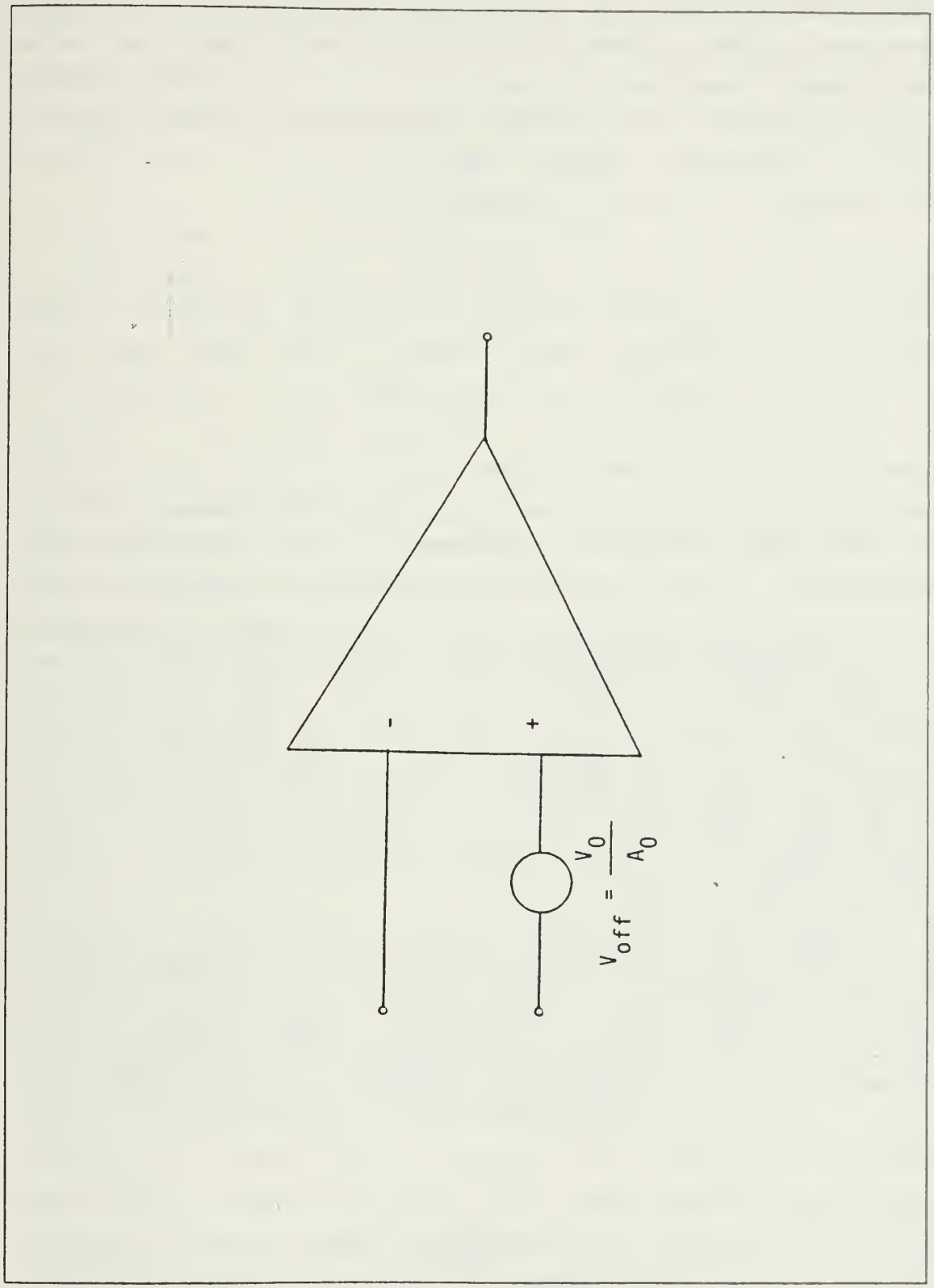

Figure 1.2 Offset Free Op-Amp

nominal values of the collector voltages and collector currents in the input differential amplifier when both inputs are grounded. This results in a non-zero differential output voltage at the op-amp's first stage, which is amplified by subsequent stages, where it may be even further aggravated by additional component mismatching.

To reduce the output offset voltage to zero, it is necessary to apply a differential input voltage of a specific amplitude and polarity. However, because of mass production techniques, even op-amps of the same type will not require an input of the same amplitude or polarity to zero the output. What is necessary then is a circuit connected to the op-amp's input terminals which will provide the flexibility of obtaining V_{off} of proper amplitude and polarity. Such a circuit is called an input offset voltage compensating network and the addition of this circuit results in an op-amp that is said to be nulled or balanced (assuming offset nulling pins are not provided on the op-amp IC). In addition, offset voltages are not necessarily constant for any given op-amp but vary with the power supply voltages applied, the operating temperature, and the age of the op-amp. This then limits the realistic value of using either internal or external nulling to compensate or correct for the offset voltage.

In closed-loop amplifiers, such as that shown in Figure 1.3, if the inputs are again connected to a common ground, the output observed will be the input offset voltage multiplied by the gain (K) of the circuit. Thus, depending upon the gain, the output voltage realized for a "zero" input may be of a significant magnitude. If an input signal is now added to the circuit, the output voltage above is superimposed on the output signal. The two major ramifications then are that the maximum possible output signal swing is reduced and that a built in system error must be accounted for (K x

V_{off}). This is exemplified by Figure 1.4 where the resulting output voltage is actually the sum of two components; one resulting from an amplification of the input signal and another from the amplification of the input offset voltage.

$$V_{out} = -\frac{R_f}{R_i} \times V_{in} \pm \left(\frac{R_f}{R_i} + 1\right) \times V_{off} \qquad (1.1)$$

Every op-amp then will have an input offset voltage and its criticality and acceptability will depend upon the application and the accuracies desired.

C. SLEW RATE LIMITATIONS OF AN OPERATIONAL AMPLIFIER

In a non-small signal situation, quite often a phenomenon called slew-rate limiting occurs in op-amps resulting in a distorted output. This is exemplified by Figure 1.5 which shows the type of distortion that is commonly observed wherein the rate of change (slope) of the input and output signals is not the same. Slew rate is a term utilized for operational amplifiers that indicates how rapidly (typical units are volts per microsecond) the output can change from one output voltage to another when the input signal experiences an instantaneous voltage-step change. That is, it is the maximum rate of change with respect to time of the output voltage that the op-amp can produce.

$$SR = \left.\frac{dV_{out}}{dt}\right|_{max} \qquad (1.2)$$

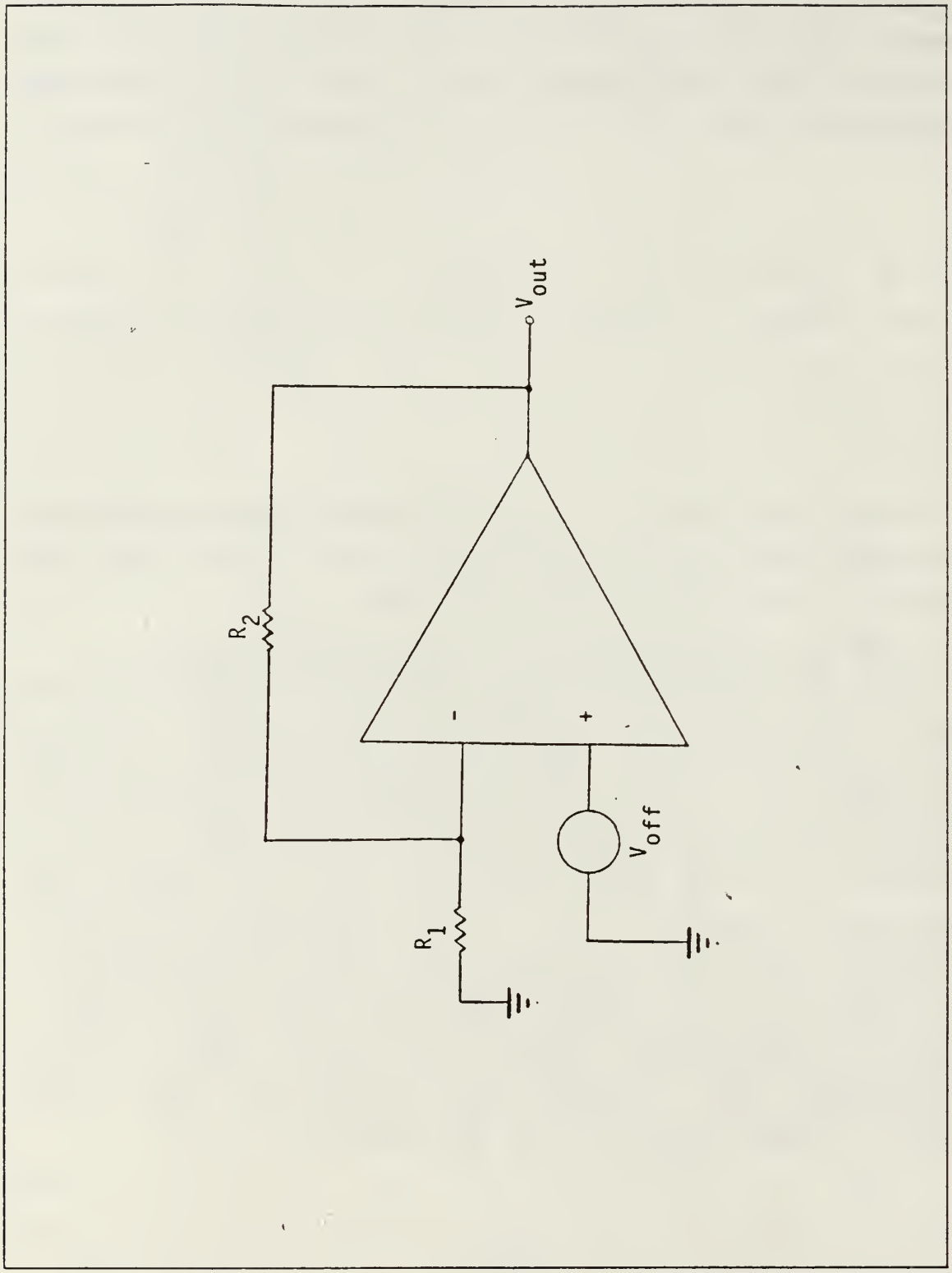

Figure 1.3 Offset Voltage in a Closed-loop Amplifier

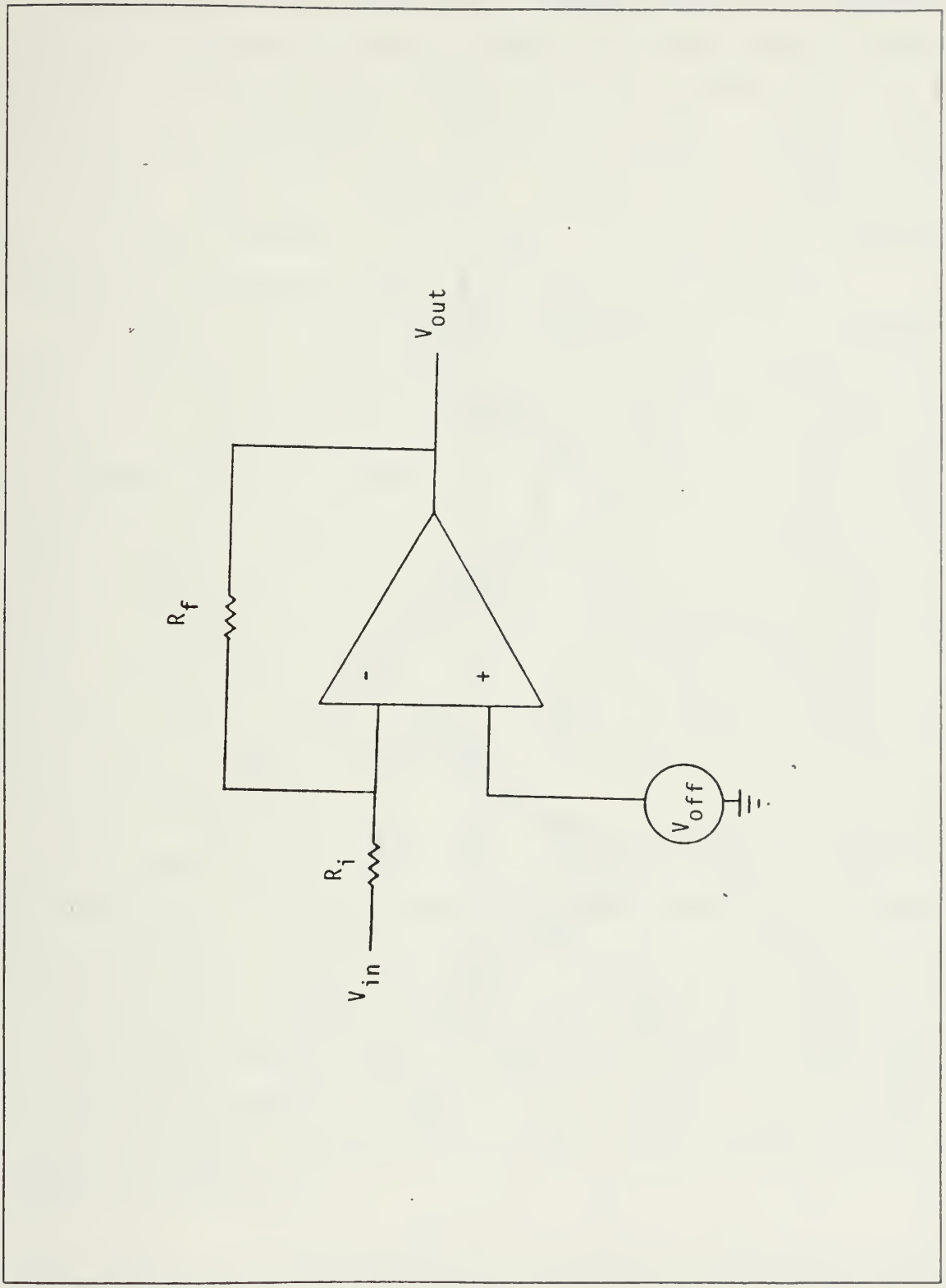

Figure 1.4 Additive Effect of Offset and Input on the Output Voltage

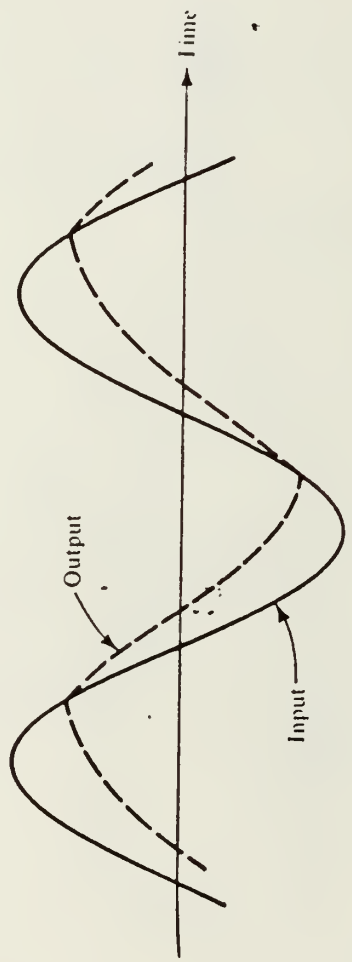

Figure 1.5 Distorted Output Sine Wave as a Consequence of Slew Rate Limiting

If, in the circuit depicted in Figure 1.6, at time t=0, a non-zero input voltage is applied, the output cannot respond instantaneously and is initially zero. This is a result of a sufficiently large differential signal, V_{in}, being applied to drive the input stage of the op-amp out of its linear range of operation. During this "transient", only limited current is available to charge the internal compensation capacitor and slew rate limiting occurs.

Slew rate is a large-signal phenomenon, ie - a signal where the amplitude is comparable to the power supply voltages. Slew rate is most commonly specified for an op-amp in a unity gain configuration and it is measured by applying a step input voltage (10Vpeak). If an op-amp's slew rate were specified as 1 V/ μs, it would imply that the output could rise or fall no faster than 1 volt every microsecond. The most desirous slew rate would be an infinite one so that the op-amp's output voltage would change simultaneously with the input. In practice, a slew rate is not truly a constant. It has been shown that it increases with higher closed-loop gains and DC supply voltages and decreases with an increase in temperature [Ref. 6].

When a large amplitude, high frequency signal is applied to an op-amp, the slew rate is limited by current limiting and saturation of the op-amp's internal stages. As a result of the current, limiting of the charge and discharge times of the internal capacitors will be reduced accordingly and will prevent the output voltage from responding immediately to a rapidly changing input. Examples of these capacitances are shown in Figures 1.7 and 1.8 for the LM 741, HA 2525, and the HA 5170. The rate at which the voltage across a capacitor changes is

$$\frac{dV_C}{dt} = \frac{I}{C} \qquad (1.3)$$

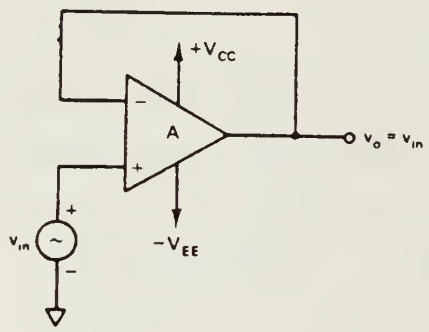

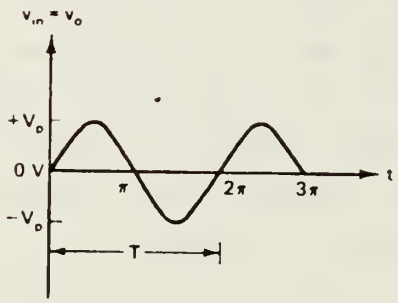

Figure 1.6 Circuit for Slew Rate Determination

Since the output voltage is the voltage across the capacitor, this equation indicates that the capacitor's charging rate is the cause of slew rate limiting.

If a large amplitude, high frequency sinusoid is applied to the voltage follower of Figure 1.6, then

$$V_{in} = V_{out} = V_p \text{SIN } \omega t \qquad (1.4)$$

The rate of change with respect to time of the output is then

$$\frac{dV_o}{dt} = V_p \, \omega \, \text{COS } \omega t \qquad (1.5)$$

The maximum rate of change will occur when cos $\omega t = 1$, implying that

$$SR = \frac{dV_{out}}{dt} = V_p \, \omega \qquad (1.6)$$

or, for the customary units:

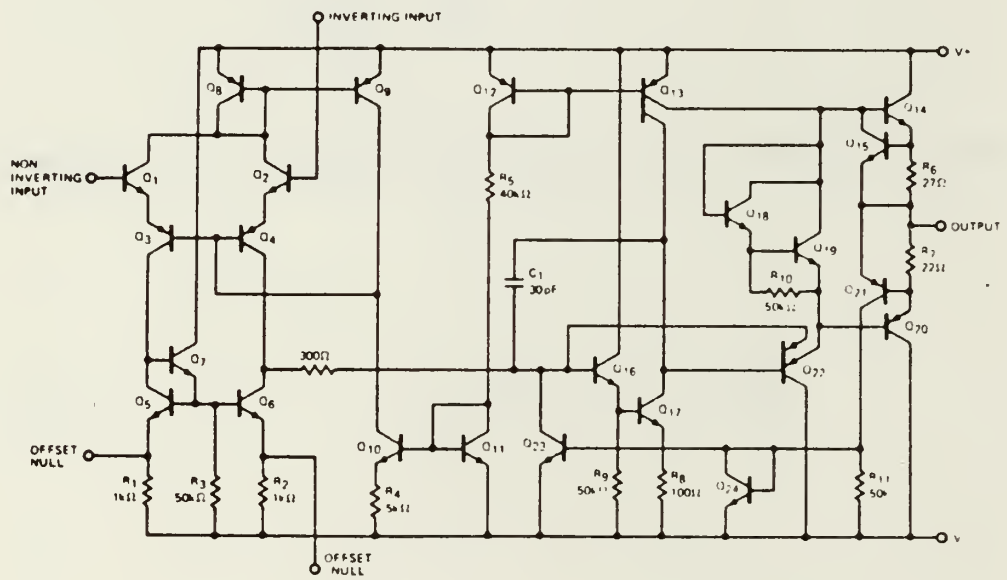

Figure 1.7 Schematic of LM 741

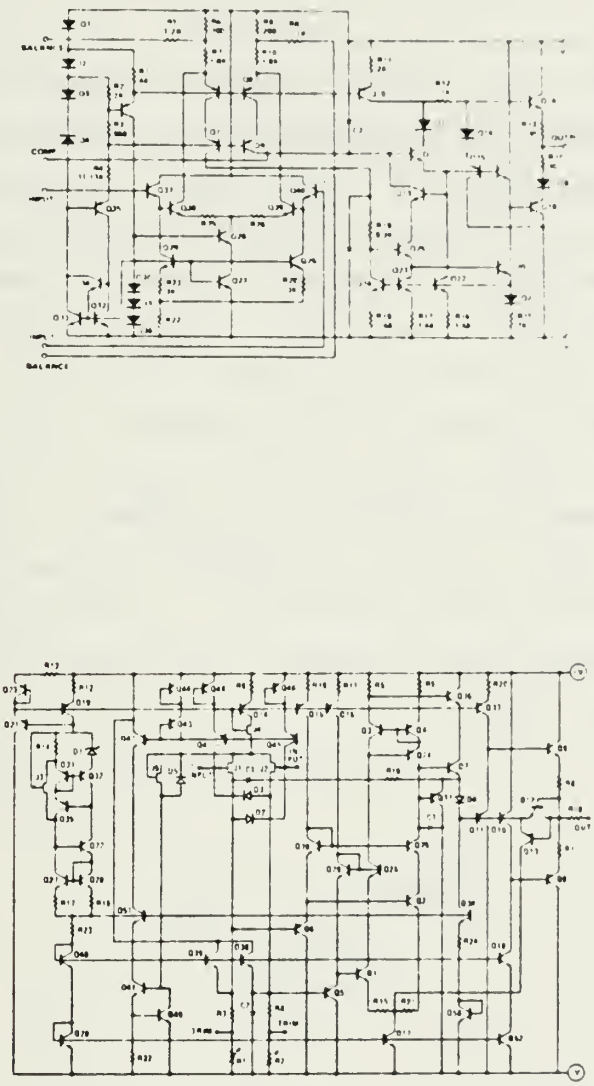

Figure 1.8 Schematics for HA 2525 and HA 5170

$$SR = \frac{2\pi f V_p}{10^6} \quad (V/\mu s) \tag{1.7}$$

where SR is the slew rate, f is the input frequency in Hertz, and V_p is the peak value of the output sine wave in volts. The implications of this equation are that the slew rate determines the maximum frequency of operation for a desired output swing, if an output free of distortion is to be achieved. Therefore, as long as the right-hand side of this equation is less than the slew rate of the op-amp, the shape of the output waveform will always be the same as that of the input, in this case, sinusoidal. If the amplitude and/or the frequency of the input signal is increased so that the slew rate of the op-amp is exceeded, then the resulting output will be distorted. If the peak voltage in Equation 1.6 equaled the maximum specified for the given op-amp ($V_p = V_{max}$), then

$$SR = \left.\frac{dV_{out}}{dt}\right|_{max} = V_{max}\,\omega_m \tag{1.8}$$

and the resulting ω_m is denoted as the amplifier's Full Power Bandwidth. This relationship now indicates the given amplifier's useable frequency range over which linear operation will be assured.

D. METHODS OF INCREASING SLEW RATE

For typical monolithic op-amps in the inverting mode, the schematic shown in Figure 1.9 has proven to be an adequate model for calculating slew rate limits [Ref. 7]. Here the op-amp is visualized as having an input stage with a small-signal transconductance of gm_1 which is connected to a large voltage gain stage (Miller integrator). It can be shown that the maximum current available to charge capacitor C is $2I_1$, where I_1 is the quiescent collector current per device in the input stage. When a large input voltage is applied, only a maximum current $I_m=2I_1$ can be delivered to the integrator in the second stage. The resulting slew rate is then:

$$SR = \left.\frac{dV_o}{dt}\right|_{max} = \frac{I_m(t)}{C} = \frac{2I_1}{C} \qquad (1.9)$$

Since $gm_1=I_1/V_i$, the integrator's small signal output voltage can be given by

$$V_o(s) = \frac{gm_1 V_i(s)}{sC} \qquad (1.10)$$

which implies

$$A_v(\omega) = \left| \frac{V_o(\omega)}{V_i(\omega)} \right| = \frac{gm_1}{\omega C} \qquad (1.11)$$

From this expression, the gain bandwidth product for the op-amp used, which is also the open-loop unity gain frequency ω_i, is

$$\omega_i = \frac{gm_i}{C} \qquad (1.12)$$

The large and small signal behavior of the op-amp can then be related by combining Equations 1.9 and 1.12 to yield:

$$SR = \left. \frac{dV_o}{dt} \right|_{max} = \frac{2\omega_i I_1}{gm_1} \qquad (1.13)$$

This equation indicates the op-amp parameters that can be modified in an effort to favorably alter the slew rate. Based upon these parameters, variations of two basic techniques have been reported in the literature [Refs. 8,9].

One method to improve the slew rate is to increase the GBWP ω_i, and in most high slew rate circuits, this is the

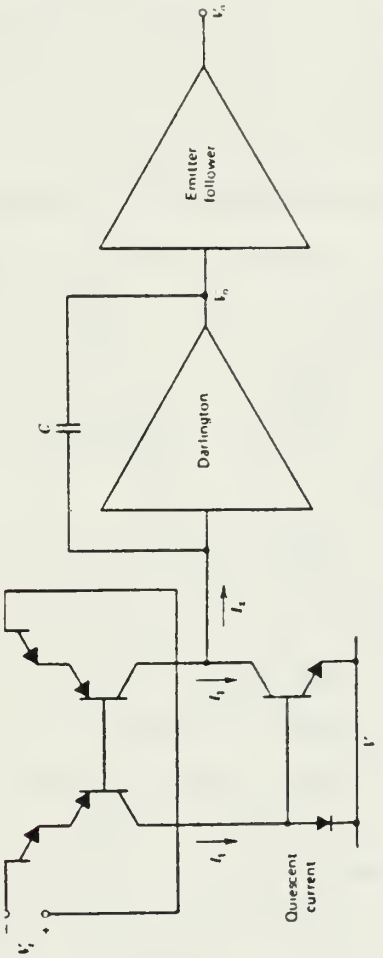

Figure 1.9 Simplified Schematic for Slew Rate Calculations of a General Purpose Op-amp

course of action chosen. However, the frequency characteristics of the transistors in the IC set an upper limit on the GBWP achievable.

The only other available means to achieve an enhancement in slew rate is to increase the ratio of the operating current to the first stage transconductance. One manner in which this can be achieved is via the inclusion of emitter-degeneration resistors in the input differential amplifier, as shown in Figure 1.10, which will reduce gm_1. The slew rate enhancement achievable by this technique is a factor of $(1+ gm_1R_E/2)$ over that given by Equation 1.13 . Improvements reported have been in the range of an eleven to twenty fold increase in slew rate . A practical limitation to this technique occurs, however, due to the mismatch in the two added emitter resistors, which results in increased input offset voltage and drift. In addition, the noise performance of the op-amp is degraded by the unavoidable addition of the resistor's thermal noise.

Another method for improving the ratio I_1/gm_1, and hence the slew rate, is by incorporating Field Effect Transistors (JFET or MOSFET) in the input stage of the amplifier, as shown in Figure 1.11 . The effect here is due to the fact that JFETs have a considerably lower transconductance when compared to bipolar devices, for a given operating current I_1. Although normally considered a disadvantage, this characteristic is highly desirable in applications requiring a fast op-amp. Slew rate enhancements via this technique have been, in special situations, as high as two orders of magnitude greater than that achievable with conventional IC op-amps. As in the previous method, however, a limitation exists on the use of FETs as input devices because of the resulting increase in the circuit's input offset voltage. This is due to the fact that FETs typically have higher input offset voltages than bipolar transistors, by at least a factor of three and often much more.

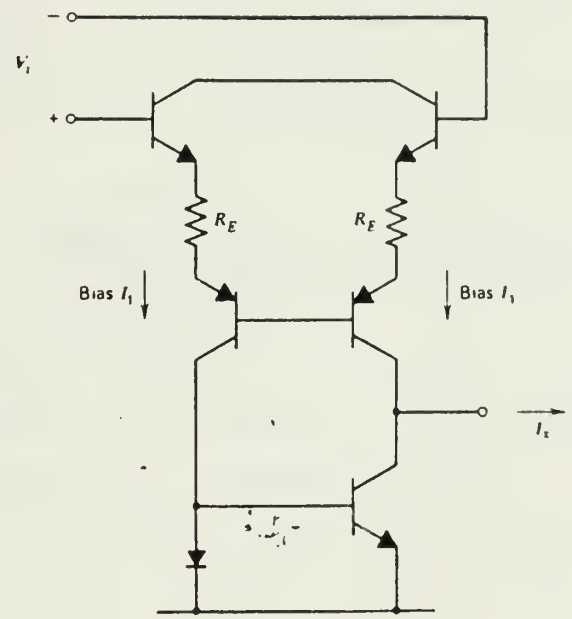

Figure 1.10 Inclusion of Emitter Resistors in First Stage of Op-amp

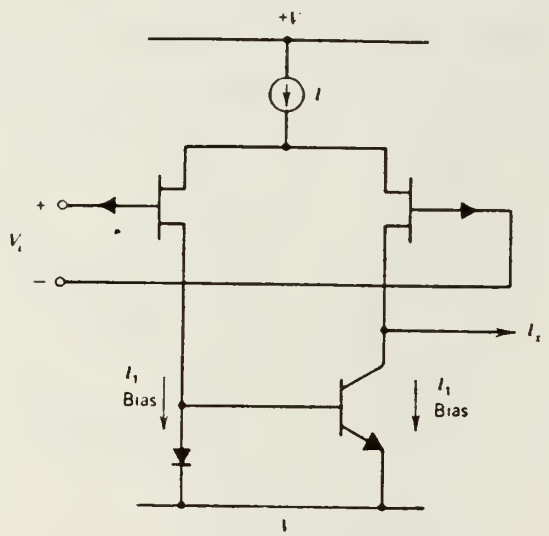

Figure 1.11 Utilization of JFETs in an Op-amp Input Stage

Other techniques for improving the slew rate have been reported, similar to that of Hearn [Ref. 9], wherein the maximum current, I_m, available for charging the compensating capacitor is increased. Although significant improvements in slew rate were achieved, again the limitation is an increase in input offset voltage.

Each of the successful methods described above results in greatly improved slew rates for monolithic op-amps. However, for each of the discussed methods, the slew rate enhancement obtained is associated with an unavoidable increase in the input offset voltage and drift, as well as some degradation in the op-amp's noise performance. Therefore, none of these methods are of any great value when the goal is an amplifier that possesses both high speed and high accuracy.

E. FREQUENCY DEPENDENT GAIN AND GAIN BANDWIDTH PRODUCT

One very important concern in designing active networks utilizing operational amplifiers is the finite op-amp frequency dependent gain, A. Figure 1.12 shows the typical frequency response of an internally compensated op-amp. To be noted are the 3-dB frequency f_L (Hz), the unity gain frequency f_i (Hz), and the uniform 20 dB per decade roll-off made possible by the internal compensating capacitor and required to ensure stable operation of the amplifier. Throughout all of this work, it is assumed that all op-amps used are internally compensated and that they exhibit this type of frequency response. Thus the gain is given by

$$A = \frac{A_o}{1 + (s/\omega_L)} \qquad (1.14)$$

where A_0 is the DC gain and ω_L is the 3 dB frequency in radians per second. For frequencies $\omega >> \omega_L$, this expression simplifies to

$$A \tilde{=} \frac{A_0 \omega_L}{s} \qquad (1.15)$$

Thus, the Gain Bandwidth Product (GBWP) of the op-amp, ω_i is given by

$$\omega_i = A_0 \omega_L \qquad (1.16)$$

which, in general, is a constant for any operational amplifier and is used as a figure of merit. The combination of the above two equations then leads to

$$A \tilde{=} \frac{\omega_i}{s} \qquad (1.17)$$

or

$$\left| A \right| \tilde{=} \frac{\omega_i}{\omega} \qquad (1.18)$$

Both A_0 and f_i are usually found to be temperature and power supply dependent. For a general purpose op-amp such as the LM741, A_0 and f_i are on the order of 100,000 and 1 MHz, respectively. Thus, in active networks in which the response is highly dependent on A_0 and/or ω_i, the responses often exhibit unpredictable variations with changes in temperature and power supply voltage. The dependency of an op-amp circuit's response on A_0 and ω_i is therefore of critical importance when comparisons or evaluations are to be made.

F. CONCLUSIONS

In this chapter, the concepts of input offset voltage, slew rate, frequency dependent gain, and gain bandwidth product, as applied to operational amplifiers, are put forth. Theoretical concepts are subsequently developed to explain the effect of each of these parameters on an op-amp's overall behavior. Previous techniques developed for slew rate enhancement are studied including their effects on areas of op-amp performance other than speed. It was demonstrated that due to the interdependence of the slew rate and input offset voltage parameters on the same subcomponents of the op-amp's input stage, it is impossible to generate a single op-amp that is both very fast and very accurate.

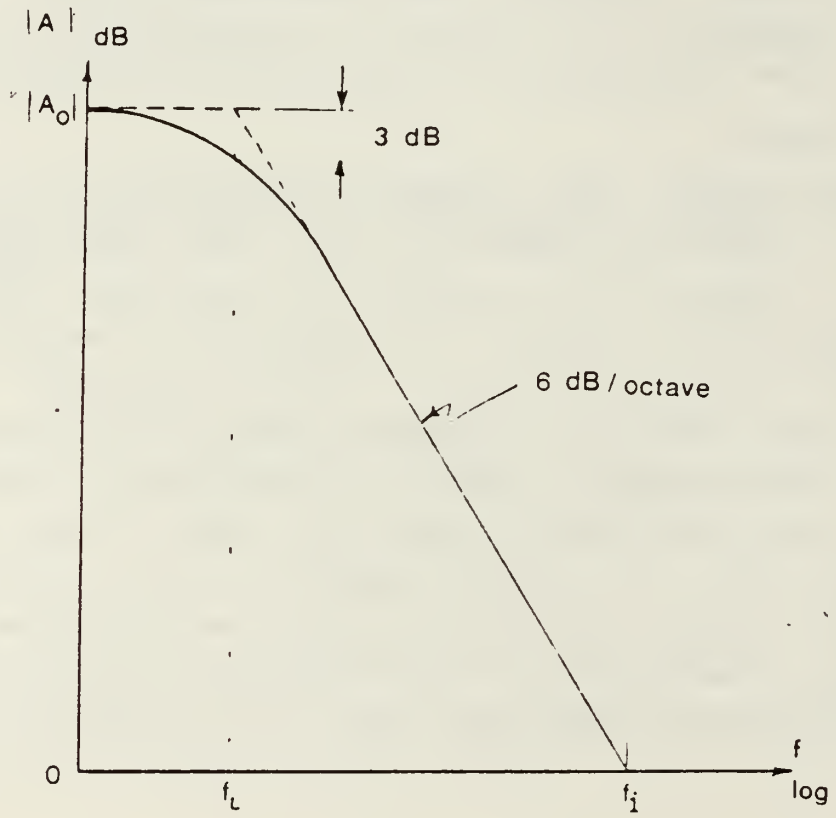

Figure 1.12 Typical Frequency Response of an Internally Compensated Operational Amplifier

II. COMPOSITE OPERATIONAL AMPLIFIERS

A. GENERATION OF COMPOSITE OPERATIONAL AMPLIFIERS

The concept of Composite Operational Amplifiers (CNOAs) was developed by W.B. Mikhael and S.N. Michael in 1981 and initial investigations into their behavior have been discussed in the literature [Refs. 1-5]. Their primary motivation was to develope a general technique of active compensation that would extend the useful bandwidth (BW) of circuits utilizing operational amplifiers. In particular, the technique would be applied to the design of active filter networks.

Starting with the basic active element, namely the op-amp itself, an exhaustive procedure was put forth for determining circuit implementations that would realize amplifiers with amplitude and phase compensation. The procedure developed utilized the concept of nullator-norator pairing [Refs. 10,11] to yield 136 possible circuit topologies (C2OAs), each containing two single op-amps. These topologies were then examined according to the following performance criteria [Ref. 12]:

1. Let A_a (s) and A_b (s) be the non-inverting and inverting open-loop gains of each of the 136 C2OAs examined. The denominator polynomial coefficients of A_a (s) and A_b (s) should have no change in sign. This satisfies the necessary (but not sufficient) conditions for stability. Also, none of the numerator or denominator coefficients of A_a (s) and A_b (s) should be realized through differences. This eliminates the need for single op-amps of matched GBWPs and results in low sensitivity of a C2OA with respect to its components.
2. The external three terminal performance of the C2OAs should resemble, as closely as possible from the

versatility point of view, those of the single op-amp.

3. No Right-Half S plane (RHS) zeroes due to the single op-amp pole should be allowed in the closed-loop gains of the C2OAs to achieve minimum phase shifts.
4. The resulting input-output relationship H_a (s) in the applications to be considered should have extended frequency operation with minimum gain and phase deviation from the ideal transfer function H_i (s). The improvement should be enough to justify the increased number of op-amps.

Twenty seven C2OA structures of the 136 examined were found to have acceptable performance according to the above criteria. From these twenty seven, four composite op-amp structures, referred to as C2OA-1, C2OA-2, C2OA-3, and C2OA-4 were found to outperform the remaining C2OA structures and were selected for further testing as one-to-one replacements for single op-amps. These structures are shown in Figures 2.1 through 2.4 .

Following the same approach, Composite Multiple Operational Amplifiers (CNOAS) for N > 2 were generated in an attempt to further extend the operating frequencies at the expense of additional amplifiers. C3OAs were obtained by starting with one of the four proposed C2OAs and replacing one of its single op-amps by any of the four C2OAs shown in Figures 2.1 through 2.4 . Thirty two possible combinations of C3OAs were thus obtained via this technique. From these, six designs proved both theoretically and experimentally to exhibit superior performance and were selected for further testing. These six configurations are illustrated in Figure 2.5 .

Similarily, C4OAs were obtained either by replacing each of the single op-amps in a C2OA with any of the C2OAs or from one of the C3OAs where any single op-amp is replaced by

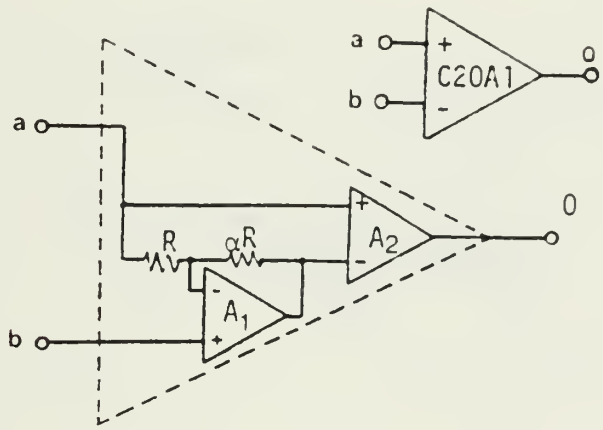

Figure 2.1 C20A-1 Composite Operational Amplifier
[Ref. 12: p. 21]

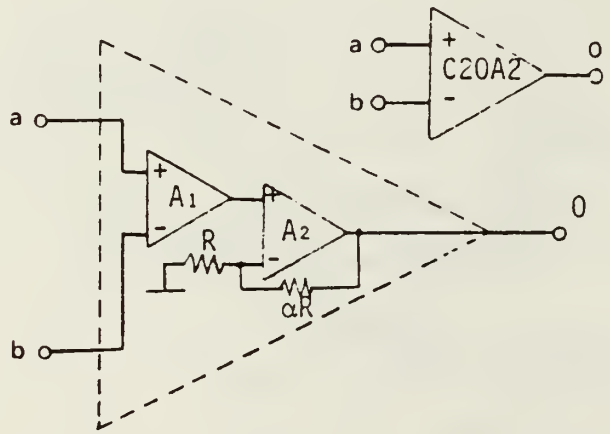

Figure 2.2 C20A-2 Composite Operational Amplifier [Ref. 12: p. 21]

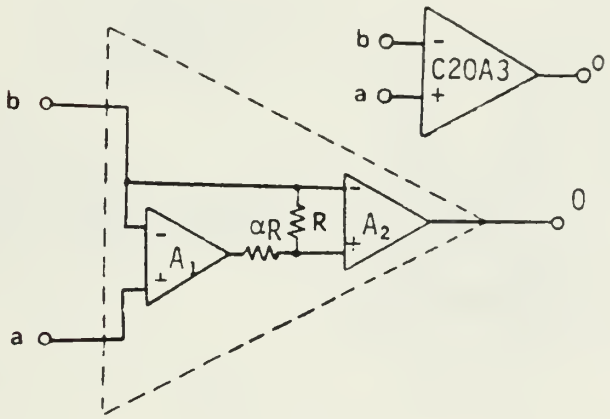

Figure 2.3 C20A-3 Composite Operational Amplifier
[Ref. 12: p. 21]

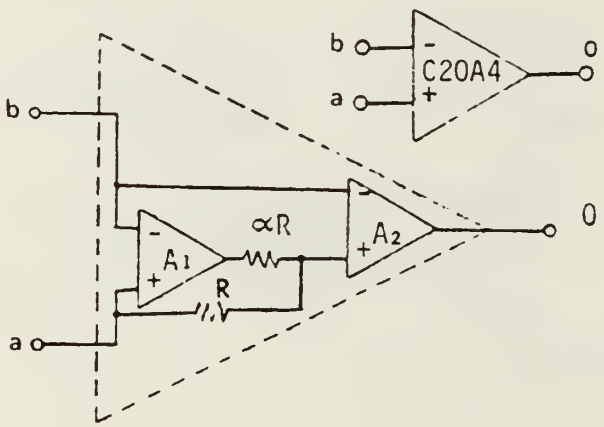

Figure 2.4 C20A-4 Composite Operational Amplifier [Ref. 12: p. 21]

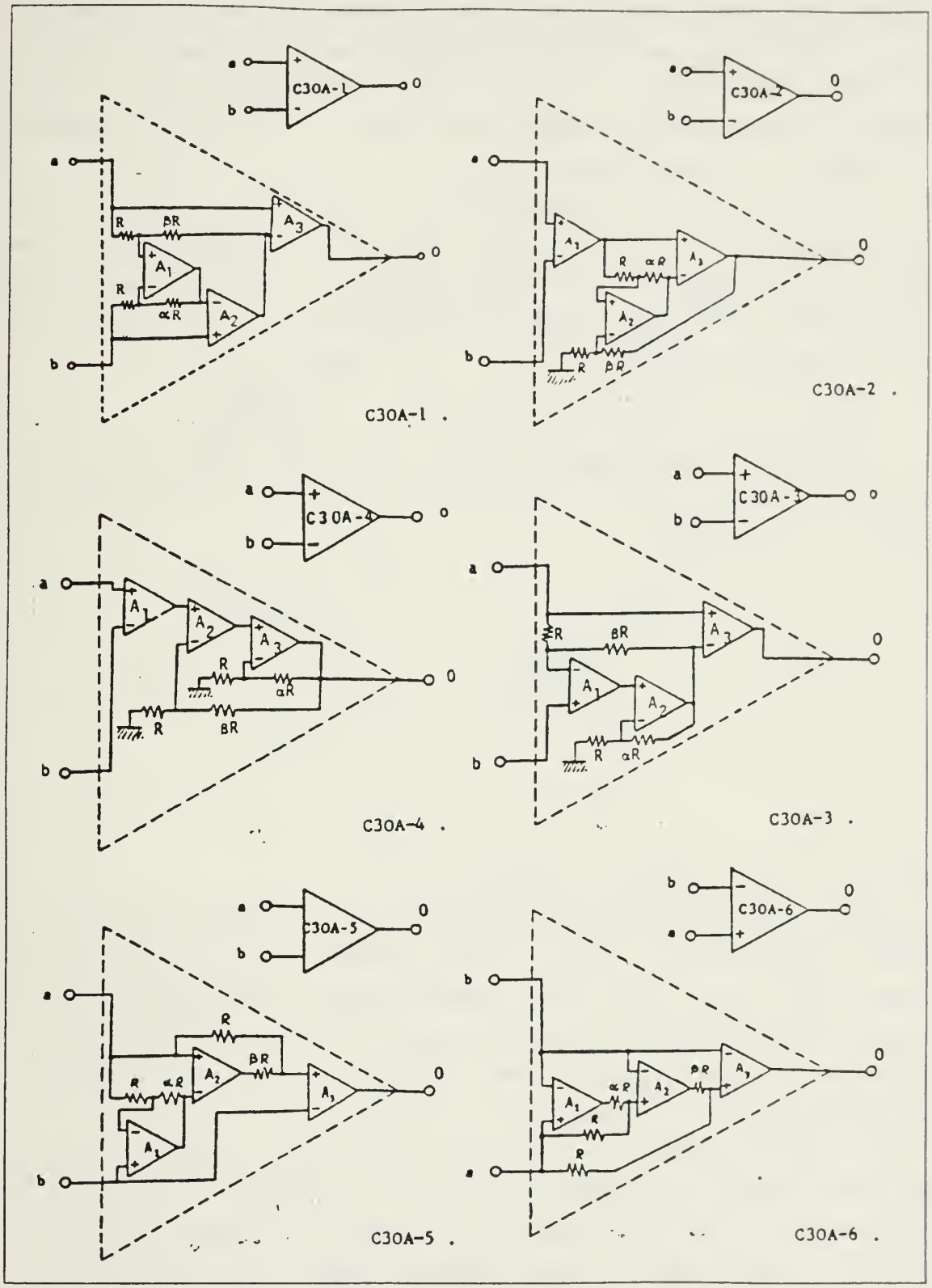

Figure 2.5 C30A Composite Operational Amplifiers [Ref. 12: p. 26]

a C20A. The novel C40As that exhibited superior characteristics, from both theoretical and experimental considerations, are shown in Figure 2.6 The open-loop gain input-output relationships for the C30As and C40As are given in Figures 2.7 and 2.8, respectively.

Although significant potential exists for many of the above composite configurations in various applications, the goal of this thesis, the generation of a fast and accurate operational amplifier, was investigated only as it pertains to the C20As.

B. SINGLE POLE VS TWO POLE ANALYSIS

Assuming a single pole model (Equation 1.14), the open loop gain of the single op-amps employed in a C20A configuration, is given by

$$A_i = \frac{A_{oi}\omega_{Li}}{\omega_{Li} + s} = \frac{\omega_i}{s + \omega_{Li}} \qquad (2.1)$$

where A_{oi}, ω_{Li}, and ω_i are the DC open loop gain, the 3 dB bandwidth, and the GBWP, respectively, of the i-th op-amp. It can be easily shown that the open loop input-output relationships of C20A-1 through C20A-4 are as listed in Figure 2.9 Here, as throughout this thesis, the variable α is the resistor ratio $\alpha R/R$ shown in Figures 2.1 - 2.4

If it is assumed that the two individual op-amps used in the composites are identical, i.e.- $A_{o1} = A_{o2} = A_o$ and $\omega_1 = \omega s'2 = \omega_i$, it is of interest to examine the open loop gains given in Figure 2.9 in the single ended inverting application, that is, $V_a = 0$. For both C20A-1 and C20A-2 the DC gain A_{oc1} is given by

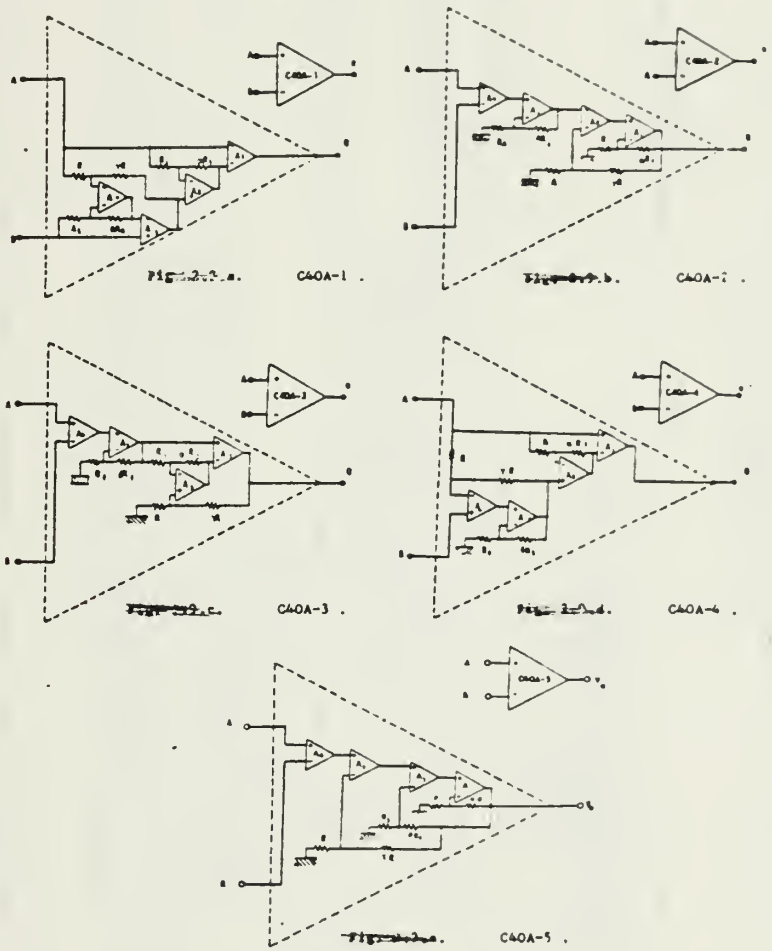

Figure 2.6 C40A Composite Operational Amplifiers [Ref. 12: p. 28]

$C30A_1$	Open Loop Gain Input-Output Relationship
C30A-1	$V_o = \dfrac{V_a[A_1A_2A_3\ (1+\beta) + A_1A_2\ \frac{(1+\beta)}{(1+\alpha)} + A_3\ (1+\beta)] - V_b[A_1A_2A_3\ (1+\beta) + A_2A_3\ (1+\beta)]}{A_1A_2 + \frac{(1+\beta)}{(1+\alpha)}\ A_1 + (1+\beta)}$
C30A-2	$V_o = \dfrac{(V_a - V_b)[A_1A_2A_3\ (1+\beta) + A_1A_3(1+\beta)]}{A_2A_3 + A_3\frac{(1+\beta)}{(1+\alpha)} + (1+\beta)}$
C30A-3	$V_o = \dfrac{V_a[A_1A_2A_3(1+\alpha)(1+\beta)+A_2A_3(1+\beta)+A_3(1+\alpha)(1+\beta)] - V_b[A_1A_2A_3(1+\alpha)(1+\beta)]}{A_1A_2(1+\alpha)+A_2(1+\beta)+(1+\alpha)(1+\beta)}$
C30A-4	$V_o = \dfrac{(V_a - V_b)[A_1A_2A_3(1+\alpha)(1+\beta)]}{A_2A_3(1+\alpha)+A_3(1+\beta)+(1+\alpha)(1+\beta)}$
C30A-5	$V_o = \dfrac{V_a[A_1A_2A_3(1+\alpha)+A_2A_3(1+\alpha)+\beta A_3] - V_b[A_1A_2A_3(1+\alpha)+A_1A_3(1+\beta)+A_3(1+\alpha)(1+\beta)]}{A_1(1+\beta)+(1+\alpha)(1+\beta)}$
C30A-6	$V_o = \dfrac{V_a[A_1A_2A_3+A_2A_3\ \alpha + A_3\ \beta(1+\alpha)] - V_b[A_1A_2A_3+A_2A_3(1+\alpha)+A_3(1+\alpha)(1+\beta)]}{(1+\alpha)(1+\beta)}$

Figure 2.7 C30A Open-Loop Gain Input-Output Relationships

[Ref. 12: p. 27]

C40A	Open Loop Gain Input-Output Relationships
C40A-1	$V_o = -\dfrac{V_a[A^2[(1+\alpha)(1+\beta)(1+\gamma)]+A^2(1+\alpha)[(1+\beta)+(1+\gamma)]+A^2(1+\alpha)(1+\gamma)(2+\beta)+A(1+\alpha)(1+\beta)(1+\gamma)) - V_b(A^2(1+A)(1+\alpha)(1+\beta)(1+\gamma))}{A^2(1+\beta)+A^2[(1+\alpha)(1+\beta)(1+\gamma)]+A(1+\gamma)[(1+\alpha)+(1+\beta)]+(1+\alpha)(1+\beta)(1+\gamma)}$
C40A-2	$V_o = \dfrac{V_a(A^2(1+\beta)(1+\gamma)) - V_b(A^2(1+\beta)(1+\gamma))}{A^2+[\frac{1+\gamma}{1+\alpha}+(1+\beta)]A^2+[(1+\gamma)+\frac{(1+\beta)(1+\gamma)}{1+\alpha}]A+(1+\beta)(1+\gamma)}$
C40A 3	$V_o = \dfrac{V_a(A^2(1+A)(1+\alpha)(1+\beta)(1+\gamma)) - V_b(A^2(1+A)(1+\alpha)(1+\beta)(1+\gamma))}{A^2(1+\alpha)+A^2[(1+\gamma)+(1+\alpha)(1+\beta)]+A(1+\gamma)[(1+\alpha)+(1+\beta)]+(1+\alpha)(1+\beta)(1+\gamma)}$
C40A-4	$V_o = \dfrac{V_a(A^2(1+\alpha)(1+\gamma)+A^2(1+\alpha)[(1+\frac{1+\gamma}{1+\beta})+A^2(1+\alpha)(1+\gamma)[1+\frac{1}{1+\beta}]+A(1+\alpha)(1+\gamma)) - V_b(A^2(1+\alpha)(1+\gamma))}{A^2+[(1+\alpha)+\frac{1+\gamma}{1+\beta}]A^2+(1+\gamma)[1+\frac{1+\alpha}{1+\beta}]A+(1+\gamma)(1+\alpha)}$
C40A-5	$V_o = \dfrac{V_a(A^2(1+\beta)(1+\gamma)) - V_b(A^2(1+\beta)(1+\gamma))}{A^3(1+\beta)+A^2(1+\gamma)+A\frac{(1+\beta)(1+\gamma)}{(1+\alpha)}+(1+\beta)(1+\gamma)}$

Figure 2.8 C40A Open-Loop Gain Input-Output Relationships

[Ref. 12: p. 29]

$$V_{0i} = V_a A_{ai}(s) - V_b A_{bi}(s) \quad (i = 1 \text{ to } 4)$$

for C20A-1:

$$V_{01} = V_a \frac{A_2 (1 + A_1) (1 + \alpha)}{A_1 + (1 + \alpha)} - V_b \frac{A_1 A_2 (1 + \alpha)}{A_1 + (1 + \alpha)}$$

for C20A-2:

$$V_{02} = V_a \frac{A_1 A_2 (1 + \alpha)}{A_2 + (1 + \alpha)} - V_b \frac{A_1 A_2 (1 + \alpha)}{A_2 + (1 + \alpha)}$$

for C20A-3:

$$V_{03} = V_a \frac{A_1 A_2}{(1 + \alpha)} - V_b \frac{A_2 (1 + A_1)}{(1 + \alpha)}$$

for C20A-4:

$$V_{04} = V_a \frac{A_2 (A_1 + \alpha)}{(1 + \alpha)} - V_b \frac{A_2 \{ A_1 + (1 + \alpha) \}}{(1 + \alpha)}$$

where α is the internal resistor ratio

Figure 2.9 C20A Open-Loop Gain Input-Output Relationships

[Ref. 12: p. 31]

$$A_{ocl} = \frac{A_o(1+\alpha)}{1 + (1+\alpha)/A_o} \tilde{=} A_o(1+\alpha) \quad \text{for } (1+\alpha) << A_o \qquad (2.2)$$

Based on the above, these two composites will have a single pole roll-off from (ω_i/A_o) to ($\omega_i/(1+\alpha)$) where the second pole will occur. This equation further implies that the DC gain will increase and the second pole frequency will decrease with increasing α.

Similarily, both C20A-3 and C20A-4 will have a DC gain given by

$$A_{oc2} = \frac{A_o^2}{1 + \alpha} \qquad (2.3)$$

which will have double poles (40 dB/decade) at (w_i/A_o), and will experience a decreasing DC gain without affecting the second pole location, as α increases.

It is important and easy to show that the first op-amp's (A1) output voltage swing for each of the four C20As is always less than the output voltage V_o, since the A1 output is an internal node. Thus, the voltage swing of the output voltage V_o solely determines the dynamic range. Hence, no harmonic distortion or dynamic range reduction of V_o should arise.

Two-pole models were next investigated for each of the configurations C20A-1 through C20A-4 to determine the effects of the internal resistor ratio (α), the composite's overall gain (K), and the individual op-amps unity gain frequencies, on the composite's overall behavior. A sample derivation is shown below for C20A-2.

A nodal analysis of the C20A-2 circuit defined by Figure 2.10 yields the following four equations:

(1) $$V_{out} = A_2 (V_3 - V_1) \qquad (2.4)$$

(2) $$V_3 = A_1 (0 - V_2) = - A_1 V_2 \qquad (2.5)$$

$$\frac{V_2 - V_{in}}{R'} = \frac{V_{out} - V_{in}}{R' (1 + K)} \qquad (2.6)$$

which implies (3) $$V_{out} = (1 + K) V_2 - KV_{in} \qquad (2.7)$$

and $$\frac{(V_1 - 0)}{R} = \frac{V_{out} - 0}{R(1 + \alpha)} \qquad (2.8)$$

which implies (4) $$V_{out} = V_1 (1 + \alpha) \qquad (2.9)$$

Combining Equations 2.4 and 2.5 yields

$$V_{out} = A_2 (-A_1 V_2 - V_1) \qquad (2.10)$$

Substitution of Equation 2.9 into Equation 2.10 yields

$$V_{out} = A_2 (-A_2 V_2 - \frac{V_{out}}{(1 + \alpha)} \qquad (2.11)$$

Substitution of Equation 2.7 into Equation 2.11 yields

$$V_{out} = A_2 \left(-A_1 \left\{ \frac{V_{out} + KV_{in}}{(1 + K)} \right\} - \frac{V_{out}}{(1 + \alpha)} \right) \qquad (2.12)$$

Rearrangement of Equation 2.12 yields

$$\frac{V_{out}}{V_{in}} = \frac{- A_1A_2K(1 + \alpha)}{(1 + K)(1 + \alpha) + A_1A_2(1 + \alpha) + A_2(1 + K)} \qquad (2.13)$$

The general expressions for ideal inverting gain transfer functions are

$$\frac{V_{out}}{V_{in}} = - K \equiv H_i \qquad (2.14)$$

and

$$\frac{V_{out}}{V_{in}} = H_i \left(\frac{1}{1 + s/\omega_p Q_p + s^2/\omega_p^2} \right) \qquad (2.15)$$

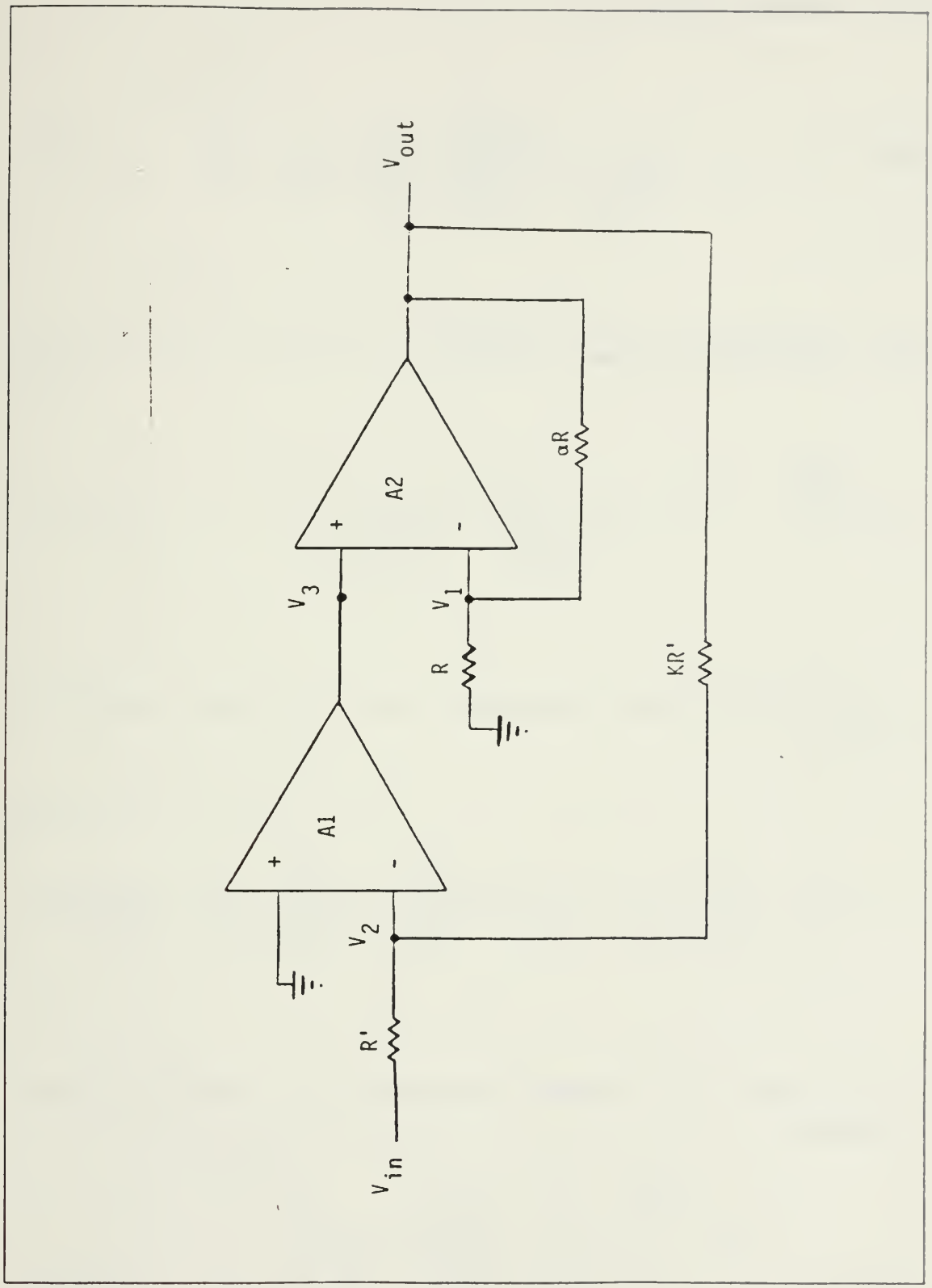

Figure 2.10 C20A-2 Model for Nodal Analysis

Hence, for the C2OA-2:

$$\frac{V_{out}}{V_{in}} = H_i \left\{ \frac{A_1A_2(1 + \alpha)}{(1 + K)(1 + \alpha) + A_1A_2(1 + \alpha) + A_2(1 + K)} \right\} \quad (2.16)$$

which, upon rearrangement, yields

$$\frac{V_{out}}{V_{in}} = H_i \left\{ \frac{1}{1 + \frac{1 + K}{A_1A_2} \quad \frac{1 + K}{A_1(1 + \alpha)}} \right\} \quad (2.17)$$

The general gain expression for a two pole model is given by

$$\frac{1}{A_i} = \frac{1}{A_{oi}} \left\{ 1 + \frac{s}{\omega_{Li}} + \frac{s}{\omega_{hi}} + \frac{s^2}{\omega_{Li}\omega_{hi}} \right\} \quad (2.18)$$

and the open loop frequency response is as shown in Figure 2.11 Hence,

$$A_1 = \frac{A_{o1}}{1 + \frac{s}{\omega_{Li}} + \frac{s}{\omega_{hi}} + \frac{s^2}{\omega_{Li}\omega_{hi}}} \quad (2.19)$$

and $$A_2 = \frac{A_{o2}}{1 + \frac{s}{\omega_{L2}} + \frac{s}{\omega_{h2}} + \frac{s^2}{\omega_{L2}\omega_{h2}}} \qquad (2.20)$$

Substitution of Equations 2.19 and 2.20 into Equation 2.17 yields

$$H = H_i \frac{N}{D} \qquad (2.21)$$

where D =

$$1 + \frac{1 + K}{A_{o1}A_{o2}}\left(1 + \frac{s}{\omega_{L1}} + \frac{s}{\omega_{h1}} + \frac{s^2}{\omega_{L1}\omega_{h1}}\right)\left(1 + \frac{s}{\omega_{L2}} + \frac{s}{\omega_{h2}} + \frac{s^2}{\omega_{L2}\omega_{h2}}\right) \qquad (2.22)$$

$$+ \frac{1 + K}{(1 + \alpha)A_o}\left(1 + \frac{s}{\omega_{L1}} + \frac{s}{\omega_{h1}} + \frac{s^2}{\omega_{L1}\omega_{h1}}\right)$$

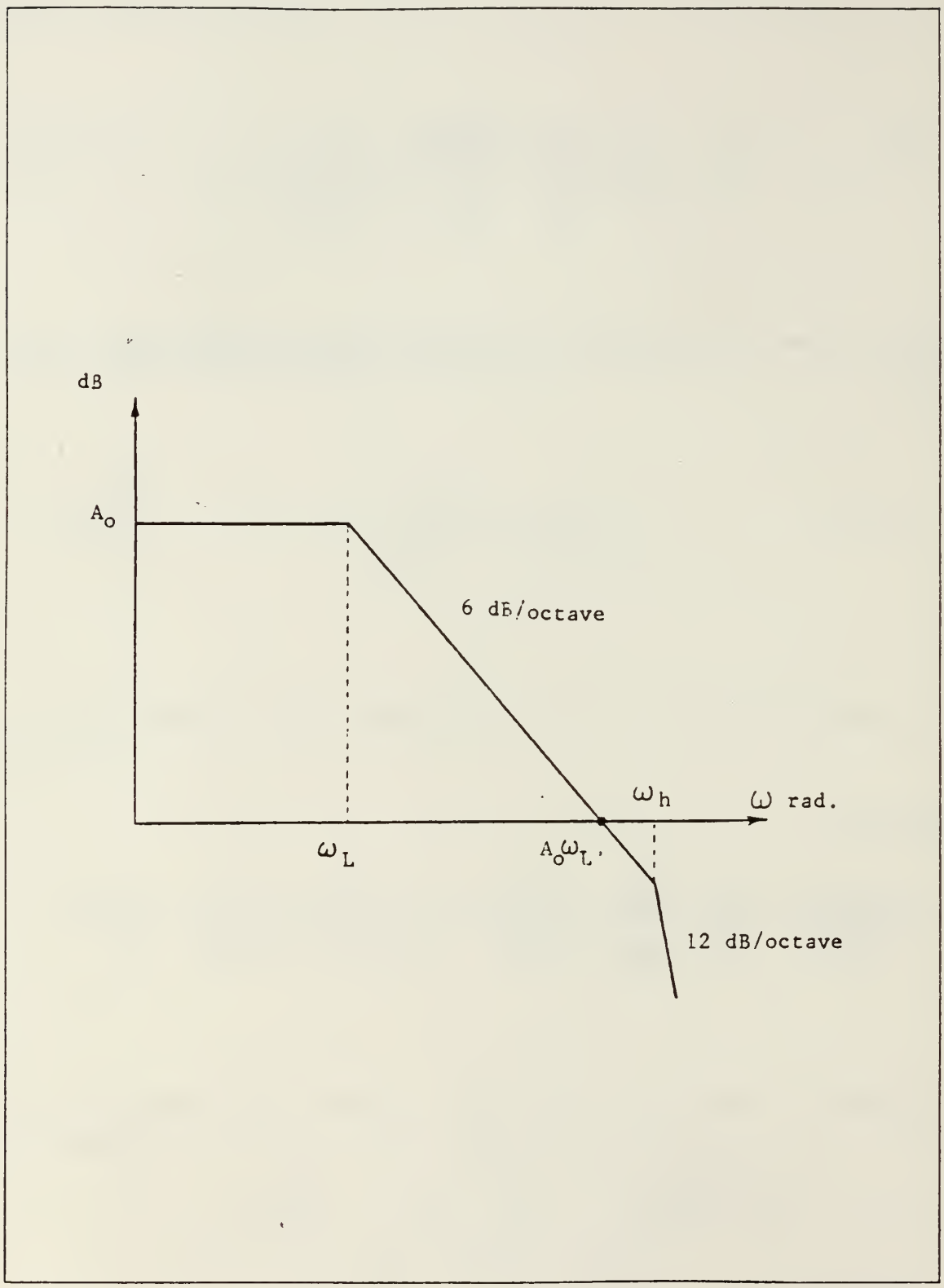

Figure 2.11 Open Loop Frequency Response for a Two Pole Model

With the reasonable assumption that ω_{h1} and ω_{h2} are both much greater than other terms appearing in the preceeding expression, and after considerable simplification:

$$D = 1 + \frac{1 + K}{1 + \alpha}\left(\frac{s}{\omega_1}\right) \frac{1 + K}{\omega_1\omega_2} s^2 \qquad (2.23)$$

where $\omega_1 = A_{o1}\omega_{L1}$ and $\omega_2 = A_{o2}\omega_{L2}$. A comparison of Equation 2.23 with the general expression shown in Equation 2.15 yields

$$\omega_p = \frac{\omega_1\omega_2}{1 + K} \qquad (2.24)$$

and

$$Q_p = \frac{1 + \alpha}{1 + K} \frac{\omega_1}{\omega_2} \qquad (2.25)$$

Equations 2.24 and 2.25 derived above, as well as the results from similar derivations for the other composites are shown in Figure 2.9 . In each case, the actual transfer

function H_a, is equal to the ideal transfer function H_i multiplied by a factor N/D (Equation 2.21). The factor N/D (N=numerator, D=denominator) then determines the amplitude and phase deviation of the actual transfer function from the ideal. The coefficients of the s and s^2 terms of the denominator polynomials, $1/\omega_p Q_p$ and $1/\omega_p 2$, respectively, are the same for each C20A configuration. The fact that none of these coefficients are realized through differences and all are positive ensures the stability of the transfer function and accounts for the low sensitivity of H_a, w_p, and Q_p to other circuit parameters.

The equations of Figure 2.9 then indicate the effects to be expected as one selects different op-amps for the fabrication of any composite(ω_1 and ω_2 altered) as well as differing internal and external resistances (α and K altered). In general, ω_p and Q_p are functions of α and K. It is desirable to select these values such that the resulting ω_p and Q_p will yield acceptable amplitude and phase deviations of the actual transfer function from the ideal and at the same time satisfy any requisite conditions for stability. Via the Routh-Hurwitz stability criterion, the necessary and sufficient conditions for stability can be shown to be:

$$1 + \alpha < \frac{1 + K}{2} \quad \text{for C20A-1 or C20A-2} \qquad (2.26)$$

$$1 + \alpha > (1 + K) \quad \text{for C20A-3} \qquad (2.27)$$

$$1 + \alpha > 4\,(1 + K) \quad \text{for C20A-4} \qquad (2.28)$$

Figure 2.12 indicates the values of α required to yield a $Q_p = 0.707$ and a $Q_p = 1.0$. From both a bandwidth and a stability point of view, C20A-1 and C20A-2 offer more attractive situations over the other two configurations.

In the generation of a finite gain amplifier using a single op-amp, the bandwidth shrinks by an approximate multiplicative factor of 1/K relative to its GBWP, ω_i. An obvious analogy to the C20As for a finite gain amplifier is the cascade of two single op-amp finite gain amplifiers, each with a gain of K, to realize an overall gain of K. Millman [Ref. 13] has shown that in this situation, the resulting bandwidth shrinks by a factor of $0.66/K$ relative to ω_i. For a $Q_p = 0.707$, it is possible to design C20A-1 and C20A-2 circuits such that the bandwidth will shrink only by a factor of approximately $1/K$, and greater than $1/K$ for $Q_p = 1.0$ ($K>>1$). Figure 2.13 compares the achievable bandwidths for these three situations.

The bandwidth extensions achievable in specific C20A configurations are presented in the following chapter. However, Michael [Ref. 12: p. 42], showed that for composites generated from 741's the bandwidth extension to be realized could be varied drastically by merely changing the value of the resistor ratio α (and thus Q_p), without sacrificing the amplifier's low sensitivity to other circuit elements and power supply variations.

$C20A_i$	$1+\alpha$	Q_p	ω_p	Stability Condition for α used
C20A-1 & C20A-2	$\sqrt{1+k}$	1	$\frac{\omega_i}{\sqrt{1+k}}$	Satisfied
	$\sqrt{\frac{1+k}{2}}$	$\frac{1}{\sqrt{2}}$	(independent of α)	Satisfied
C20A-3	0	$Q_{p_{min}} = \sqrt{1+k}$	$\frac{\omega_i}{\sqrt{1+k}}$	Unsatisfied
C20A-4	(1+k)	1	$\frac{\omega_i}{1+k}$	Unsatisfied
	2(1+k)	$\frac{1}{\sqrt{2}}$	$\frac{\omega_i}{\sqrt{2}(1+k)}$	Unsatisfied

Figure 2.12 Values of for Max Flat ($Q_p = 0.707$) and $Q_p = 1.0$

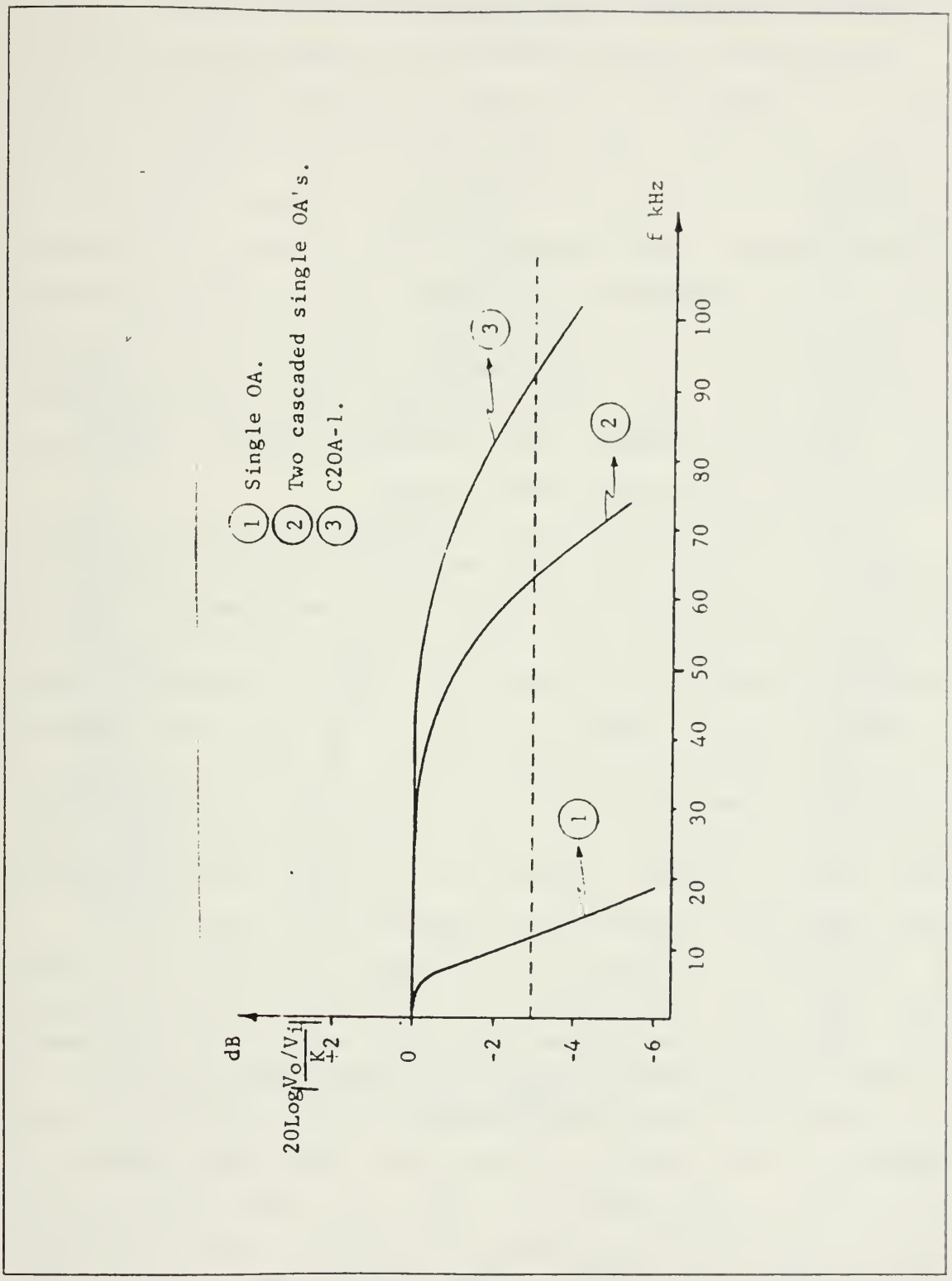

Figure 2.13 Comparison of Bandwdths Achievable From Single Op-Amps, Cascaded Op-Amps, and Composite Op-Amps

[Ref. 12: p. 40]

C. COMPUTER GENERATED FREQUENCY RESPONSE ANALYSIS

The previous section presented an example derivation for C20A-2 to demonstrate the manner in which the finite gain transfer functions, ω_p's, and Q_p's shown in Figure 2.9 were developed. To prove the validity of the assumptions and approximations utilized to develope these equations a computer program (see Appendix A) was written to calculate and plot the frequency responses of the four composite op-amps. Since exact specifications were not available from the manufacturer, the low frequency poles (ω_{Li}) and high frequency poles (ω_{hi}) were estimated from the experimentally determined GBWPs and approximate open loop gains available from the op-amp data sheets.

In the C20A-2 derivation presented, the exact transfer function, utilizing two pole models for each op-amp, was presented as Equations 2.21 and 2.22 . The transfer function assuming a single pole model for each op-amp is that represented by Equations 2.21 and 2.23 . Pairs of equations such as these for each composite were inserted into the computer program to determine what differences (errors), if any, are incurred by assuming single pole behavior of the op-amps. Figures 2.14 through 2.21 show the results obtained where those titled "general expression" indicate the single pole model equations illustrated by Equations 2.21 and 2.23 .

For C20A-1, a comparison of Figures 2.14 and 2.15 indicates that any differences are negligible. The frequency range over which the single pole model accurately represents the behavior of C20A-2, however, is not nearly as large, as may be seen by comparing Figures 2.16 and 2.17 . For this composite, the results indicate that the approximation is only valid to approximately 5 MHz, at which point a non-negligible deviation is noted. For C20A-3, shown in Figures 2.18 and 2.19, and C20A-4, shown in Figures 2.20 and 2.21, the valid ranges are 15 MHz and 10 MHz, respectively.

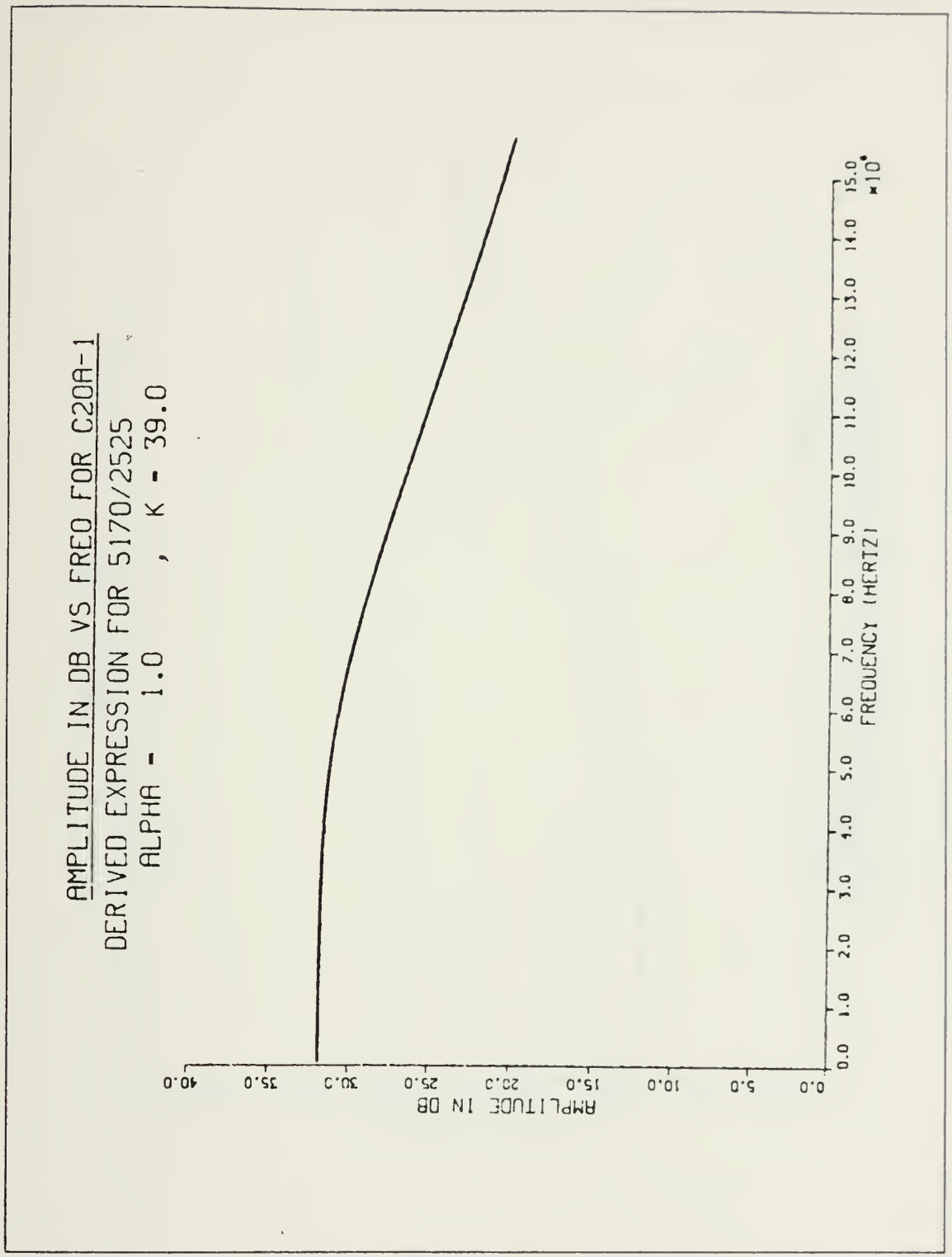

Figure 2.14 Computer Generated Frequency Response of C20A-1 Utilizing a Two Pole Model

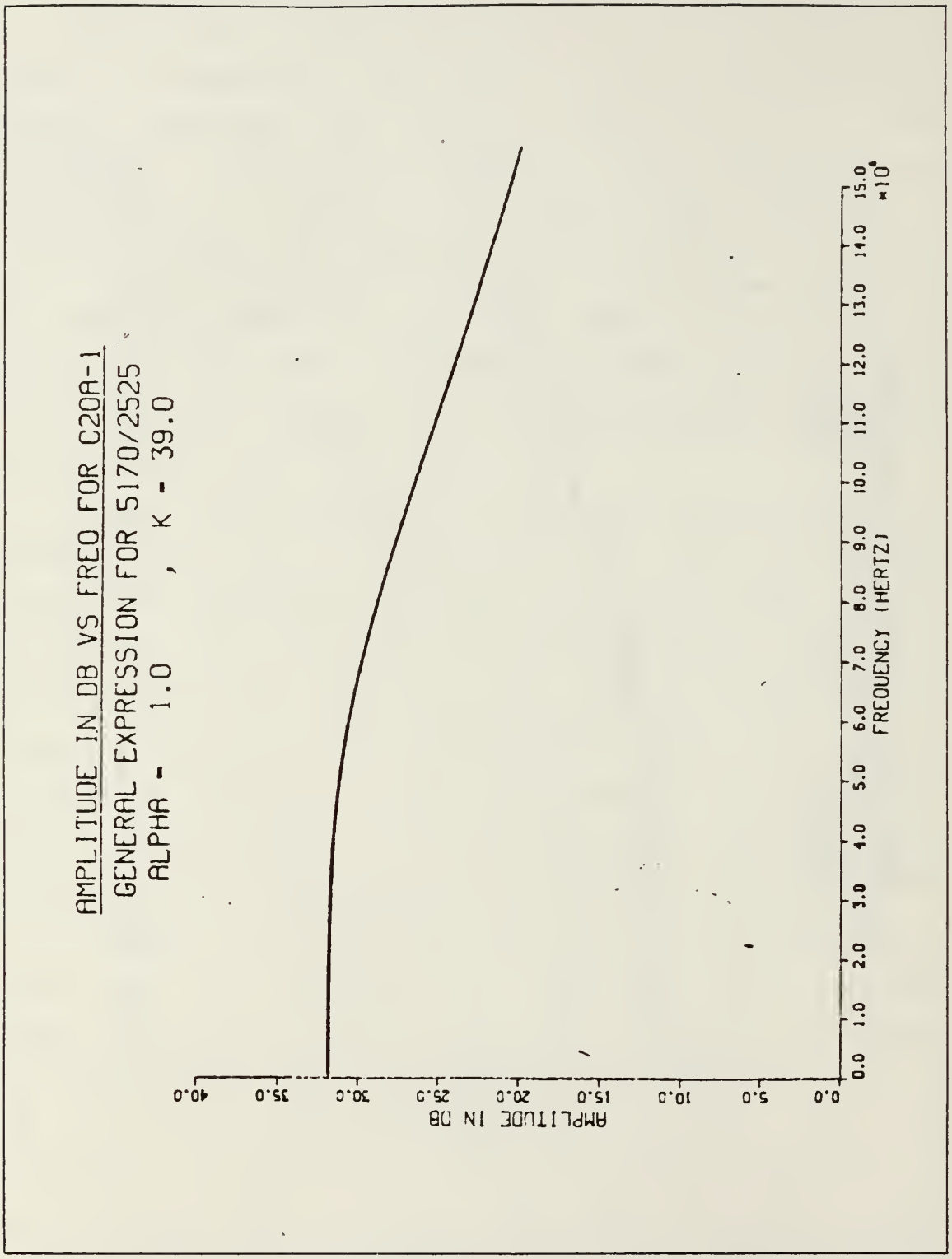

Figure 2.15 Computer Generated Frequency Response of C20A-1 Utilizing a Single Pole Model

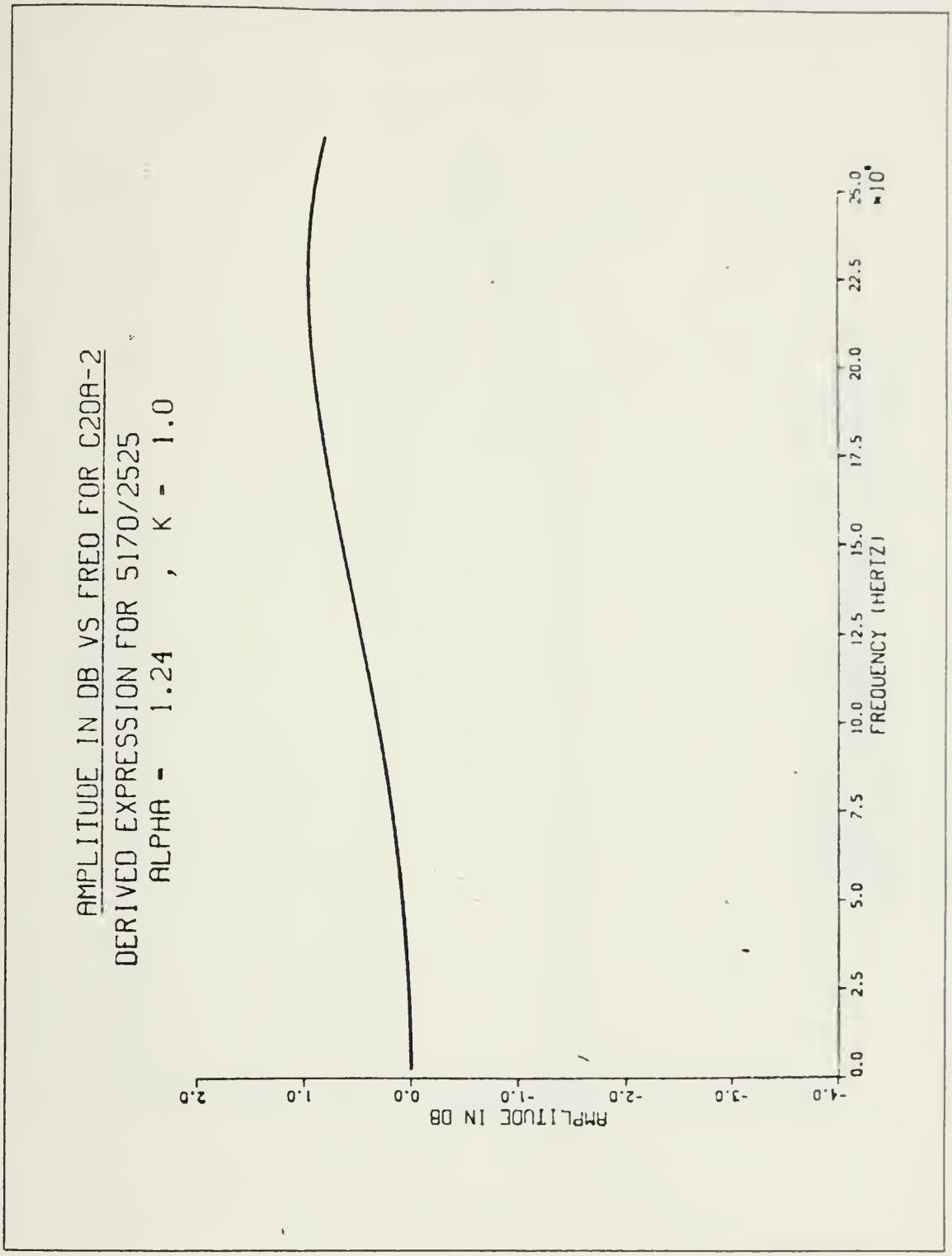

Figure 2.16 Computer Generated Frequency Response of C20A-2 Utilizing a Two Pole Model

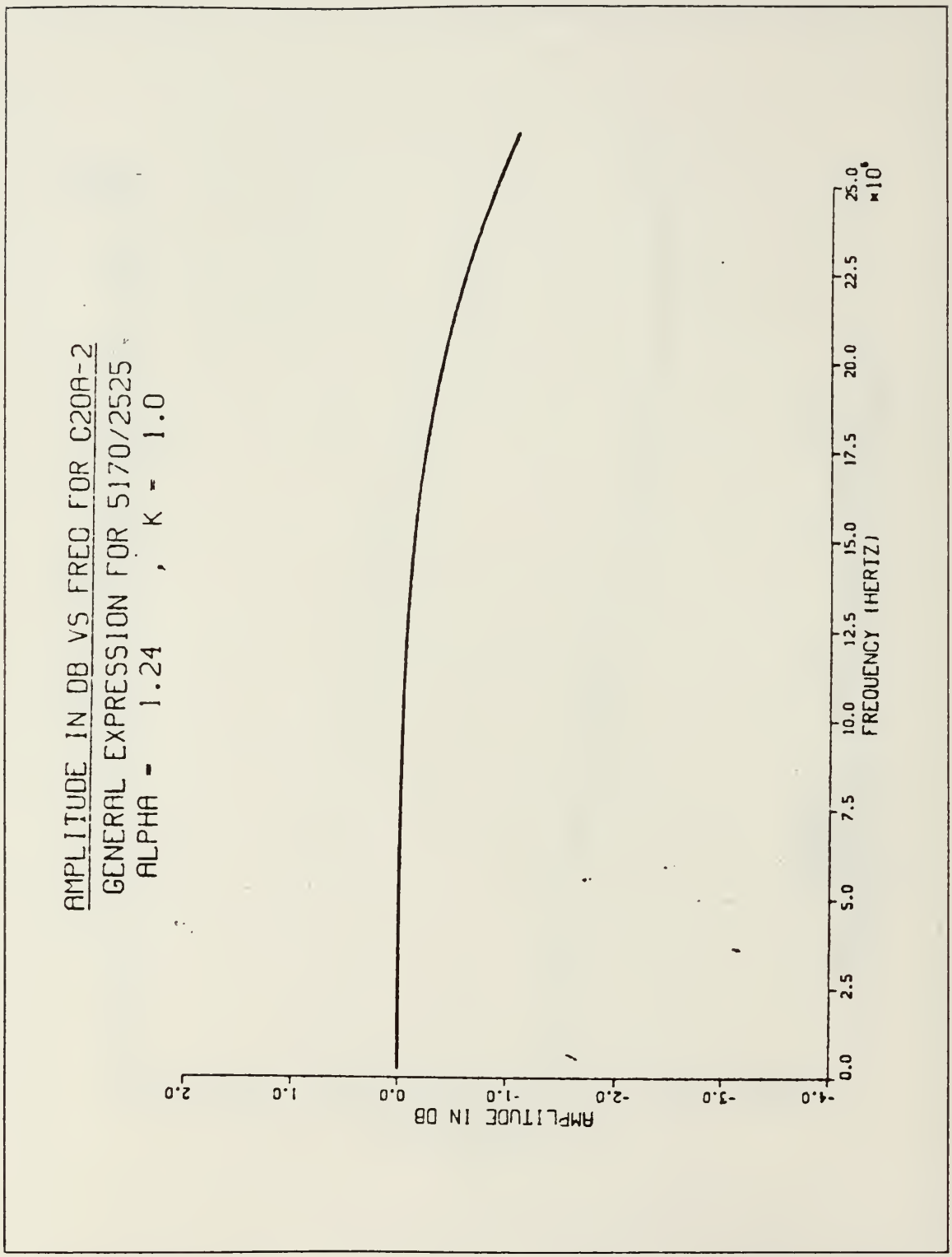

Figure 2.17 Computer Generated Frequency Response of C20A-2 Utilizing a Single Pole Model

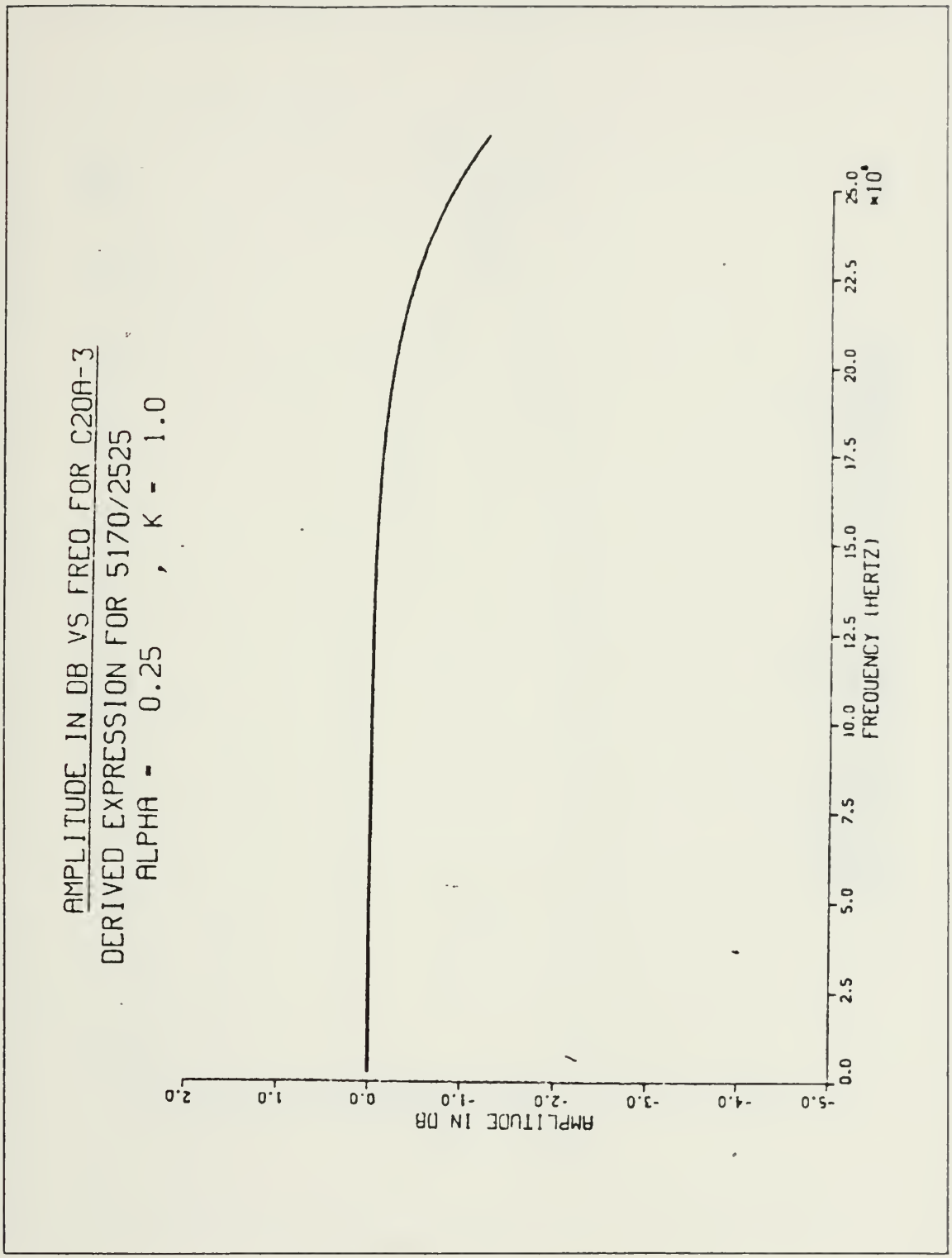

Figure 2.18 Computer Generated Frequency Response of C20A-3 Utilizing a Two Pole Model

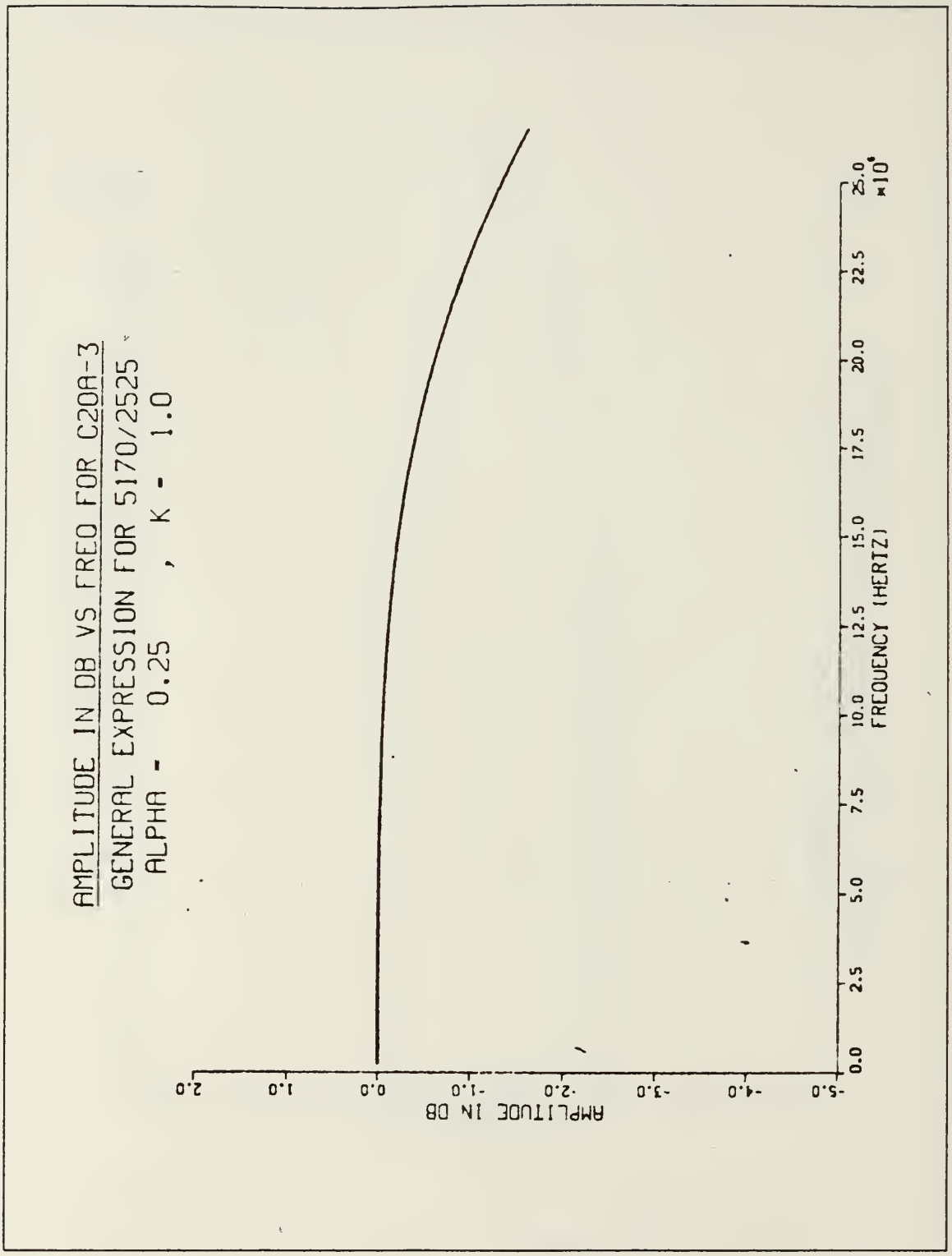

Figure 2.19 Computer Generated Frequency Response of C20A-3 Utilizing a Single Pole Model

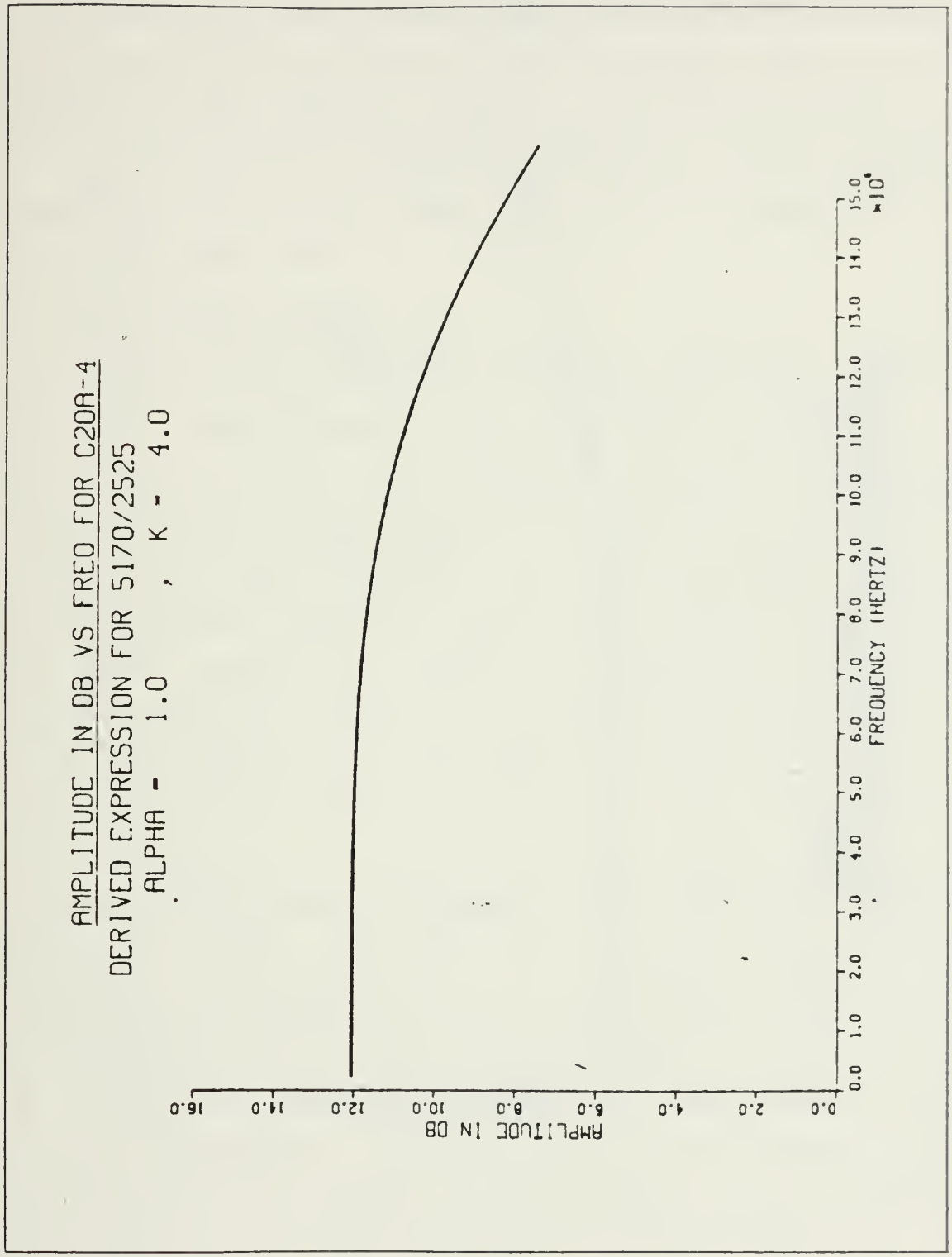

Figure 2.20 Computer Generated Frequency Response of C20A-4 Utilizing a Two Pole Model

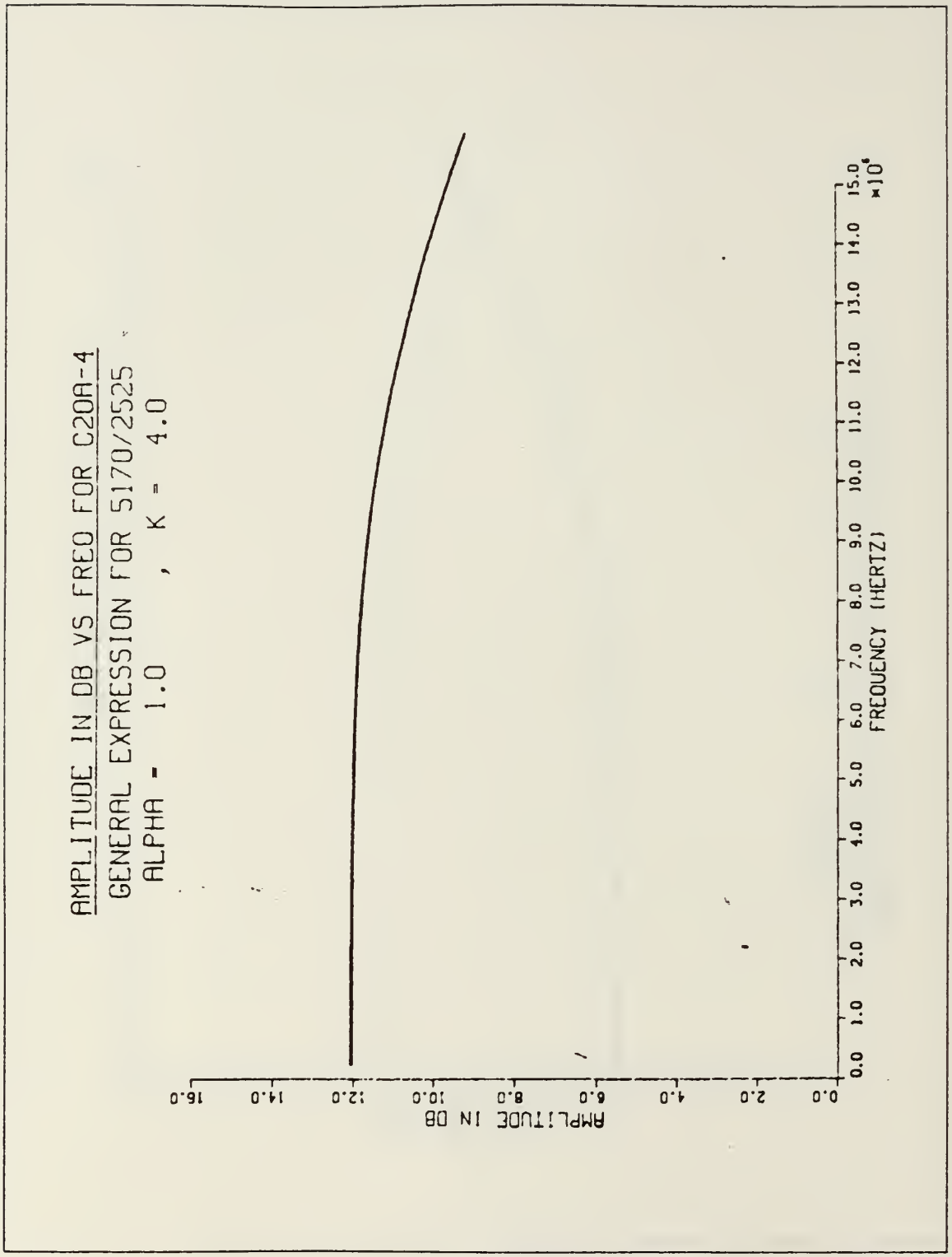

Figure 2.21 Computer Generated Frequency Response of C20A-4 Utilizing a Single Pole Model

In each case, the op-amps used were the HA-5170 in the A1 position and the HA-2525 in the A2 position. The α and K parameters were chosen to yield a maximally flat (Q_p = 0.707) response, as given by the equations listed in Figure 2.9 . These results indicate that the single pole approximation is valid out to quite respectable frequencies for each of the four C2OAs.

D. INPUT OFFSET VOLTAGE

As previously addressed, one very important aspect concerning the performance of an operational amplifier is its input offset voltage, since it places a lower limit on the DC voltage that can be accurately detected and amplified. Because no two op-amps can be produced in an identical fashion, offset voltages must be treated as random parameters, arising from randomly occurring mismatches between pairs of devices utilized in the op-amp's input stage. This then makes calculating offsets a fundamentally different operation than that employed for other common op-amp parameters, since they are best described by a probability distribution with some standard deviation about some mean (ideally zero).

Gray [Ref. 7: pp. 402-407], in this fashion, gives an exhaustive statistical derivation for the input offset voltage of a 741. Even with a circuit of this relative simplicity, the derivation is , by necessity, fraught with assumptions and generalities even though much is known about the specifications of the components used to fabricate the 741. For high performance op-amps then, such as those used in this investigation, a similar effort would be essentially worthless since the op-amp vendors view most of the information required for the derivation as proprietary and not releasable.

In the case of the 741, however, Gray's results were

$$V_{off} = V_T \left[\frac{2}{1 + \frac{I_{c5-6} R_{1-2}}{V_T}} \right] \left[\frac{\Delta I_{s5-6}}{I_{s5-6}} \right] \qquad (2.29)$$

$$- \left[\frac{2 \frac{I_{c5-6} R_{1-2}}{V_T}}{1 + \frac{I_{c5-6} R_{1-2}}{V_T}} \right] \left[\frac{\Delta R_{1-2}}{R_{1-2}} \right]$$

where the notation is relative to that given in Figure 2.22 . This equation demonstrates that the major contributors to the input offset voltage of a 741 are mismatches between transistors Q5 and Q6, Q1 and Q2, Q3 and Q4, resistors R1 and R2, and the Beta values for Q3 and Q4.

Since an exact determination of the input offset voltage from the transistor level appeared unlikely, an effort was made to attempt to predict the input offset voltage that would result given the offset voltages of the op-amps to be used in a given composite. Fortunately, this approach was not as difficult. As an example, the overall input offset voltage of the C20A-3 configuration is obtained as shown below.

From Figure 2.23, Equations 2.30 and 2.31 may be written.

$$V_1 = A_1 V_3 \qquad (2.30)$$

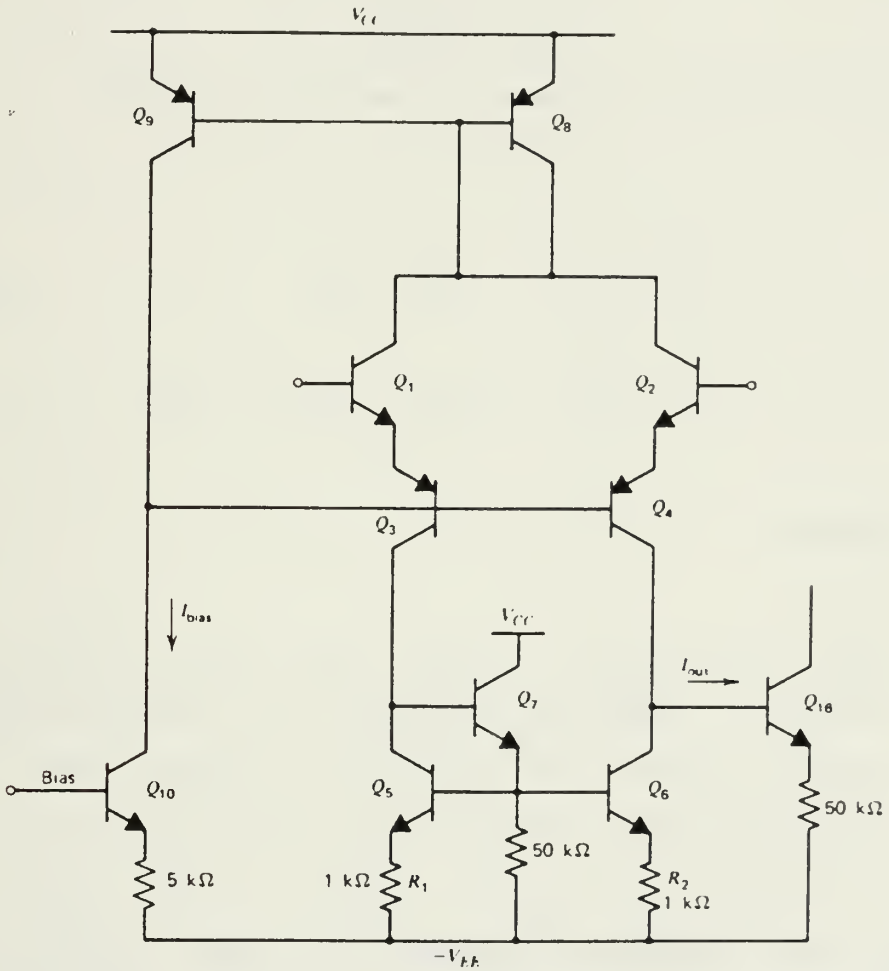

Figure 2.22 Circuit for Calculating the Input Offset Voltage of the 741

$$\frac{V_2 - V_1}{\alpha R} = \frac{V_3 - V_2}{R} \qquad (2.31)$$

Substitution of the latter into the former yields

$$V_2 - A_1 V_3 = \alpha V_3 - \alpha V_2 \qquad (2.32)$$

which implies

$$V_3 = V_2 \frac{1 + \alpha}{A_1 + \alpha} \qquad (2.33)$$

If V_{off2}, the voltage required to offset op-amp A2, is reflected back to the input, then

$$V_3 = V_{off2} \left(\frac{1 + \alpha}{A_1 + \alpha} \right) \qquad (2.34)$$

Since the voltage required to offset op-amp A1 is V_{off1}, the input offset voltage for the composite, V_{off} may be written as

$$V_{off} = V_{off1} + V_{off2} \left(\frac{1 + \alpha}{A_1 + \alpha} \right) \qquad (2.35)$$

or

$$V_{off} = V_{off1} + V_{off2} \left(\frac{1 + \alpha}{A_1} \right) \qquad (2.36)$$

since α << A1.

Similarily, the input offset voltages for the other C20As can be shown to be those illustrated in Figure 2.24 . In each case, except for C20A-1, the portion of the total offset due to the second or A2 op-amp is divided by the open loop gain of the A1 op-amp. This then implies that the overall input offset voltage of the composites is essentially the same as the input offset voltage of the op-amp in the A1 position. The same can also be said for the C20A-1 configuration, given α large.

The significance of these equations is that very accurate composites (low V_{off}) can be generated merely by selecting an op-amp with a very small input offset voltage and placing it in the composite's A1 position.

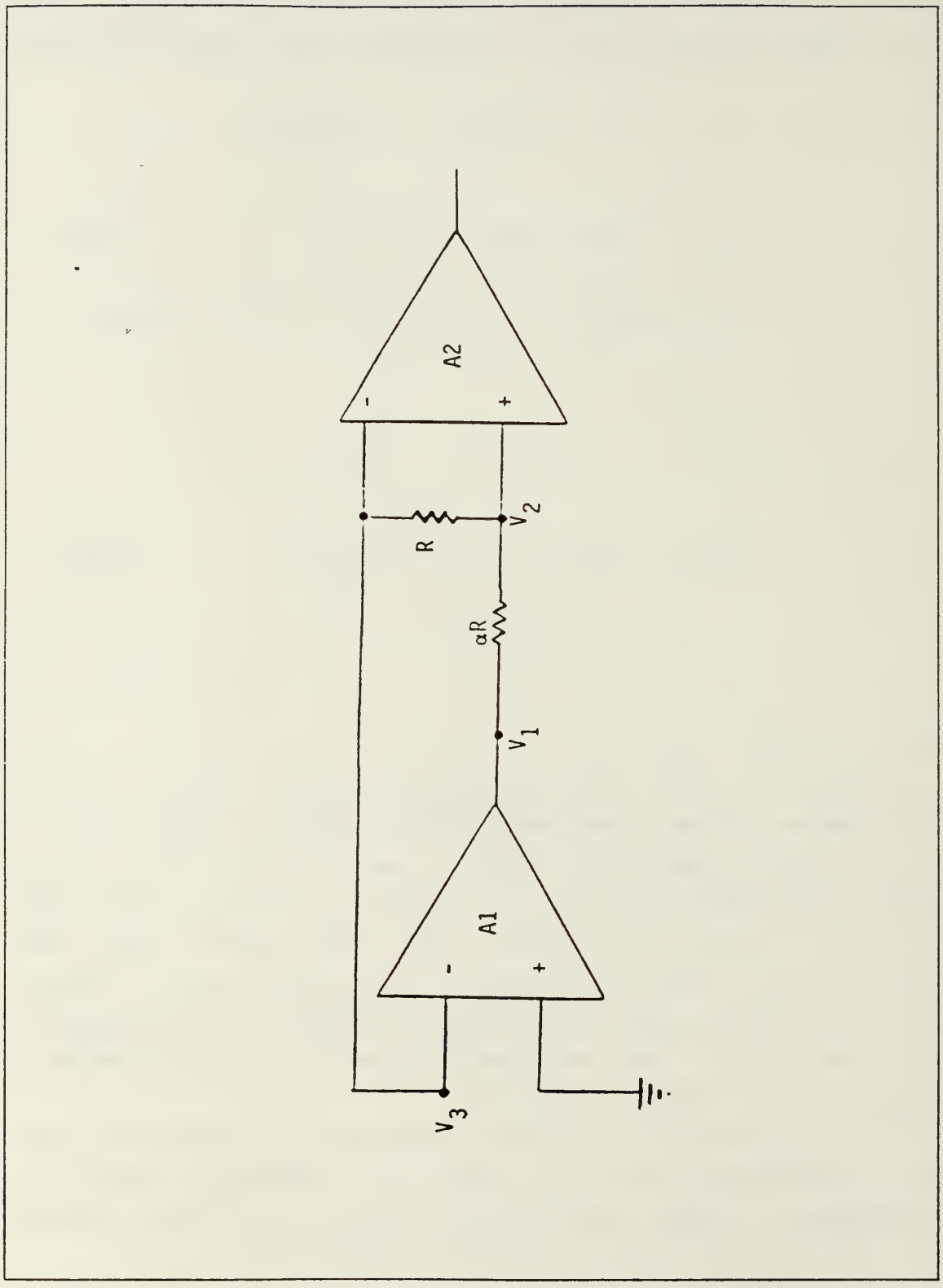

Figure 2.23 Circuit for Calculating the Input Offset Voltage of the C20A-3

C20A-1	$V_{off} \simeq V_{off1} + (V_{off2} / \alpha)$
C20A-2	$V_{off} = V_{off1} + (V_{off2} / A1)$
C20A-3	$V_{off} = V_{off1} + \{ V_{off2} (1 + \alpha) / A1 \}$
C20A-4	$V_{off} = V_{off1} + \{ V_{off2} (1 + \alpha) / A1 \}$

Figure 2.24 C20A Input Offset Voltages

E. SIGNIFICANCE OF THE COMPOSITE APPROACH

As indicated previously, several successful methods exist that greatly improve the slew rate of operational amplifiers. But, with each of these high frequency performance improvements, an unavoidable increase in the input offset voltage resulted. It was envisioned that, owing to the fact that the composite operational amplifier families are tolerant of mismatching of individual op-amp GBWPs, they might provide an excellent opportunity to construct CNOAs tailored to certain specifications. This could be achieved by selecting different and proper op-amps capable of providing the required performance.

In accordance with the theory developed earlier, the use of a precision op-amp that contributes little DC error, in place of the A1 op-amp in any of the C2OAs would provide excellent front-end characteristics for the composite and serve as the controlling component in determining the input offset voltage. Similarily, the selection of a high slew rate, fast settling, and wide bandwidth op-amp in place of the A2 op-amp, would result in a fast output stage.

An analysis of the design described above can easily show that the resulting composite operational amplifier should have almost the same excellent resolution and high accuracy of the precision op-amp used in its front-end. This is true since the effect of the non-precision op-amp used in the output stage would be drastically reduced at the front-end of any of the C2OAs. Similarily, the limitation of the slew rate and bandwidth of the front-end op-amp would have very little effect on the high-speed performance of the resulting composite op-amp. This is also true since it can be easily shown that the voltage swing at the first op-amp (A1) output, which is an internal node in each of the C2OAs, will always be much less than the output voltage swing. Thus , no dynamic range reduction or harmonic distortion should

arise due to the limited power bandwidth of the front-end op-amp and the composite should exhibit a high-speed performance similar to the fast op-amp used in its output stage.

F. CONCLUSIONS

In this chapter, the concept of composite operational amplifiers and a general approach for their generation was presented, thus yielding operational amplifiers that potentially can be very fast, very accurate, while extending the useful operating frequencies of the linear active networks realized by their use. Of all the possible C2OA combinations achievable via this technique, four were shown to satisfy the suggested performance criteria and hence should exhibit superior performance.

Single pole and two pole analyses were performed for the C2OAs. The results of these analyses, as confirmed by computer simulation, indicate that the composite's expected behavior can be effectively modeled by considering that each of its parent op-amps contributes only a single pole instead of two to the composite's overall frequency response. Thus, a considerably simpler analysis may be utilized on networks employing composites.

Theoretical expressions were derived indicating that the input offset voltage exhibited by a composite operational amplifier should approximate that of the parent op-amp occupying its A1 position.

In addition, arguments were introduced expounding the fact that while the A1 op-amp should determine the composite's overall accuracy, the A2 op-amp should determine both the speed and the bandwidth of the composite. The fact that GBWP mismatching is tolerated by the composites allows an accurate, but slow op-amp to be used in the A1 position, with a fast, but less accurate op-amp in the A2 position , to generate an operational amplifier that is both fast and accurate.

III. REALIZATION OF HIGH-SPEED, HIGH-ACCURACY OPERATIONAL AMPLIFIERS

A. EXPERIMENTAL TECHNIQUES

Because one of the goals in this investigation was the maximization of slew rate, it was determined that a standard electronic "bread-board" could not be used due to the stray capacitances added to the circuit at each pin connection. Therefore, a circuit board with no metal connections was utilized in consort with specially designed sockets to formulate a plug-in-module design for each of the four C20As (Figure 3.1). Thus, a degree of standardization was achieved in that for a test on any given configuration, only the op-amps and the four resistors used to determine α and K would possibly be different. In addition, all measurements recorded utilized the same signal generator (HP-3312A), oscilloscope (HP-1741A--100MHz), power supply (Tektronix PS 503A), and probes. The power supply voltages were uniformly set at +15 Volts and -15 Volts, and each was filtered by a capacitor connected to ground.

The C20As were uniformly tested in their inverting configurations as shown in Figures 3.2 through 3.5 . These figures include the pin assignments to correlate them to Figure 3.1 . For all slew rate determinations, the square wave input signal was at a nominal frequency of 1 KHz and its magnitude was adjusted so that the amplified output signal level was 10 V peak-to-peak. Slew rates were determined by measuring the slope of the up-ramp portion of the output square wave, with the horizontal axis (time) expanded as much as practicable, to increase the accuracy of the measurements.

All connecting wires and resistor leads were made as short as possible to minimize any stray capacitances.

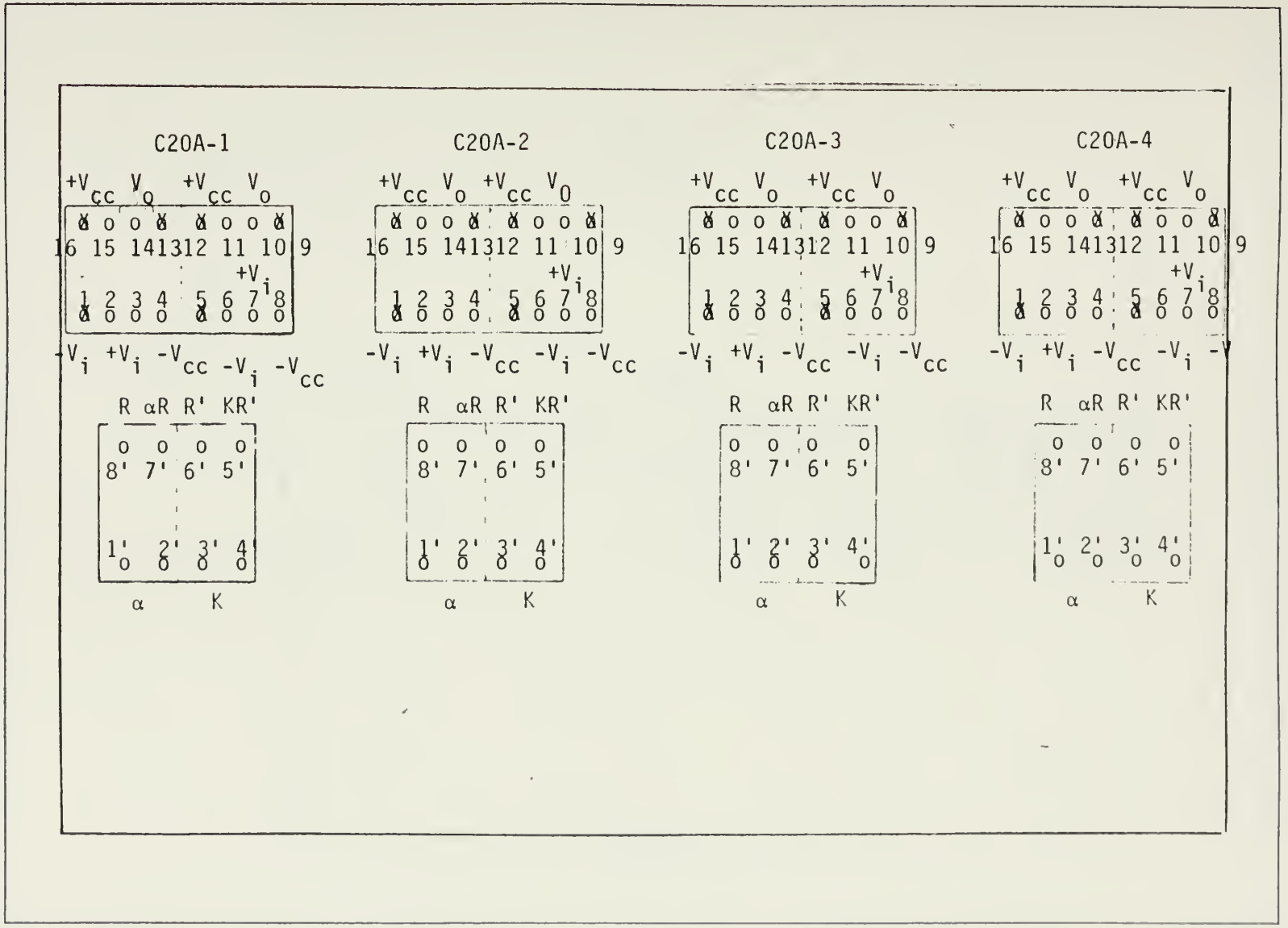

Figure 3.1 Slew Rate Test Board for C20As

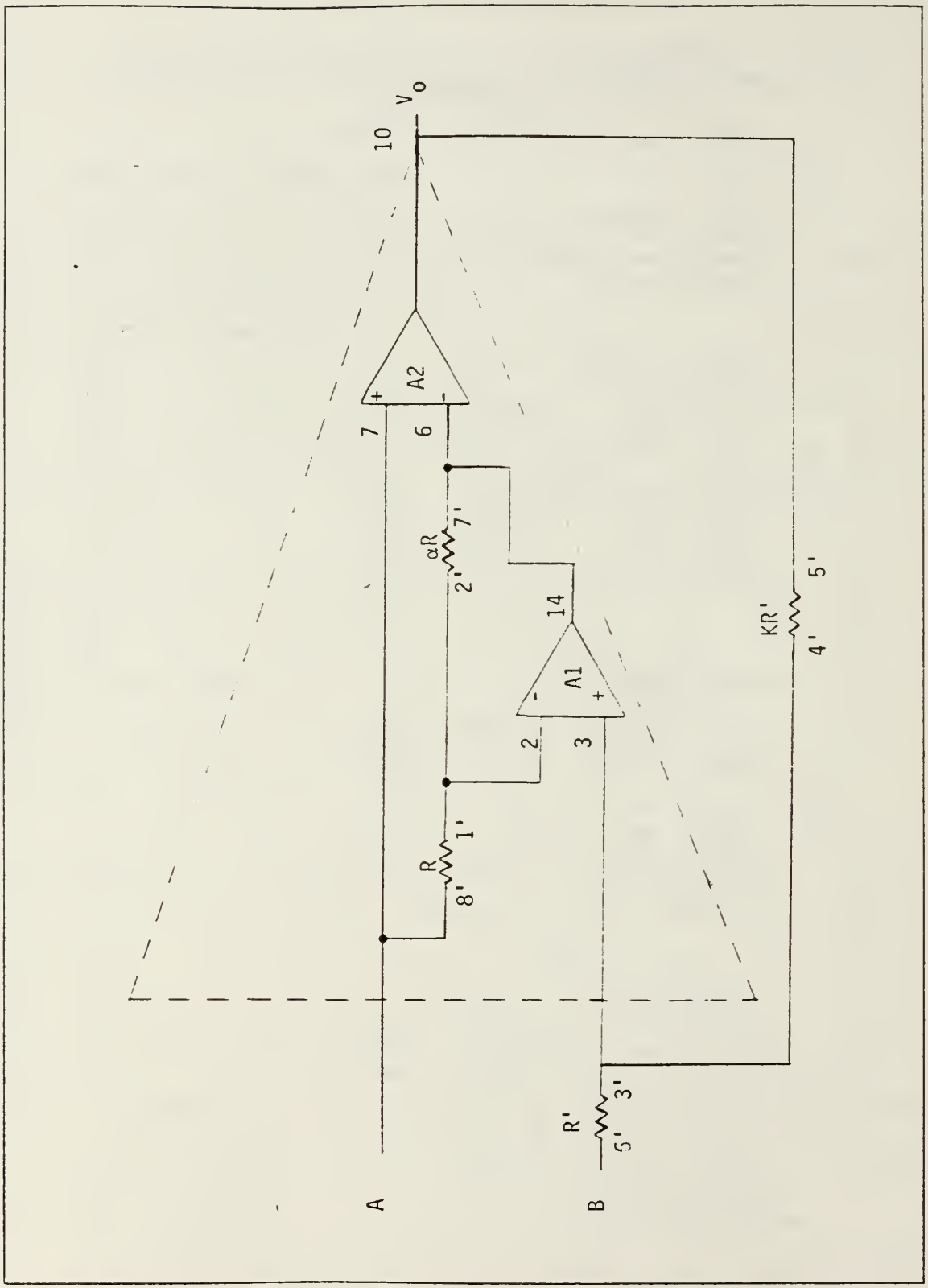

Figure 3.2 C20A-1 Test Configuration

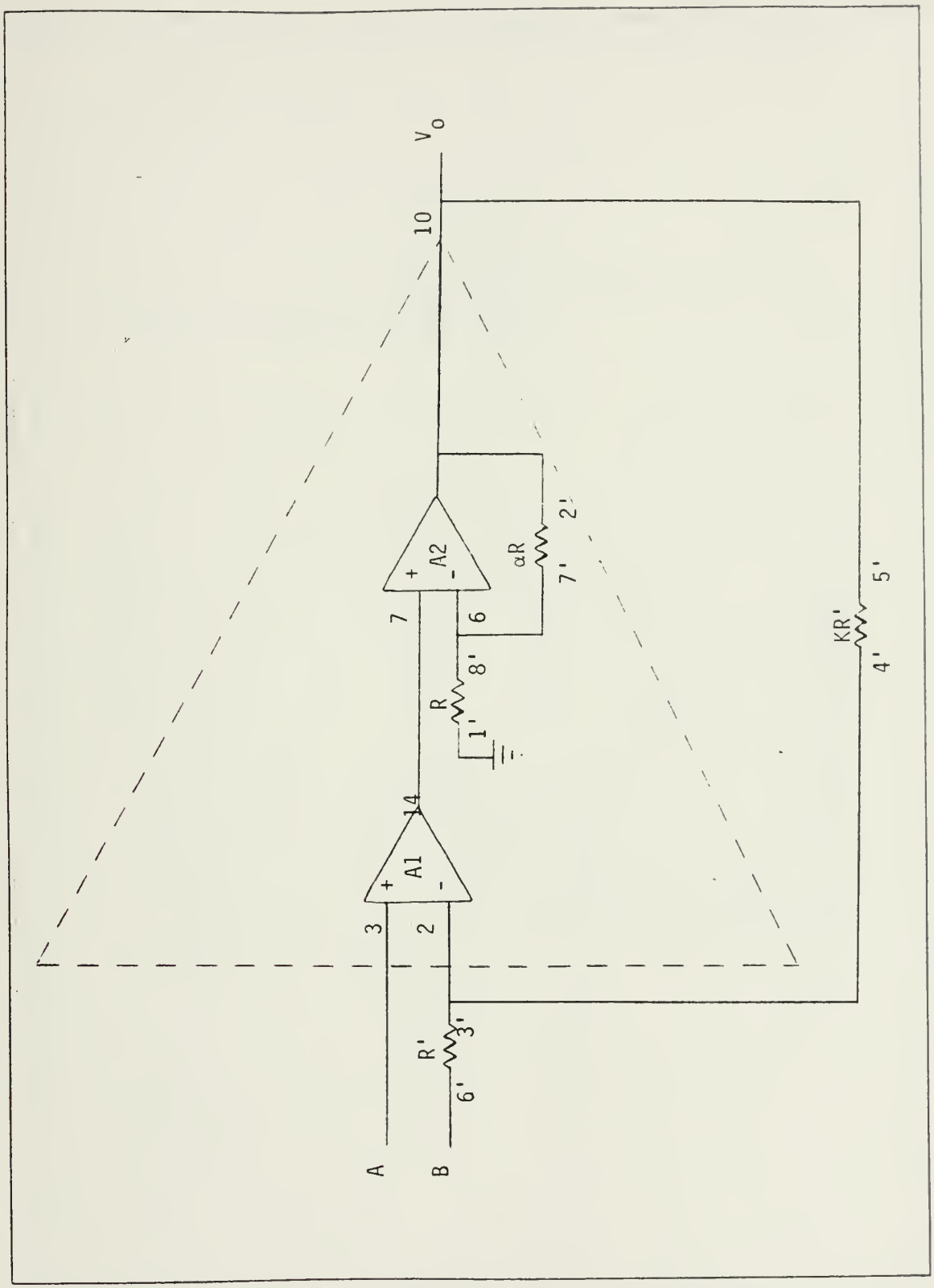

Figure 3.3 C20A-2 Test Configuration

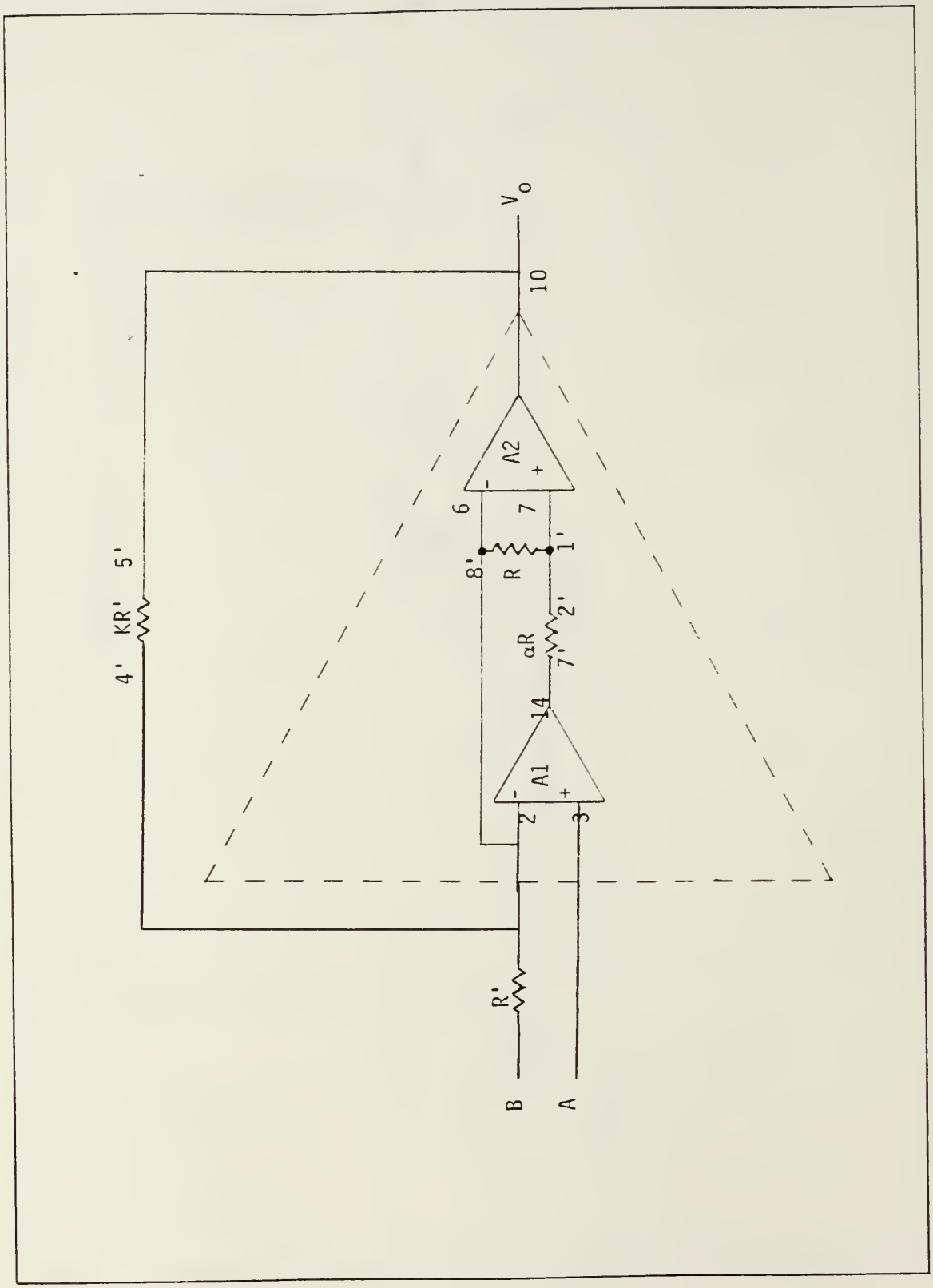

Figure 3.4 C20A-3 Test Configuration

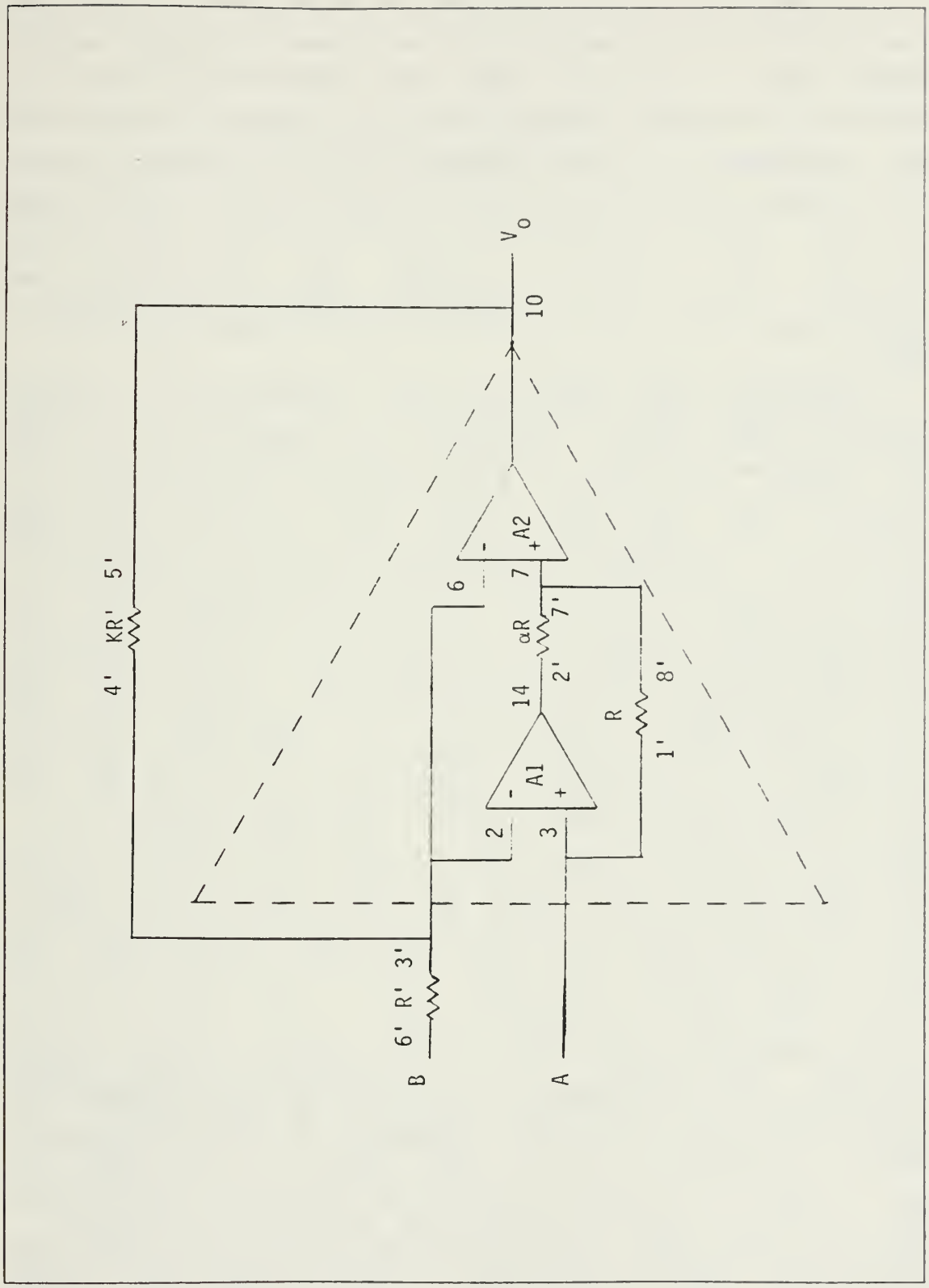

Figure 3.5 C20A-4 Test Configuration

The GBWPs of all op-amps used were measured in the test configuration specified on the data sheets at the recommended gain. A sinusoidal input was applied such that the level of the output sinusoid was 10 V peak-to-peak. The input frequency was then increased until the output signal had dropped to a level of 0.707 times this value. The frequency of the signal was then measured on a Data Precision 5740 frequency counter and this value was multiplied by the circuit gain to arrive at the op-amp's GBWP.

A special test circuit was also constructed for measuring the input offset voltages. This circuit utilized the very accurate HA-5170 in a non-inverting configuration with a gain of 100. The amplifier was made offset free by the addition of an external voltage source, in the manner of Figure 1.2 . The output test voltage was then measured on a Tektronix DM502 digital multi-meter and this raw data was recorded. Such a circuit was necessary due to the extremely small input offset voltages expected to be achieved. For the C20A-2 and C20A-3 configurations, an additional resistor equivalent to the parallel combination of R' and KR' was placed between ground and the non-inverting terminal (A) of the amplifier being tested. Due to time limitations and the fact that the goal was a very fast and very accurate amplifier, input offset voltages were not routinely measured, but rather were measured when the front-end op-amp (A1) was a very accurate one.

All data reported, both for the parent op-amps and the composite configurations, are experimentally determined (single data points) for the individual op-amps reported. In general, performance values were noted to vary among op-amps of the same type. Therefore, the op-amp selected for an application was done to maximize the effect expected to be demonstrated. Thus, the HA2525 (1) was selected for the A2

position of composites since it is faster than HA2525 (2) and maximization of speed was the goal.

Initial investigations were performed with LM741s followed by subsequent trials involving high-performance op-amps, graciously provided by Harris Corporation. The experimentally determined performance factors for all of the op-amps used in this thesis are provided in Figure 3.6 .

B. EXPERIMENTAL RESULTS FOR C2OA-1

The data presented in this section are the experimental results realized for the C2OA-1 configuration illustrated in Figure 3.2 . For C2OA-1, as well as the other three configurations, investigations began with 741s and progressed to the faster Harris op-amps listed in Figure 3.6 . GBWPs were determined only in select cases so that any trends might be illuminated. The feature of bandwidth extension was only of secondary interest since this property of CNOAs has been previously shown and discussed. Offset measurements were made only on the fastest circuits since a very accurate amplifier was only of interest if the op-amp was fast as well. All slew rates (SR) reported have the units $V/\mu S$ and all GBWPs have the units of MHz unless otherwise specified.

Figure 3.7 shows the results when op-amp 741(1) was placed in the A1 position followed by 741(2), thereby creating a situation with the faster of the two op-amps in the output or A2 position. Here it is seen that in every case, the slew rate of the composite exceeds that of the op-amp in the A2 or speed determining position. There appears to be a definite trend that the slew rate increases with increasing α and slightly increases with increasing K. A maximum slew rate enhancement of approximately 26% was achieved (K = 9.67, α = 60.97).

Figure 3.8 shows the results achieved for HA-2505(2) and HA-2505(1)in the A1 and A2 positions, respectively. Here again, with the faster of the two op-amps in the A2

OP-AMP	SLEW RATE (V/μs)	GBWP (MHz)	V_{off}
741 #1	0.847	1.20	
741 #2	0.862	1.61	
741 #3	0.649	1.04	
HA-2505 #1	35.70	13.43	1.52 mV
HA-2505 #2	34.48	12.90	
HA-2525 #1	140.80	23.10	6.68 mV
HA-2525 #2	128.20	21.76	
HA-2539	714.3	436.7	3.0 mV
HA-5170	8.0	4.6	121 μV

Figure 3.6 Experimentally Determined Performance Factors for Op-Amps Used in This Investigation

(A) K = 1.00

ALPHA	1.96	4.11	8.05	15.85	60.97
SLEW RATE	0.93	0.96	1.00	1.00	1.06

(B) K = 2.08

ALPHA	1.00	1.96	4.11	8.05	15.85
SLEW RATE	0.93	0.94	0.98	1.00	1.03

(C) K = 9.67

ALPHA	1.00	1.96	4.10	8.05	15.85	60.97
SLEW RATE	0.97	0.97	0.99	1.01	1.04	1.09

Figure 3.7 Results for C20A-1 Composed of Two 741s

position, the composite exhibits a faster slew rate. The slew rate is observed to increase with increasing α, but no clear pattern regarding a dependence upon K is indicated.

Figure 3.9 shows the results obtained for 741(3) in the A1 position with either the HA-2505(1) or the HA-2525(1) in the A2 position. In both cases the results were quite poor in that the composite's slew rate never approached that of the parent op-amp in the A2 position. This poor behavior is noted when the A1 op-amp is a 741 (while the A2 op-amp is not), thus indicating that perhaps the GBWP mismatch in these situations is too severe. It should be noted, however, that the bandwidth still increased over that of the parent op-amp in the A2 position by as much as a factor of three.

Figure 3.10 reports the results for the combinations HA-2505(1)/HA-2525(1) and HA-2525(2)/HA-2525(1), in the A1 and A2 positions , respectively. Here, slew rates are observed to be on the order of, or greater than, the HA-2525 in the A2 position, with the largest slew rate enhancement again on the order of 25%. Bandwidth extensions by a factor of between two and three were noted as well.

Figure 3.11 shows the results obtained for the HA-5170 in the A1 position with HA-2525(1) in the A2 position. Here, for the first time, a very high accuracy op-amp is utilized as the front-end amplifier. The slew rates observed varied from approximately 2% to 85% of that of the A2 op-amp and again, small GBWP extensions were observed. The striking observation to be made though, is that the input offset voltage of the composite is approximately half that of the very accurate A1 op-amp. This was totally unexpected considering the expression derived for the theoretical input offset voltage (Figure 3.1) in conjunction with α equal to zero. Nevertheless, an amplifier was created whose speed approached that of the parent fast op-amp and exceeded the accuracy of the parent precision op-amp. In this case and

(A) K = 1.00

ALPHA	1.00	1.96
SLEW RATE	38.46	41.67

(B) K = 4.25

ALPHA	1.00	1.96	4.10	8.05
SLEW RATE	35.71	34.48	37.03	38.46

(C) K = 9.72

ALPHA	1.00	2.05	4.10
SLEW RATE	35.71	36.36	37.74

Figure 3.8 Results for C20A-1 Composed of Two HA-2505s

(A)

ALPHA	0.48	1.00	1.96
K	53.9	100.7	222.7
SLEW RATE (V/μs)	14.7	12.5	9.35
GBWP (MHz)	33.9	48.4	79.5

(B)

ALPHA	1.00	0.48	1.00
K	179.0	99.2	87.9
SLEW RATE (V/μs)	14.08	19.61	23.81
GBWP (MHz)	93.5	70.3	64.3

Figure 3.9 Results for C2OA-1: (a) 741(3)/HA-2505(1) (b) 741(3)/HA-2525(1)

(A)

ALPHA = 1.00

K = 12.9

SLEW RATE = 137.9 V/μs

(B)

ALPHA	1.00	4.10	0.48	1.00
K	8.45	53.90	3.98	5.77
SLEW RATE (V/ s)	166.7	85.1	166.7	175.4
GBWP (MHz)	54.4	230.9	54.7	64.9

Figure 3.10 Results for C20A-1: (a) HA-2505/HA-2525 (b) Two HA-2525s

others to follow in which the offset is less than that of the parent A1 op-amp, it is no doubt due to V_{off1} and V_{off2} having opposite signs. Thus a subtractive situation occurs yielding a composite more accurate than the A1 op-amp.

The final C2OA-1 test involved the HA-5170 with the HA-2539, a combination of the most accurate and the fastest op-amps available. Unfortunately, no useable results were obtained. This is perhaps due to the fact that, in this situation, the GBWP mismatch is approximately two orders of magnitude.

C. EXPERIMENTAL RESULTS FOR C2OA-2

Figure 3.12 shows the results when op-amp 741(1) was placed in the A1 position, followed by 741(2) in the A2 position. Clearly the slew rate increases with both α and K. A maximum slew rate enhancement of approximately 12% was achieved.

Figure 3.13 shows the results obtained with either HA-2505(2) or 741(3) in the A1 position while HA-2505(1) occupied the A2 position. Here again, the slew rate appears to increase with both α and K. Few data points were attempted, however, since it did not appear that both a fast and accurate op-amp would be achievable. In addition, for the 741/2505 case, once again the GBWP mismatch is in excess of a factor of ten.

Figure 3.14 shows the results obtained from a combination of HA-2525(2) (A1) with HA-2525(1) (A2) and a combination of HA-5170 (A1) with HA-2525(1) (A2). In the case of the former, high slew rates were not achievable at either low or high values of α and K but was achievable at intermediate values of these variables. However, an increase in the GBWP by approximately a factor of ten was realized. For the latter op-amp combination, an intermediate value for α was selected and applied over a range of gains (K). No dramatic results occured and therefore the offset measurement was not attempted.

ALPHA	1.08	1.08	2.00	0.00	0.00
K	15.06	37.58	34.34	15.06	10.76
SLEW RATE (V/μs)	104.17	48.78	3.23	62.50	117.60
GBWP (MHz)	55.69	29.65	---	---	49.50
OFFSET (μV)	---	---	---	---	60

Figure 3.11 Results for C20A-1 Composed of HA-5170/HA-2525

(A) K = 1.00

ALPHA	1.00	1.96	4.10	8.05	60.98
SLEW RATE	0.80	0.80	0.83	0.87	0.87

(B) K = 2.08

ALPHA	1.00	1.96	4.10	8.05	60.98
SLEW RATE	0.81	0.86	0.88	0.89	0.91

(C) K = 9.67

ALPHA	1.00	1.96	4.10	8.05	15.85
SLEW RATE	0.86	0.89	0.92	0.94	0.96

Figure 3.12 Results for C20A-2 Composed of Two 741s

(A)

ALPHA	1.00	0.00
K	9.72	9.72
SLEW RATE (V/μs)	33.33	29.41

(B)

ALPHA	4.10	8.05	19.00
K	3.25	11.90	11.90
SLEW RATE (V/μs)	3.15	5.13	10.00
GBWP (MHz)	3.8	---	7.4

Figure 3.13 Results for C20A-2: (a) Two HA-2505s (b) 741(3)/HA-2505(1)

(A)

ALPHA	1.00	4.10	8.05	4.76
K	5.34	39.16	126.9	21.27
SLEW RATE (V/μs)	83.30	133.3	58.80	142.9
GBWP (MHz)	---	235.0	262.8	---

(B)

ALPHA	3.92	3.92	3.92
K	9.77	3.68	14.92
SLEW RATE (V/μs)	45.45	71.43	37.04

Figure 3.14 Results for C20A-2: (a) Two HA-2525s (b) HA-5170/HA-2525

When the HA-5170 was combined with the extremely fast HA-2539, no useable results were obtained. Again, this combination is tantamount to a GBWP mismatch of approximately 100.

In general, the same type of trends were observed for the C20A-2 as for the C20A-1, but, in the case of the former, the results were not as dramatic or satisfying in terms of goal achievement.

D. EXPERIMENTAL RESULTS FOR C20A-3

The results obtained for the combination 741(1) and 741(2) in the A1 and A2 positions, respectively, are shown in Figure 3.15 . Although the slew rates still increase with K, these results conflict with earlier trials in that they do not necessarily increase with α.

Attempts to combine an HA-2525 or an HA-5170 with an HA-2539 yielded no useable results.

Figure 3.16 shows the results for the other three op-amp combinations attempted: two HA-2525s, 741(3) with HA-2505(1), and HA-5170 with HA-2525(1). The first two added little to the information base but the combination of the very accurate HA-5170 with the very fast HA-2525 was interesting in that, just as in the C20A-1 case, an op-amp as fast and as accurate as the parents was realized, but for the case of the C20A-3, the GBWP decreased by a considerable amount. The usual tendency is for the slew rate and GBWP to go hand-in-hand.

E. EXPERIMENTAL RESULTS FOR C20A-4

Figure 3.17 shows the results for 741s number two and one in the A1 and A2 positions, respectively. Although a slew rate enhancement is noted for K = 9.72, for this configuration, unlike the other three, the slew rate does not appear to vary at all with α.

(A) K = 1.00

ALPHA	1.00	1.96	4.10	8.05	15.80
SLEW RATE	0.88	0.88	0.89	0.89	0.91

(B) K = 2.08

ALPHA	1.00	1.96	4.10	8.05	15.80
SLEW RATE	0.89	0.89	0.89	0.91	0.91

(C) K = 10.70

ALPHA	1.00	1.96	4.10	8.05	15.80
SLEW RATE	0.96	0.96	0.94	0.92	0.89

Figure 3.15 Results for C20A-3 Composed of Two 741s

(A)

ALPHA	0.00	1.00	1.96	4.10	8.05
K	1.00	1.00	1.00	1.00	1.00
SLEW RATE	31.25	33.25	34.48	32.26	33.33

(B)

ALPHA	1.00	4.10	0.48	1.00	1.00
K	2.20	0.26	3.10	5.34	25.84
SLEW RATE	26.67	21.74	35.70	31.25	2.63
GBWP	3.10	0.34	4.10	4.00	1.81

(C)

ALPHA	0.43	0.43	0.43
K	2.71	4.77	1.82
SLEW RATE	133.3	100.0	142.8
GBWP	11.58	---	10.41
OFFSET	---	---	123 μV

Figure 3.16 Results for C20A-3: (a) Two HA-2505s
(b) 741/HA-2505
(c) HA-5170/HA-2525

(A) K = 1.00

ALPHA	1.00	1.96	4.10	8.05	15.80
SLEW RATE	0.88	0.86	0.86	0.86	0.86

(B) K = 2.08

ALPHA	1.00	1.96	4.10	8.05	15.80
SLEW RATE	0.89	0.89	0.89	0.89	0.89

(C) K = 9.72

ALPHA	1.00	1.96	4.10	8.05	15.80
SLEW RATE	0.96	0.96	0.96	0.96	0.96

Figure 3.17 Results for C20A-4 Composed of Two 741s

Figure 3.18 shows the results for the 2505(2)/2505(1) combination as well as the 741(3)/2505(1) combination. In the former case, the slew rate remained approximately constant or decreased with increasing α, depending on the value of K selected. For the 741/2505 combination, the values obtained for both slew rate and GBWP were disappointingly poor.

Figure 3.19 shows the results for the combinations HA-2525(2)/HA-2525(1), HA-5170/HA-2525(1), and HA-5170/HA-2539. For the first combination, slew rate enhancements of approximately 15% were noted as well as GBWP extensions of 30 - 60%. For the 5170/2525 combination, slew rate enhancements up to 10% were noted as well as a 50% extension of the GBWP. This particular configuration, with α = 3.29 and K = 11.26, yielded the most accurate composite yet, with an input offset voltage of only 53 μV. This marks the second occurrence wherein a composite was generated with an accuracy substantially superior to the parent op-amp in the A1 position. The last configuration, utilizing a 5170 and a 2539, is the first composite with the 2539 in the A2 position where very high slew rates were achieved.

Figure 3.20 shows the final results for the C20A-4 configuration. Included are the 2525(1)/2539 combination and the 2525(1)/5170 combination where, as throughout the results, the amplifier in the A1 position is listed first. The first case is important in that it resulted in the largest slew rate ever recorded, 714.2 V/μS, which equals that of the parent HA-2539. The second combination is very important in that it demonstrates the validity of the theory previously developed. That is, with the 2525 in the A1 position, the input offset voltage of the composite should approximately equal that of the 2525. With the 5170 in the A2 position, the composite should exhibit a slew rate approximately that of the 5170. This, in conjunction with

(A) K = 1.00

ALPHA	1.00	4.10	15.80
SLEW RATE	33.33	33.33	33.33

(B) K = 19.1

ALPHA	15.80	40.20	61.0	73.17
SLEW RATE	33.33	29.41	27.03	25.64

(C)

ALPHA	1.00	4.10	0.48	1.00	1.00
K	11.80	31.50	8.49	25.84	99.24
SLEW RATE	2.56	1.45	3.12	1.67	1.11
GBWP	1.34	2.42	1.52	1.62	3.68

Figure 3.18 Results for C20A-4: (a) Two HA-2505s (b) 741/HA-2505

(A)

ALPHA	4.80	8.05	18.94	4.80
K	2.95	5.34	12.52	6.70
SLEW RATE	166.7	166.7	100.0	160.0
GBWP	33.72	33.08	30.35	36.92

(B)

ALPHA	3.29	3.29	3.29	3.29	3.29
K	410.0	85.4	59.7	11.26	7.13
SLEW RATE	100.0	27.02	32.25	142.9	153.85
GBWP	---	---	---	35.04	---
OFFSET	---	---	---	53 μV	---

(C)

ALPHA	9.90	9.90	4.95
K	4.10	8.0	7.0
SLEW RATE	571.0	444.4	555.5

Figure 3.19 Results for C20A-4: (a) Two HA-2525s, (b) HA-5170/HA-2525 (c) HA-5170/HA-2539

Figure 3.19, which is the same except that the op-amp positions are reversed, demonstrates conclusively that the composite should exhibit an offset approximately equal to that of the op-amp in the A1 position, as well as a slew rate approximately equal to that of the amplifier in the A2 position.

F. CONCLUSIONS

This chapter briefly discussed the techniques utilized in this investigation and presented the experimental results achieved for each of the C20As using a variety of op-amps. In general, slew rates appear to increase with increasing α, whereas the value of K is not a prime contributor to slew rate enhancement.

In situations where the GBWP mismatch was greater than a factor of ten, all configurations, except for C20A-4, fail to generate fast composites. GBWP extensions were noted in most trial combinations although they varied very small increases up to one order of magnitude. This maximum bandwidth extension was achieved with C20A-2, and except for this one bright spot, the C20A-2 did not fair well.

C20A-4 seems to tolerate GBWP mismatch much better than the other configurations. It is the only one where useable results were obtained when using the very fast HA-2539. This confiuration also produced the most accurate composite, with an input offset voltage of 53 μV, and the fastest composite, with slew rate of 714.2 V/μS.

The results for the C20A-4 combinations of 5170/2525 and 2525/5170 proved conclusively the theory expounded in the previous chapter, indicating that a composite's input offset voltage will be determined by the A1 op-amp, while its slew rate and GBWP will be determined by the op-amp in the A2 position.

C20A-1, C20A-3, and C20A-4, using the 5170/2525 combination, all produced composites whose accuracies and slew

(A)

ALPHA	1.00	1.00	1.00	1.94	1.94	4.95	4.95	9.90
K	6.90	24.4	3.70	3.70	24.2	2.75	24.5	4.80
SLEW RATE	480.0	222.2	571.4	625.0	180.0	714.2	100.0	666.7

(B)

ALPHA = 19.50

K = 2.07

SLEW RATE = 6.20

OFFSET = 6.7 mV

Figure 3.20 Results for C20A-4: (a) HA-2525/HA-2539 (b) HA-2525/HA-5170

rates were on the order of, or better than, their parent op-amps, thus generating composite operational amplifiers that were both very fast and very accurate.

IV. APPLICATIONS OF PRECISION, HIGH SLEW RATE OPERATIONAL AMPLIFIERS IN ACTIVE NETWORKS

A. INTRODUCTION

Based on the results presented in the previous chapter, the op-amps selected for the applications to be addressed in this chapter are the HA-5170 (SR = 8.0 V/μs, V_{off} = 121 μV, GBWP = 4.6 MHz) and the HA-2525 (SR = 140.8 V/μs, V_{off} = 6.7 mV, GBWP = 23.1 MHz). The use of the former as the front-end op-amp results in a composite with accuracies comparable to the 5170, while the use of the 2525 as the output op-amp provides the composite with a speed on the same order of magnitude and a higher GBWP.

Three sample applications have been selected for presentation in this chapter to illustrate the utility and value of the C20As in active networks. They are a square wave generator, an improved version of a precision half-wave rectifier, and a novel sample and hold circuit design.

B. SQUARE WAVE GENERATOR

Figure 4.1 shows the square wave generator circuit constructed for this investigation of a non-linear op-amp application. Figure 4.2 shows the circuit's output when an LM741 is used as the op-amp. The input frequency used was only 150 Hz, as higher frequencies yielded an even more drastic deviation from the desired square wave output.

Figure 4.3 shows the output obtained when the op-amp used was the HA-2525. The input frequency used to generate this output was 312 KHz. Further increase of the input frequency, as in the case of the 741, produced what was considered as unacceptable distortion.

Figure 4.4 shows the results achievable when a composite op-amp is utilized. Here the C20A-4 configuration was used

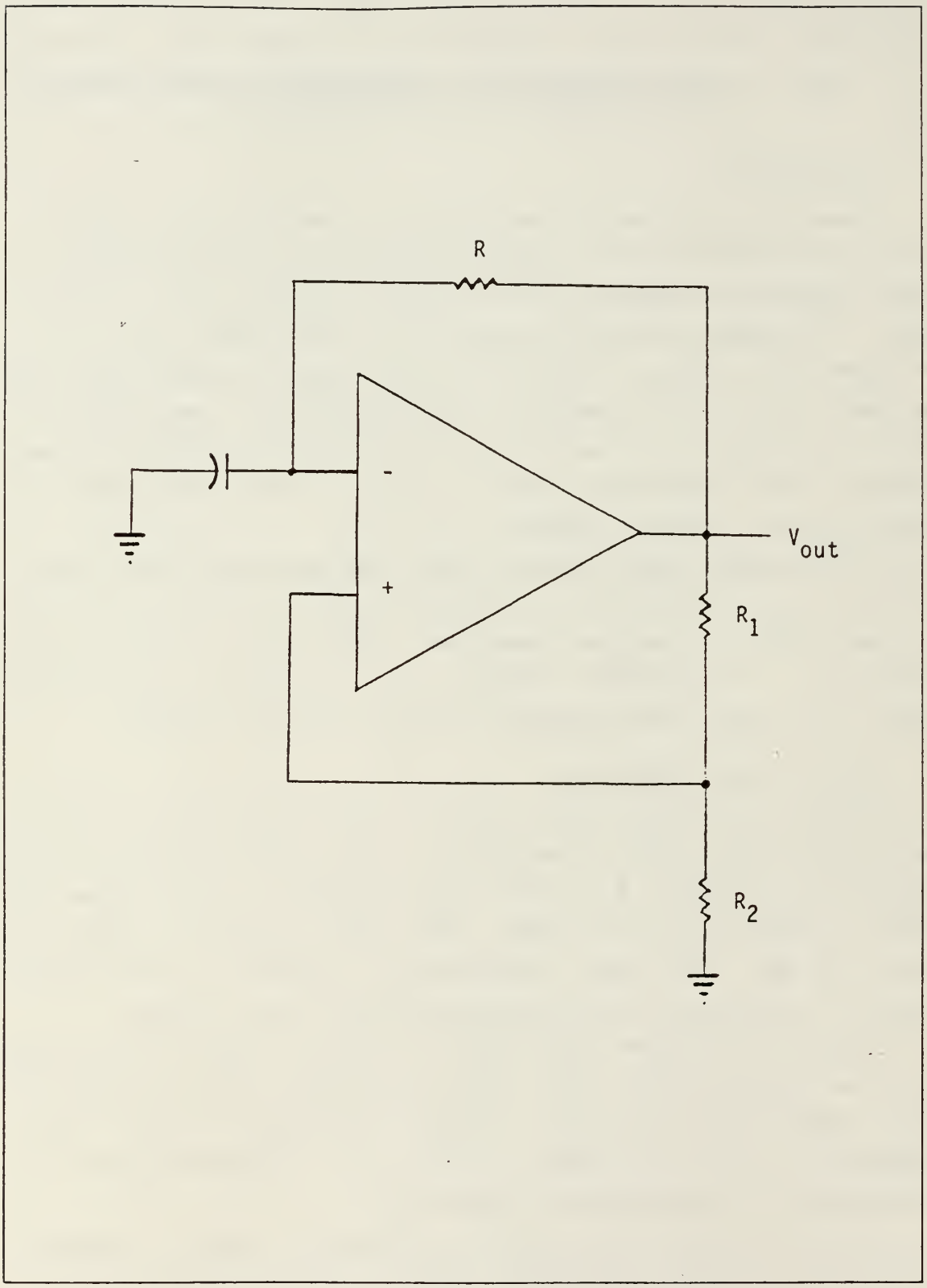

Figure 4.1 Square Wave Generator Circuit

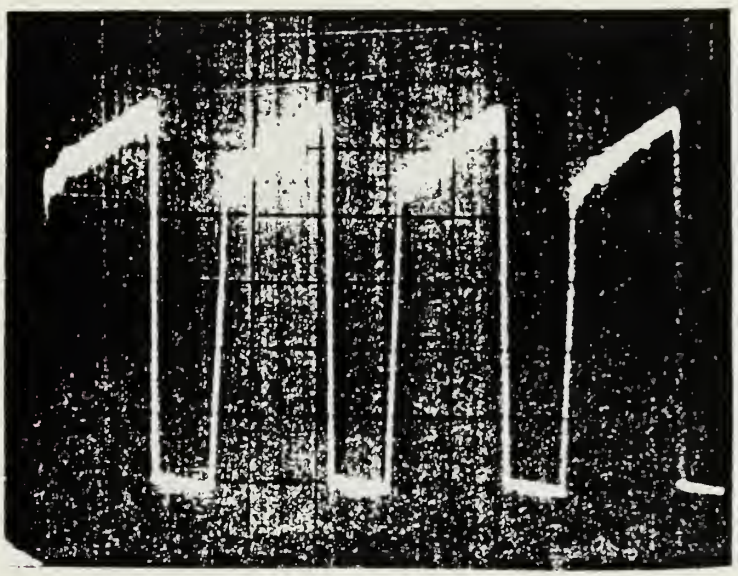

Figure 4.2 Output of a Square Wave Circuit Using an LM741

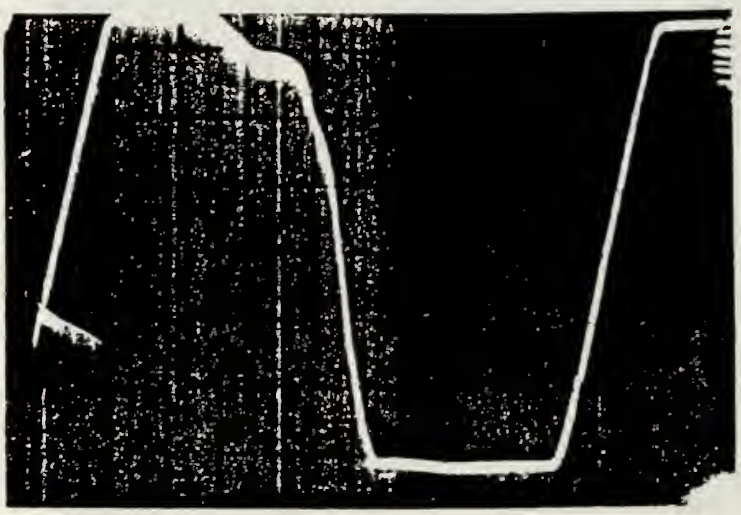

Figure 4.3 Output of Square Wave Circuit Using an HA-2525

with the 5170 in the A1 position and the 2525 in the A2 position. It was noted that the internal resistor ratio α had little effect on the output and the output shown here for α = 2.6 was typical. The input frequency utilized was 625 KHz. Although higher frequencies once again yielded further distortion from the ideal, this demonstrates that the composite circuit was able to produce a better square wave at twice the frequency of the single HA-2525.

C. IMPROVED PRECISION HALF-WAVE RECTIFIER

In light of the stability problems and other difficulties reported by Ismail [Ref. 14] in utilizing composite op-amps to generate either a superdiode or a half-wave rectifier, the improved version of a precision half-wave rectifier illustrated in Figure 4.5 was constructed. In this non-linear situation, as with many others, an op-amp is used in conjunction with other circuit devices (ex. diodes, transistors, etc.), all operating in their non-linear modes. However, these devices also exhibit their own non-ideal characteristics which often exacerbate a given problem. In this particular instance, the real semiconductor diodes suffer from a finite voltage drop that limits their usefulness in small-signal applications.

Assuming a silicon diode with a reverse bias voltage of 0.7 V, it has been shown that the superdiode depicted in Figure 4.6 (a) has a reverse bias voltage of 0.7/A , where A is the finite open-loop gain of the op-amp [Ref. 15]. This fact permits the rectification of much smaller signal levels, although the operating frequency may be limited by the dynamics of the op-amp. Figure 4.6 (b) shows the superdiode proposed by Ismail which utilizes a composite op-amp, in an effort to improve the circuit's dynamic behavior. For this circuit, it was shown that the reverse bias voltage is further reduced by a factor of 1/A2, where A2 is the open-loop gain of the composite's output op-amp. Figure 4.7 shows

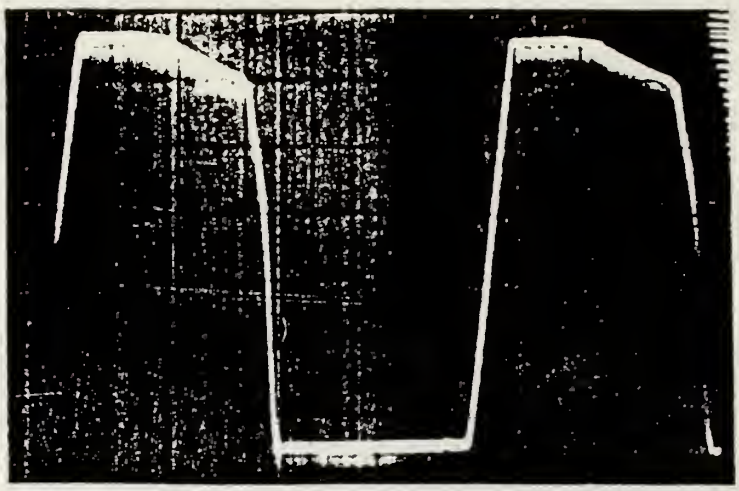

Figure 4.4 Output of Square Wave Circuit Using the C20A-4 Composite

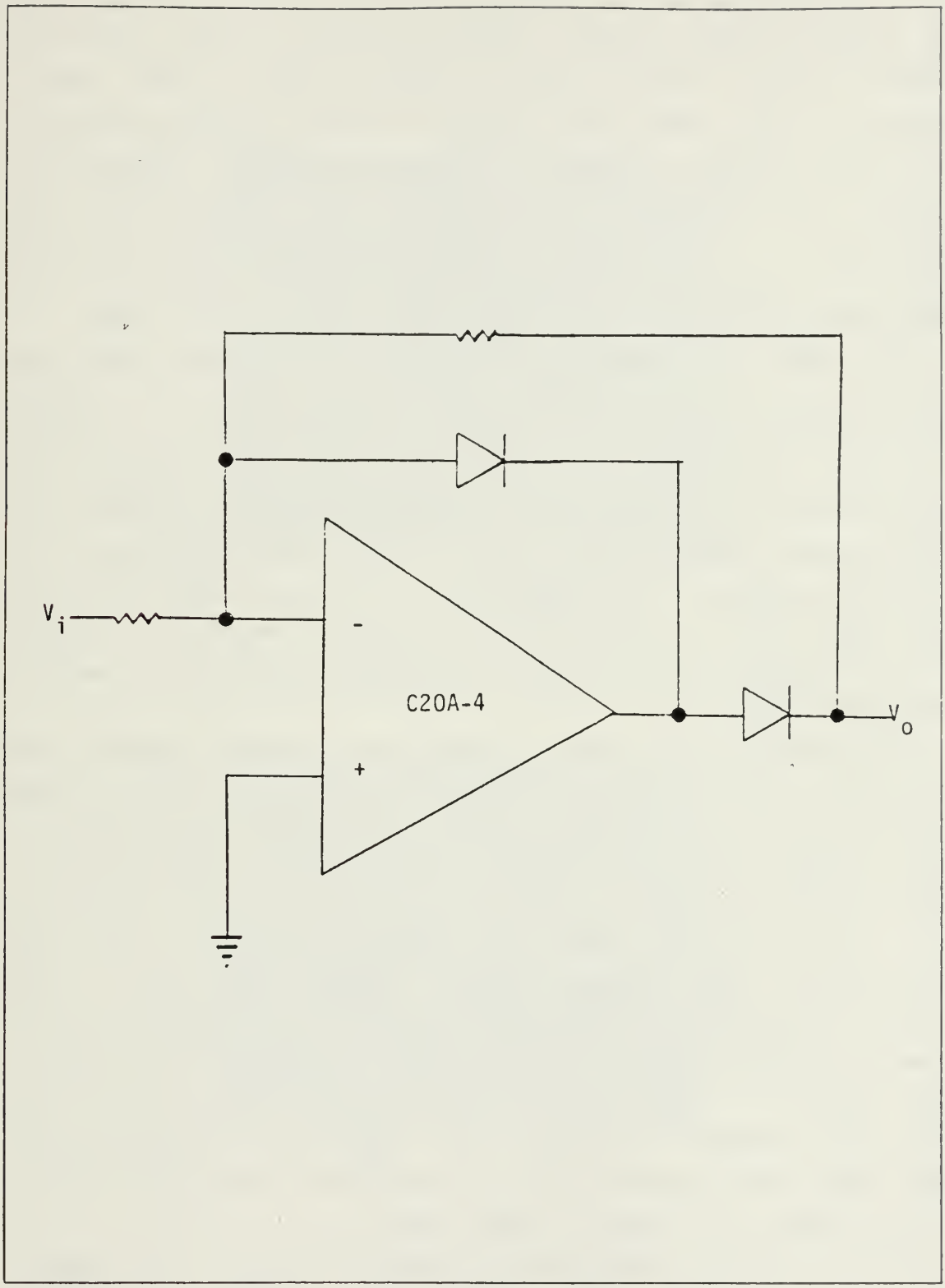

Figure 4.5 Improved Version of a Precision Half-Wave Rectifier Circuit

the results obtained by Ismail for this circuit. Figure 4.7 (a) shows the best output achieved for the circuit shown in Figure 4.6 (b), with a 400 mV peak-to-peak, 2 KHz input. Figure 4.7 (b) shows the transfer characteristic obtained for this circuit. Ismail's improved composite superdiode circuit of Figure 4.6 (c) yielded the results shown in Figure 4.8 . In part (a) is shown the half-wave rectification of a 5 KHz, 750 mV peak-to-peak signal, while part (b) shows the results for a 15 KHz, 40 mV peak-to-peak input.

The C20A configuration utilized in the above work was not one of the four C20A configurations that have been discussed throughout this thesis. As indicated in Chapter II, C20A-1 through C20A-4 were obtained by a process of eliminating from among all of the possible two-amplifier combinations, those that theoretically would yield poor or marginal stability and performance. It was therefore felt that these four composite configurations should be tested for their applicability before proceeding to try more exotic configurations.

Once again, the C20A-4 configuration was selected and the same two op-amps, the HA-5170 and the HA-2525, were utilized. Using a sinusoidal input of 23 KHz with a peak-to-peak voltage of 11.0 V yielded the transfer characteristic shown in Figure 4.9 (a). Again, the resistor ratio seemed to have little effect. Since the composite should allow the rectification of smaller signal levels, it came as no surprise that a very nice rectification was achievable with a peak-to-peak input of 45 mV, at a frequency of 23 KHz. This result is shown in Figure 4.9 (b). Figure 4.10 (a) shows the transfer characteristic obtained for these same conditions, and Figure 4.10 (b) shows the rectified output for a 6 KHz , 45 mV peak-to-peak input.

These results indicate the superiority of the C20A-4 since it rectified lower peak input signals at higher frequencies than did the other circuits discussed.

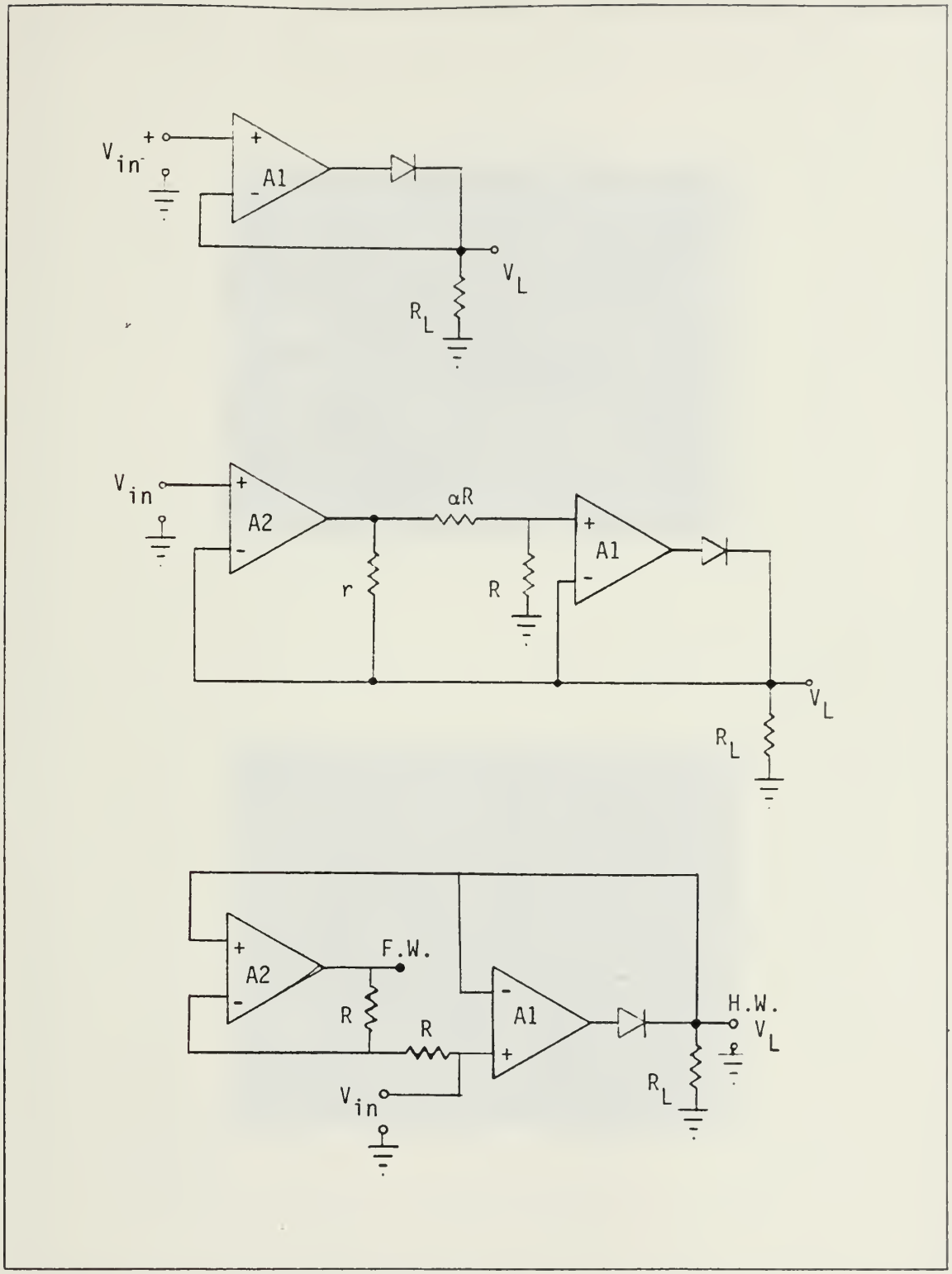

Figure 4.6 (a) Superdiode Circuit
(b) Composite Superdiode Circuit
(c) Improved Composite Superdiode Circuit

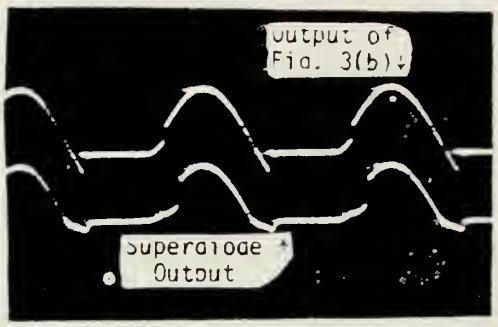

Figure 4.7 (a) Output for Fig 4.6 (b)
(b) Transfer Characteristic for Fig 4.6 (b)

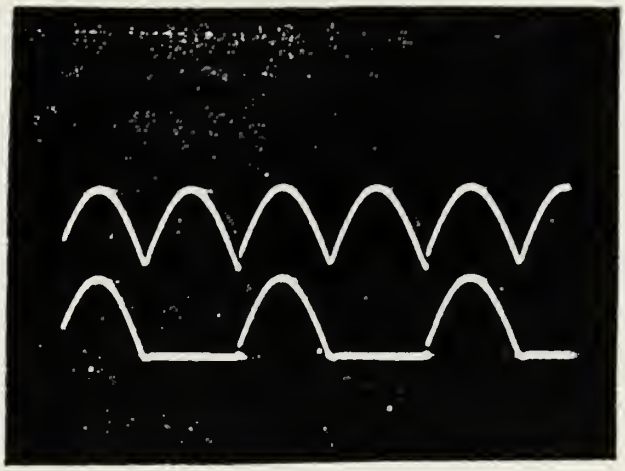

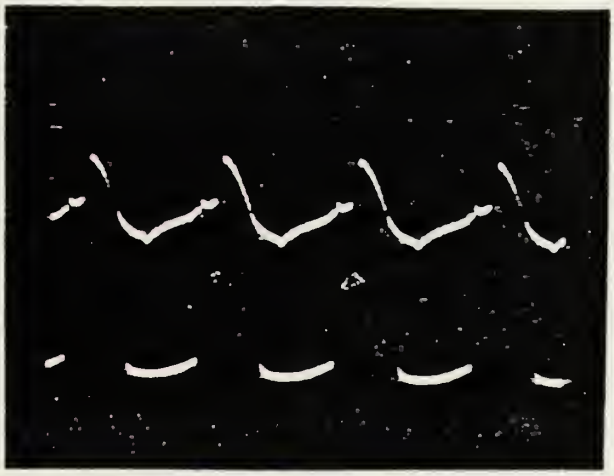

Figure 4.8 (a) Output of Figure 4.6 c for 5 KHz Input
(b) Output for Figure 4.6 c for 15 KHz Input

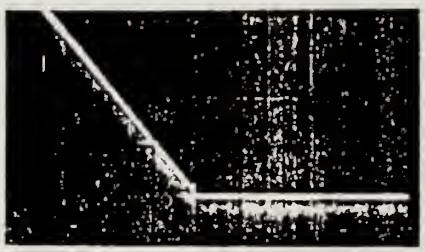

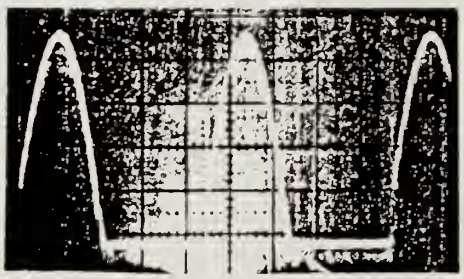

Figure 4.9 (a) Transfer Characteristic for C20A-4 (V =11 V)
(b) Output Resulting from 23 KHz, 45 mV Signal

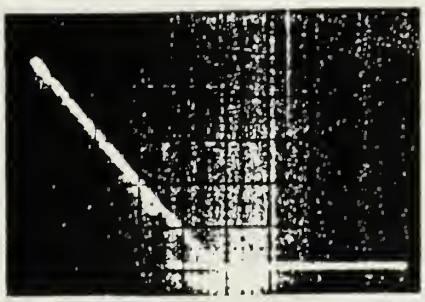

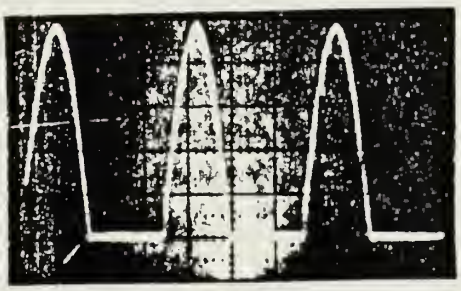

Figure 4.10 (a) Transfer Characteristic for C20A-4 (V =45mV)
(b) Output Resulting From 6 KHz, 45 mV Signal

D. NOVEL SAMPLE AND HOLD CIRCUIT

The final application to be discussed, a sample and hold circuit, is the most dramatic of all in that the real utility of the composite op-amps is in those areas demanding both a very high-speed and very high-accuracy operation.

In today's technology, signal processing is more and more often accomplished using digital methods. Since most of the events occuring in the physical world we live in are analog by nature, the desire to process information digitally requires a conversion of the analog signal into a digital one, and after processing, from digital back to analog. Central to the analog to digital (A/D) and digital to analog (D/A) converters that perform these operations are sample and hold circuits.

Sample and hold circuits are used to sample an analog signal at a given instant of time and hold the sampled value as long as the system requires. The simplest form of a sample and hold circuit is a switch in series with a capacitor. If the switch is closed, the capacitor will track the input voltage. When the switch is opened, the capacitor holds the voltage level at a constant value.

One of the simplest practical sample and hold circuits is shown in Figure 4.11 . Here, an electronically controlled switch, often a MOSFET device, provides a means for rapidly charging the capacitor to the sampled voltage and then isolating the input voltage source from the circuit so that the capacitor can store the desired input voltage level. In order for the sample and hold circuit to produce a good approximation of the input waveform being sampled, it is necessary for the frequency of the "clocking" control voltage to be substantially higher than that of the input signal. As with most practical sample and hold circuits, an op-amp is here employed by the circuit to present a low driving circuit impedance and a high load impedance across

the capacitor. For many critical applications, the utilization of a precision and/or high-speed op-amp is essential.

To get a better understanding of the requirements that might be imposed upon such a circuit, it can be visualized in conjunction with an A/D converter as the interface between an analog system and a 16 bit digital system. Given a 10 V maximum input implies the least significant bit (LSB) would represent 153 μV (voltage / 2 raised to the Nth power). The results presented in Chapter III indicated that the slew rate and input offset voltage achieved by the HA-5170/HA-2525 combination in the C20A-1, C20A-3, or C20A-4 configuration would fulfill the requirements, ie. - an LSB of 153 μV and a very high clock rate. The C20A-3, although the least accurate of the three, was selected since it coincidently exhibited exactly the accuracy required for the LSB of the 16 bit system.

Figure 4.12 shows the novel sample and hold circuit constructed utilizing the C20A-3 with α = 0.43 and K = 2.0. The switching control voltage (Vs) was applied at a frequency of 2.6 MHz. The placement of the capacitor between the switch and the non-inverting terminal of the HA-2525 was selected so that during hold periods the capacitor would not be able to discharge due to the open switch an one side and the high input impedance of the 2525 on the other.

Figure 4.13 shows the results obtained for this circuit. Here the input signal was a 100 KHz sinusoid. The photograph shows both the input and the output wave forms intentionally offset. It clearly demonstrates that the circuit amplified the signal by a factor of two and was able to sample at the 2.6 MHz clocking rate; i.e. - 26 samples per cycle were made and recorded.

These results do not represent the upper limits of this novel design. The clocking rates and α and K parameters were chosen merely to illustrate the utility of the circuit

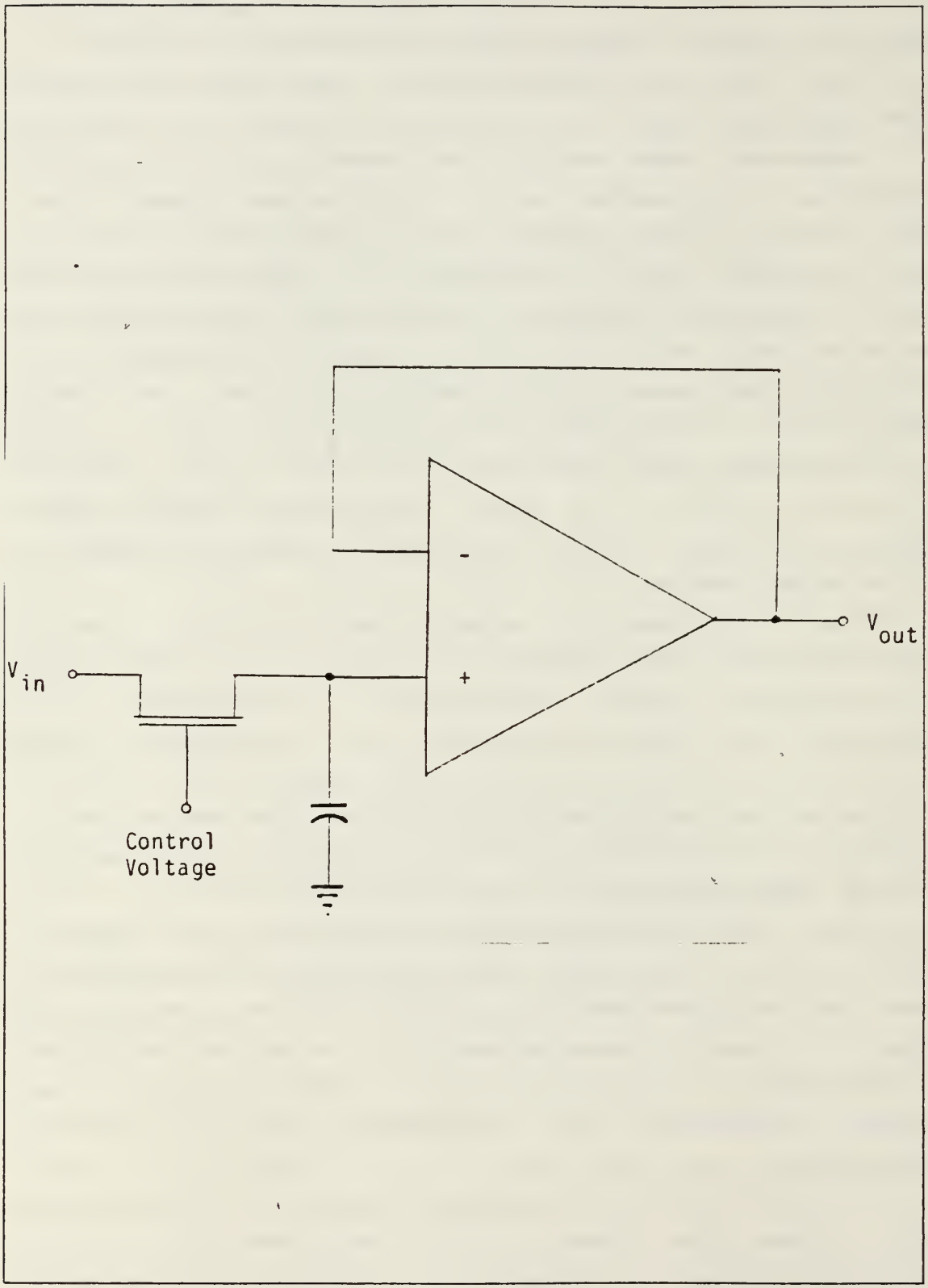

Figure 4.11 Practical Sample & Hold Circuit

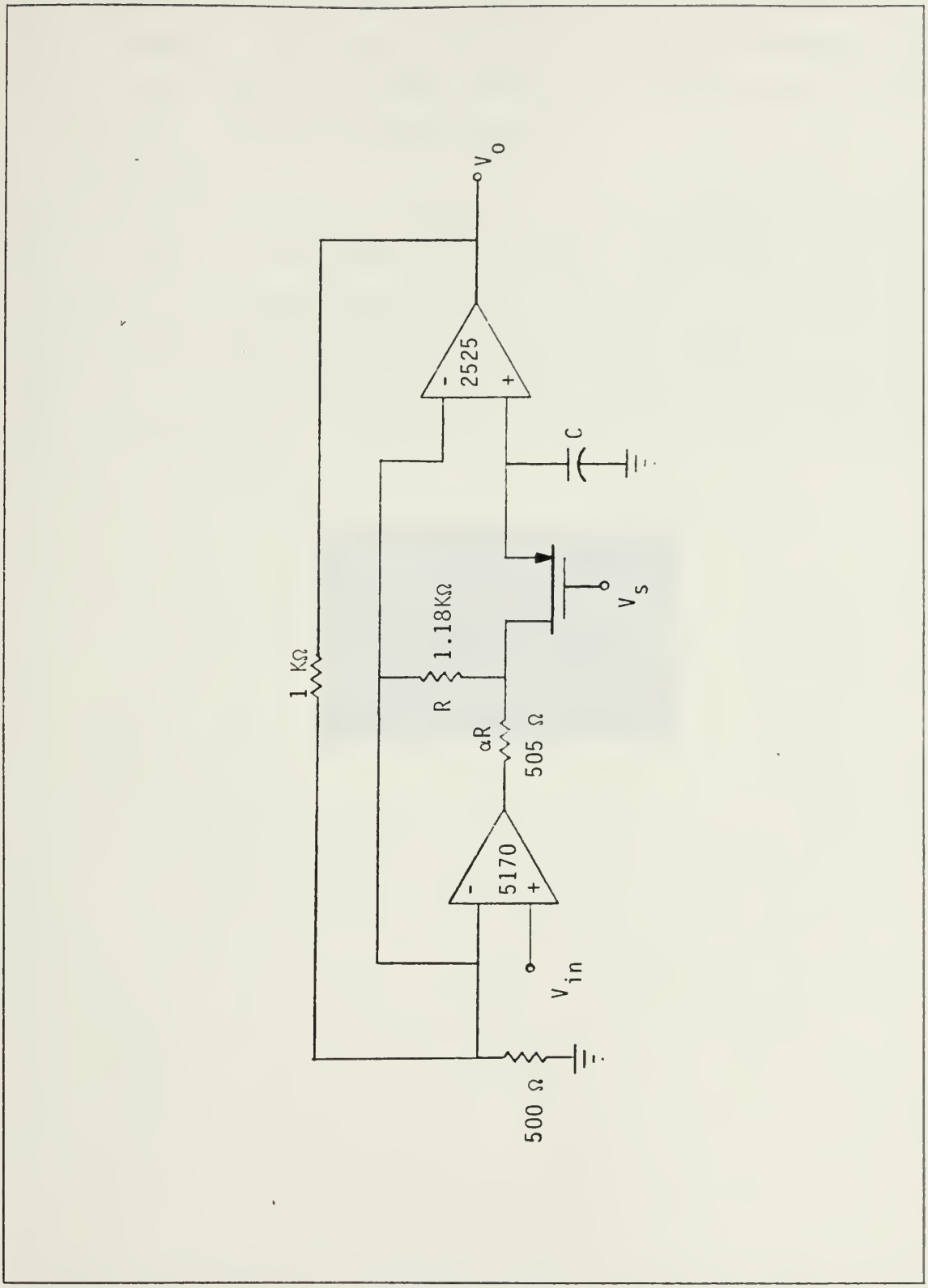

Figure 4.12 Novel Sample & Hold Circuit

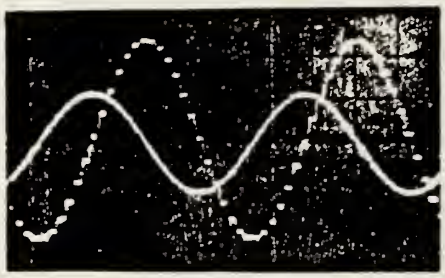

Figure 4.13 Results for Novel Sample & Hold Circuit

and that it would perform adequately in a demanding situation. Higher clock rates are quite likely permissable and better results may have been achievable with the other, more accurate and faster configurations.

E. CONCLUSIONS

The three applications presented in this chapter illustrate the utility of composite operational amplifiers in both linear and non-linear applications. Further, the capability of the composites to operate at very high speeds, in tasks requiring a high degree of precision, has been demonstrated. This constitutes a considerable improvement over presently available circuits.

V. CONCLUSIONS

The goal of this research effort was the realization of a high-speed, high-accuracy operational amplifier, an entity heretofore unknown.

In Chapter I, the concepts governing the behavior of an operational amplifier were discussed and theoretical expressions were derived which indicated the interdependence of an op-amp's slew rate and input offset voltage. The fact that both of these parameters are ultimately dependent upon the same transistors and resistors in the op-amp's first stage precludes the concurrent improvement of each. A variety of very successful techniques cited in the literature for slew rate enhancement were examined, and with each, the above observation was born out. That is, when an enhancement of slew rate was achieved, the input offset voltage was degraded.

Chapter II presented the relatively new concept of composite operational amplifiers (CNOAs) for N = 2, 3, or 4. The technique for their development was discussed and extensive theoretical analyses were developed indicating that this class of operational amplifiers should be able to perform with concurrent high-speed and high-accuracy.

Of all the possible C2OAs (N=2), four were shown to satisfy the suggested performance criteria and thus should exhibit superior performance. Arguments were introduced indicating that the composite's input op-amp (A1) should ultimately determine the overall input offset voltage achievable. Similarily, the output op-amp (A2) should determine the slew rate and bandwidth realizable by the composite. Since the composites were known for their ability to tolerate GBWP mismatching between the A1 and A2 op-amps, this provided an excellent opportunity to build into a composite any reasonable combination of speed and accuracy.

These precepts were then applied in Chapter III to a variety of op-amps covering the gamut of speed and accuracy. It was found that three of the four configurations yielded composite op-amps that exhibited accuracies on the order of, or better than, that of the very accurate amplifier in the A1 position, while simultaneously achieving speeds comparable to that of the high-speed op-amp in the composite's A2 position.

With these results in hand, Chapter IV presented three sample applications of these new high-speed, high-accuracy op-amps to illustrate their utility in both linear and nonlinear applications. Of particular importance was the development of a new sample and hold circuit that performed excellently in a situation demanding extreme precision while operating at a very high speed.

Thus, the novel design described in this thesis has resulted in a composite amplifier that combines the excellent performance of the precision op-amp used in its front-end, with the speed and wide bandwidth of the op-amp used in its output stage. Such optimum composite amplifiers not only offer significantly improved AC and DC performance over currently available devices, but they also make no new demands on technology, since they require only those devices that can be produced with available linear monolithic techniques.

APPENDIX A

PROGRAM TO CALCULATE THE FREQUENCY RESPONSE OF C2OAS

```
      DIMENSION HMAG(220),HPHASE(220),OMEGA(220)
      COMPLEX HH,S,DENOM
      REAL K,ANUM
c     THE FOLLOWING ARE CONSTANTS TO BE UTILIZED:A01=>DC
GAIN OF FIRST c     OPAMP;A02=>DC GAIN OF SECOND OPAMP;K=>
GAIN OF COMPOSITE OPAMP; c     ALPHA=>RATIO OF INTERNAL
RESISTORS
      Q = 1.0
      PI = 3.1415927
      AOQ = 2.24E4
      A02 = 1.E5
      K =   1.0
      ALPHA = 1.24
C     THE FOLLOWING ARE THE POLES FOR THE TWO OPAMPS; L
=>LOWER FREQ C     POLE, H=> HIGHER FREQ POLE, 1=> FIRST
OPAMP, 2=> SECOND OPAMP
      PLQ = 2.071E2*PI
      PHQ =  2.0E7*PI
      PL2 = 2.31E2*PI
      PH2 =  8.0E7*PI
      W1 = AOQ*PLQ
      W2 = A02*PL2
      OMEKA = -9999.
      DO 99 M = 1,220
         OMEKA = OMEKA + 150000.
         OMEGA(M)=OMEKA
         S = CMPLX(0.0,OMEKA)
C         NUM=> NUMERATOR & DENOM=> DENOMINATOR OF THE
TRANSFER C         FUNCTION " HH". HMAG=> MAGNITUDE OF THE
```

```
FREQ RESPONSE, C        HPHASE=> PHASE OF THE FREQ RESPONSE,
OMEGA=> FREQ, HR=> C        REAL PART OF TRANSFER FUNCTION,
HI=> IMAGINARY PART
C
C       THE FOLLOWING LINES SHOULD BE USED FOR THE
NUMERATOR AND C        DENOMINATOR TERMS FOR C20A-1:
C
C       ANUM = -K
C       DENOM =  Q+(Q+K)/(AO2*(Q+ALPHA))+(Q+K)/(AOQ*AO2)+
C                                                        *
((Q+K)/(AOQ*AO2))*S*(Q/PLQ+Q/PL2+Q/PHQ+Q/PH2+
C    *           AOQ/((Q+ALPHA)*PL2)+AOQ/((Q+ALPHA)*PH2))+
C                                                        *
((Q+K)/(AOQ*AO2))*S**2*(Q/(PLQ*PL2)+Q/(PLQ*PHQ)+
C                                                        *
Q/(PLQ*PH2)+Q/(PL2*PHQ)+Q/(PL2*PH2)+Q/(PHQ*PH2)+
C                                                        *
AOQ/((Q+ALPHA)*PL2*PH2))+((Q+K)/(AOQ*AO2))*S**3*
C    *           (Q/(PLQ*PL2*PHQ))+((Q+K)/(AOQ*AO2))*S**4*
C    *           (Q/(PLQ*PL2*PHQ*PH2))
C
C         THE FOLLOWING LINES SHOULD BE USED FOR THE
NUMERATOR AND C        DENOMINATOR TERMS FOR C20A-2:
C
C       ANUM = -K
C        DENOM =  Q+(Q+K)/(AOQ*(Q+ALPHA))+(Q+K)/(AOQ*AO2)+
C    *           (Q+K)/(AOQ*AO2)*S*(Q/PHQ+Q/PL2+Q/PHQ+Q/PH2+
C    *           AO2/((Q+ALPHA)*PLQ)+AO2/((Q+ALPHA)*PHQ))+
C                                                        *
(Q+K)/(AOQ*AO2)*S**2*(Q/(PLQ*PL2)+Q/(PLQ*PHQ)+
C                                                        *
Q/(PLQ*PH2)+Q/(PL2*PHQ)+Q/(PL2*PH2)+Q/(PHQ*PH2)+
C                                                        *
AO2/((Q+ALPHA)*PLQ*PHQ))+((Q+K)/(AOQ*AO2))*S**3*
C    *           (Q/(PLQ*PL2*PHQ))+((Q+K)/(AOQ*AO2))*S**4*
```

```
C     *            (Q/(PLQ*PL2*PHQ*PH2))
C
C          THE  FOLLOWING  LINES  SHOULD  BE  USED  FOR  THE
NUMERATOR AND C         DENOMINATOR TERMS FOR C20A-3:
C
C        ANUM =(Q+Q/AOQ+(Q/AOQ)*S*(Q/PLQ+Q/PHQ)+(Q/AOQ)*S**2*
C     *          (Q/(PLQ*PHQ)))*(-K)
C         DENOM = Q+Q/AOQ+((1+ALPHA)*(1+K)/(AOQ*AO2))+
C                                                              *
((1+ALPHA)*(1+K)/(AOQ*AO2))*S*(AO2/(PLQ*(1+ALPHA)*
C                                                              *
(1+K))+AO2/(PHQ*(1+ALPHA)*(1+K))+Q/PLQ+Q/PL2+Q/PHQ+
C                                                              *
Q/PH2)+((1+ALPHA)*(1+K)/(AOQ*AO2))*S**2*(AO2/(PLQ*
C                                                              *
PHQ*(1+ALPHA)*(1+K))+Q/(PLQ*PH2)+Q/(PLQ*PL2)+Q/(PLQ*
C                                                              *
PH2)+Q/(PL2*PHQ)+Q/(PHQ*PH2))+((1+ALPHA)*(1+K)/(AOQ*
C                                                              *
AO2))*S**3*(Q/(PLQ*PL2*PHQ)+Q/(PL2*PHQ*PH2)+Q/(PLQ*
C                                                              *
PL2*PHQ)+Q/(PLQ*PHQ*PH2))+((1+ALPHA)*(1+K)/(AOQ*AO2))*
C     *            S**4*Q/(PLQ*PL2*PHQ*PH2)
C
C          THE  FOLLOWING  LINES  SHOULD  BE  USED  FOR  THE
NUMERATOR AND C         DENOMINATOR FOR THE C20A-4:
C
C                                                          ANUM
=(AOQ*AO2+AO2*(Q+ALPHA)+AO2*(Q+ALPHA)*S*(Q/PLQ+Q/PHQ)+
C     *          AO2*(Q+ALPHA)*S**2*(Q/(PLQ*PHQ)))*(-K)
C                                  DENOM                       =
(Q+ALPHA)*(Q+K)+AOQ*AO2+AO2*(Q+ALPHA)+(Q+ALPHA)*
C                                                              *
(Q+K)*S*(Q/PL2+Q/PH2+Q/PLQ+Q/PHQ+AO2/((Q+K)*PLQ))+
```

```
C                                                                    *
(Q+ALPHA)*(Q+K)*S**2*(Q/(PL2*PH2)+Q/(PLQ*PL2)+
C                                                                    *
Q/(PLQ*PH2)+Q/(PL2*PHQ)+Q/(PHQ*PH2)+Q/(PLQ*PHQ)+
C    *          A02/((Q+K)*PLQ*PHQ))+(Q+ALPHA)*(Q+K)*S**3*
C                                                                    *
(Q/(PLQ*PL2*PH2)+Q/(PL2*PHQ*PH2)+Q/(PLQ*PL2*PH2)+
C    *          Q/(PLQ*PHQ*PH2))+(Q+ALPHA)*(Q+K)*S**4*
C    *          (Q/(PLQ*PL2*PHQ*PH2))
C
C
C         THE FOLLOWING LINES SHOULD BE USED FOR THE
NUMERATOR AND C        DENOMINATOR FOR C20A-1 IF YOU ASSUME
THAT WH1 AND WH2 ARE C        BOTH INFINITE. I.E.-- OVERALL
COMPOSITE IS REPRESENTED BY C        A TWO POLE MODEL, WHICH
IMPLIES EACH INDIVIDUAL OP-AMP IN C        THE COMPOSITE IS
TREATED AS HAVING A SINGLE POLE.
C
C       WP = SQRT((W1*W2)/(Q+K))
C       QP = (Q+ALPHA)*(SQRT(W2/(W1*(Q+K))))
C       ANUM = -K
C       DENOM = Q+S/(WP*QP)+(S**2)/(WP**2)
C
C         THE FOLLOWING LINES SHOULD BE USED FOR THE
NUMERATOR AND C        DENOMINATOR FOR C20A-2 IF YOU ASSUME
THAT WHQ & WH2 ARE C        BOTH INFINITE.
C
        WP = SQRT((W1*W2)/(Q+K))
        QP = (Q+ALPHA)*SQRT(W1/(W2*(Q+K)))
        ANUM = -K
        DENOM = Q+S/(WP*QP)+(S**2)/(WP**2)
C
C         THE FOLLOWING LINES SHOULD BE USED FOR THE
NUMERATOR AND C        DENOMINATOR FOR C20A-3 IF YOU ASSUME
THAT WHQ & WH2 ARE C        BOTH INFINITE.
```

```
C
C       WP = SQRT((W1*W2)/((Q+ALPHA)*(Q+K)))
C       QP = SQRT(((Q+K)*(Q+ALPHA)*W1)/W2)
C       ANUM = -K*(Q+S/W1)
C       DENOM = Q+S/(WP*QP)+(S**2)/(WP**2)
C
C         THE  FOLLOWING  LINES  SHOULD  BE  USED  FOR  THE
NUMERATOR AND C        DENOMINATOR FOR C20A-4 IF YOU ASSUME
THAT WHQ & WH2 ARE C        BOTH INFINITE.
C
C       WP = SQRT((W1*W2)/((Q+K)*(Q+ALPHA)))
C       QP = SQRT(((Q+K)*W1)/((Q+ALPHA)*W2))
C       ANUM = -K*(Q+(Q+ALPHA)*S/W1)
C       DENOM =  Q+S/(WP*QP)+(S**2)/(WP**2)
C
      HH = ANUM/DENOM
      HMAG(M)=20.*ALOG10(CABS(HH))
      HR = REAL(HH)
      HI = AIMAG(HH)
      HPHASE(M)= ATAN2(HI,HR)
      OMEGA(M)= OMEGA(M)/2.*PI
      WRITE(6,200) OMEGA(M),HMAG(M),HPHASE(M)
99    CONTINUE
  200 FORMAT(5X,E14.5,5X,F14.5,5X,F14.5)
C-----------------------------------------------------------------
C GRAPHICS PARAMETERS FOR MAGNITUDE IN DBS VS FREQUENCY
C-----------------------------------------------------------------
      CALL LRGBUF
      CALL TEK618
C .....     SETUP THE PLOTTING AREA
      CALL PAGE (11.0,8.5)
      CALL NOBRDR
      CALL AREA2D(9.0,6.5)
C .....  LABEL THE X & Y AXES
      CALL XNAME('FREQUENCY (HERTZ)$',100)
```

```
      CALL YNAME('AMPLITUDE IN DB$',100)
      CALL HEADIN ('AMPLITUDE IN DB VS FREQ FOR
C20A-2$',-100,1.4,3)
      CALL HEADIN ('GENERAL EXPRESSION FOR
5170/2525$',100,1.4,3)
C       CALL HEADIN('DERIVED EXPRESSION FOR 5170/2525
$',100,1.4,3)
      CALL HEADIN ('ALPHA = 1.24 , K = 1.0
$',100,1.4,3)
C .....  DEFINE THE AXES
      CALL GRAF(0.0,'SCALE',1.5E7, -4. ,'SCALE', 2.0)
C..... DRAW THE CURVES
      CALL THKCRV(0.02)
      CALL CURVE(OMEGA,HMAG,199,0)
C       CALL RLMESS('PROBLEM 1A (NEG) OF PROBLEM SET
2$',100,2.0,25.0)
C..... TERMINATE THIS PLOT
      CALL ENDPL(0)
      CALL DONEPL
      STOP
      END
```

LIST OF REFERENCES

1. Mikhael, W.B. and Michael, S.N.,"Generation of Actively Compensated Composite Operational Amplifiers and Their Use in Extending the Operating Frequencies of Linear Active Networks," Proceedings of the IEEE Symposium on Circuits and Systems, Newport Beach, CA, May 1983.

2. Mikhael, W.B. and Michael, S.N., "Actively Compensated Composite Operational Amplifiers," Proceedings of the Midwest Symposium on Circuits and Systems, Albuquerque, NM, June 1981.

3. Mikhael, W.B. and Michael, S.N., "Active Filter Design for High Frequency Operation," Proceedings of the Midwest Symposium on Circuits and Systems, Houghton, MI, Aug 1982.

4. Michael, S.N. and Gariano, P., "Optimization of High-Speed, High-Accuracy Integrated Operational Amplifiers," Proceedings of the Midwest Symposium on Circuits and Systems, Louisville, KY, Aug 1985.

5. Michael, S.N. and Gariano, P., "Applications of Precision, High-Slew Rate Op-Amps in Active Networks," Proceedings of the Midwest Symposium on Circuits and Systems, Louisville, KY, Aug 1985.

6. Gayakwad, R.A., Op-Amps and Linear Integrated Circuit Technology, p. 220, Prentice Hall, 1983.

7. Gray, P.R. and Meyer, R.G., Analysis and Design of Analog Integrated Circuits, p. 573, John Wiley and Sons, Inc., 1984.

8. Solomon, J.E., Davis, W.R., and Lee, P.L., "A Self Compensated Monolithic Op Amp with Low Input Current and High Slew Rate," ISSCC Dig. Tech. Papers, pp. 14-15, 1969.

9. Hearn, W.E., "Fast Slewing Monolithic Operational Amplifier," IEEE J. of Solid-State Circuits, Vol. SC-6, pp. 20-24, Feb 1971.

10. Davies, A.C., "The Significance of Nullators, Norators and Nullors in Active-Network Theory," Radio Electron Eng., Vol. 34, pp. 259-267, 1967.

11. Tellegen, B.D., "On Nullators and Norators," IEEE Trans. on Circuit Theory, Vol. CT-13, pp.466-469, 1966.

12. Michael, S.N., Composite Operational Amplifiers and Their Applications in Active Networks, Ph.D. Dissertation, West Virginia University, Morgantown, West Virginia, August 1983.

13. Millman, J. and Halkias, C., Integrated Electronics, Analog and Digital Circuits and Systems, p. 217, McGraw-Hill, Inc., 1972

14. Ismail, M., Zarabadi, S., Meyers, G., "Application of Composite Op-amps in Nonlinear Circuits," Proceedings of Midwest Symposium on Circuits and Systems, Morgantown, WV, June, 1984, pp. 44-47.

15. Sedra, A.S. and Smith, K.C., Microelectronic Circuits, HRW Series in Electrical Engineering, New York, 1982, pp. 155-161.

INITIAL DISTRIBUTION LIST

		No. Copies
1.	Defense Technical Information Center Cameron Station Alexandria, Virginia 22304-6145	2
2.	Library, Code 0142 Naval Postgraduate School Monterey, California 93943-5100	2
3.	Chairman, Department of Electrical and Computer Engineering, Code 62 Naval Postgraduate School Monterey, California 93943-5100	1
4.	Prof. Sherif Michael, Code 62XP Department of Electrical and Computer Engineering Naval Postgraduate School Monterey, California 93943-5100	2
5.	Prof. Larry Abbott, Code 62AT Department of Electrical and Computer Engineering Naval Postgraduate School Monterey, California 93943-5100	1
6.	LCDR Patrick Gariano Jr., Code 61V2 Space and Naval Warfare Systems Command Washington, DC 20363	2

21251

Thesis
G192
c.1

Gariano
Generation of an optimum high speed high accuracy operational amplifier.

thesG192
Generation of an optimum high speed high
3 2768 000 62965 3
DUDLEY KNOX LIBRARY